Finite Element Modelling of Magma Convection and Attendant Groundwater Flow

A Thesis Submitted to

Rhodes University

in fulfilment of the requirements

for the degree of

Master of Science

by

Keith Harrison

January 1998

Physics Department

Rhodes University

Grahamstown

6140

Abstract

This thesis describes preliminary two- and three-dimensional modelling of mass and heat transport of hot, molten magma in crustal intrusions and of the associated thermally induced flow of groundwater contained in the surrounding country rock. The aim of such modelling is to create a tool with which to predict the location of mineral deposits formed by the transport and subsequent precipitation of minerals dissolved in the convecting groundwater.

The momentum equations (Navier-Stokes equations), continuity equation and energy equation are used in conjunction with specially constructed density and viscosity relationships to govern the mass and heat transport processes of magma and groundwater. Finite element methods are used to solve the equations numerically for some simple model geometries. These methods are implemented by a commercial computer software code which is manipulated with a control program constructed by the author for the purpose.

The models are of simple two- or three-dimensional geometries which all have an enclosed magma chamber surrounded completely by a shell of country rock through which groundwater is free to move. Modelling begins immediately after the intrusive event when the magma (in most cases rhyolitic) is at its greatest temperature. Heat is allowed to flow from the magma into the country rock causing thermal convection of the groundwater contained therein. The effect of the country rock as a porous medium on the flow of groundwater is modelled by including a distributed resistance term in the momentum equation.

The computer code that controls the modelling is such that adaptions made to the models to represent real physical intrusive systems are trivial.

Results of the research at this stage allow approximate prediction of the location of mineral deposits. Enhanced predictions can be made by effecting improvements to the models such as a more detailed representation of chemical processes, adaption of the computer code to allow multiple injections of magma and the modelling of frozen magma as a porous medium which admits the flow of groundwater.

Acknowledgements

Thanks to Anglo American, BHP, Goldco (formerly Gencor and Goldfields), Rio Tinto Mining and Exploration and the Foundation for Research Development for funding the project; to Dr P. Nathanson (H.O.D. Physics); to Prof. P. Kaye (H.O.D. Chemistry), Prof. H. Parolis (H.O.D. Pharmacy) and Prof. P. Clayton (H.O.D. Computer Science) for granting me extensive use of the Chemistry, Pharmacy and Computer Science computer hardware; to *Ansys*, Inc. (Southpointe, 275 Technology Drive, Canonsburg, PA, USA, 15317) for the use of their *FLOTRAN* software and to Steve van Wyk (Tetra Technology, Pretoria) for his help and advice.

Special thanks to my supervisor Prof. Alan Rice; to Prof. Fabio Frescura and to Andrè Botha.

Contents

	List of Figures	vii
	List of Tables	ix
1	**Introduction**	**1**
	1.1 Thesis Description and Aims	1
	1.2 Methodology	2
	1.3 Content of the Thesis	3
2	**The Intrusion-Country Rock System**	**5**
	2.1 Behaviour of Magmatic Melts in Crustal Intrusions	5
	2.1.1 Behaviour of Magmatic Fluids	*6*
	2.1.2 Viscosity	*6*
	2.1.3 Density	*7*
	2.1.4 Thermal Conductivity and Specific Heat	*8*
	2.1.5 Flow Regime	*9*
	2.2 Porous Media and Groundwater Flow	10
	2.2.1 Structure of Porous Media	*10*
	2.2.2 Behaviour of Porous Media during an Intrusive Event	*11*
	2.2.3 Groundwater Flow	*13*
3	**Equations Governing Magma and Groundwater Flow**	**16**
	3.1 Magma Flow	16
	3.2 Porous Media Flow	18
	3.3 Treatment of the Equations by *FLOTRAN*	20
4	**Numerical Solution of the Governing Equations by Finite Element Methods**	**22**
	4.1 Finite Element Analysis	22
	4.2 Representing the Problem Domain	23
	4.3 Representing a Solution	25
	4.4 Perfecting the Trial Solution	26
	4.5 Discretizing the Governing Equations	27
	4.5.1 Diffusion and Source Terms	*28*
	4.5.2 Transient Term	*29*

4.5.3 Advection Term 30
4.6 Determining Pressure 35
4.6.1 Velocity-Pressure Coupling Equations 36
4.6.2 The Incompressible Flow Pressure Equation 37
4.7 Solving the Discrete System 38
4.7.1 General Solution Sequence 38
4.7.2 The TDMA Matrix Solver 40
5 Model Structure and Control **41**
5.1 *Ansys* and *FLOTRAN* 41
5.2 The *FLOTRAN* Fluid Element 42
5.3 The Process Modelled 43
5.4 The Models 46
5.4.1 Two-dimensional Square Chamber 47
5.4.2 Two-dimensional Wedge-shaped Chamber 48
5.4.3 Three-dimensional Cylindrical Chamber 48
6 Results **52**
6.1 Results Displays 52
6.1.1 Contour Plots 52
6.1.2 Vector Plots 53
6.1.3 Particle Traces 53
6.2 Mesh Refinement Experiments 53
6.3 Square Magma Chamber 54
6.4 Country Rock Surrounding the Square Magma Chamber 55
6.5 Wedge-shaped Magma Chamber 55
6.6 Transient Results Sequences 56
6.7 Three-dimensional Cylindrical Magma Chamber and Surrounding Country Rock 56
6.8 Animations 57
7 Discussion and Conclusions **77**
7.1 Square Magma Chamber and Surrounding Country Rock 77
7.2 Wedge-shaped Magma Chamber and Surrounding Country rock 79
7.3 Cylindrical Magma Chamber and Surrounding Country Rock 80
7.4 Animations 80
7.4.1 Sill-shaped Magma Chamber 80

7.4.2 Sill-shaped Magma Chamber with Conductive Country Rock *81*
7.4.3 High Aspect Ratio Cylindrical Magma Chamber *81*
7.4.4 Visualization Techniques *82*
7.5 Predicting the Location of Mineral Deposits 82
7.6 Problems with the Models and Suggestions for Improvements 83
References 85
Appendix 1 Derivation of Equations Governing Fluid Flow **88**
a1.1 The Continuity Equation 88
a1.2 The Momentum Equation 90
a1.3 The Energy Equation 93
Appendix 2 APDL Macros for the Coupled Solution of Magma Chamber and Country Rock Models **96**

List of Figures

Figure 1.1	Simplified map showing surface exposures of the Bushveld Complex.	2
Figure 2.1	Plot of the variation of viscosity with temperature of a rhyolitic melt.	7
Figure 2.2	Thermal conductivity of a typical basaltic magma.	9
Figure 4.1	The process of finite element analysis.	24
Figure 4.2	A finite element mesh with quadrilateral elements.	25
Figure 4.3	The shape of the linear interpolation function $N_L(x,y)$.	26
Figure 4.4	A quadrilateral element showing the quantities required to test the top right node (node j) for downwindedness.	31
Figure 4.5	Flow rates through the edges of a quadrilateral element with downstream node $j = 1$.	32
Figure 4.6	(a) Triangular and (b) tetrahedral elements showing the streamline that passes through the downwind node (node 1 in both cases) and its upstream point of entry into the element. Mass flow rates through element edges or faces are also shown.	33
Figure 4.7	Flow chart showing the major steps in *FLOTRAN*'s solution procedure.	39
Figure 5.1	Model used to investigate the effects of mesh refinement on solution accuracy.	47
Figure 5.2	(a) Two-dimensional square magma chamber mesh and (b) and surrounding country rock mesh. Note that (a) is not to the same scale as (b) and has been enlarged for clarity. With the scales equal, (a) fits exactly into the central cavity in (b) and all nodes along the contact boundaries coincide.	50
Figure 5.3	Two-dimensional wedge-shaped chamber (a) and surrounding country rock (b).	50
Figure 5.4	Vertical sections through the centres of the three-dimensional cylindrical magma chamber (a) and the surrounding country rock (b).	51
Figure 6.1	Plot of the heat flux (a) and temperature (b) at the central contact element in the mesh experiment model. The legend gives the total number of elements along the contact edge for each curve.	58

Figure 6.2 Temperature distributions in the two-dimensional square magma chamber (1 km by 1km) after (a) 90.2 and (b) 190 years. 59

Figure 6.3 Temperature distribution in the two-dimensional square magma chamber (1km by 1 km) after 385 years. 60

Figure 6.4 Particle traces in the two-dimensional square magma chamber (1km by 1 km) calculated after (a) 0.2 and (b) 90.2 years. The arrows indicate the direction of flow. 61

Figure 6.5 Velocity distributions in the two-dimensional square magma chamber (1km by 1 km) after (a) 0.2 and (b) 8.0 years. 62

Figure 6.6 Velocity distributions in the two-dimensional square magma chamber (1km by 1 km) after (a) 8.5 and (b) 10.7 years. 63

Figure 6.7 (a) Velocity distribution in the two-dimensional square magma chamber (1km by 1 km) fter 90.2 years and (b) the same distribution overlaid with the corresponding temperature distribution. 64

Figure 6.8 Velocity distribution in the two-dimensional square magma chamber (1km by 1 km) after (a) 1083 and (b) 2600 years. 65

Figure 6.9 Temperature distributions in the two-dimensional country rock surrounding the square magma chamber after (a) 190 and (b) 1083 years. 66

Figure 6.10 (a) Velocity distribution in the two-dimensional country rock surrounding the square magma chamber after 2600 years and (b) particle trace after 15200 years. The arrows in the particle trace indicate the direction of flow. 67

Figure 6.11 Velocity distributions in the two-dimensional country rock surrounding the square magma chamber after (a) 10.7 and (b) 90.3 years. 68

Figure 6.12 Velocity distributions in the two-dimensional country rock surrounding the square magma chamber after (a) 1083 and (b) 2600 years. 69

Figure 6.13 (a) Magnified view of the velocity and temperature distributions in the two-dimensional country rock surrounding the square magma chamber after 2600 years. (b) Velocity distribution in 15200 years. 70

Figure 6.14 (a) Temperature distribution in the two-dimensional wedge-shaped magma chamber after 38.2 years. (b) Particle trace calculated after 20.7 years. The arrows indicate the direction of flow. 71

Figure 6.15 Velocity distribution in the two-dimensional wedge-shaped magma chamber after 20.7 years. 72

Figure 6.16 Development of the temperature distribution in the two-dimensional square chamber and the surrounding country rock over the first 27000 years with frames approximately 5400 years apart. 73

Figure 6.17 Development of the velocity distribution in the two-dimensional square chamber and the surrounding country rock over the first 5300 years with frames approximately 1060 years apart. The upper scale in each picture refers to the country rock while the bottom scale refers to the magma. 74

Figure 6.18 Development of the velocity distribution in the two-dimensional wedge-shaped chamber over 9 years, starting from 12.8 years with frames approximately 1.8 years apart. 75

Figure 6.19 (a) Sectioned view of half of the three-dimensional country rock model showing the temperature distribution after 200 years. (b) The same sectioned view showing the velocity distribution after 200 years. (c) Sectioned view of the corresponding three-dimensional magma chamber showing the temperature distribution after 200 years. 76

Figure a1.1 Flow through a small cubic volume. 89

Figure a1.2 Torques about the centre of a small fluid element. 92

List of Tables

Table 3.1 Correspondence between the general scalar transport equation and the five governing equations. 21

Table 5.1 The physical properties used for modelling magmatic fluid. 44

Table 5.2 The physical properties used for modelling groundwater. 45

Table 5.3 Boundary and initial conditions applied to the square magma chamber model. 48

Table 5.4 Boundary and initial conditions applied to the cylindrical magma chamber model. 49

Chapter 1

Introduction

1.1 Thesis Description and Aims

The main objective the project reported in this thesis was to produce a general model of fluid flow in intrusive systems. An intrusive system in this context can be regarded as a chamber of molten magma which is injected in a single event over an infinitesimal time period into the crust from the mantle and proceeds to cool and solidify. Heat from the magma is conducted into the country rock which completely surrounds the chamber and causes convective transport of the groundwater contained within. The total effort of the project was initiated by treating problems akin to granitic stocks because they require fewer computational resources.

A particular focus of the project was the Bushveld Complex in South Africa, shown in **Figure 1.1** (Eales et al., 1993). Although a full model of the Complex itself has not yet been made, much work has been done on the modelling of simpler, associated structures. The information gleaned from these models should be of great use in understanding the processes at work during the cooling of the Bushveld Complex magma.

Such a study of the Bushveld Complex is extremely important, because, despite the extensive research and experimentation (including regional gravity surveys, ground and aeromagnetic surveys, time domain electromagnetic surveys, DC resistivity soundings and regional reflective seismic studies), there is still much that is unclear.

In particular, there is confusion about the origin of certain layered sequences in the complex, many of which are rich in economically valuable minerals. Knowledge of associated geological

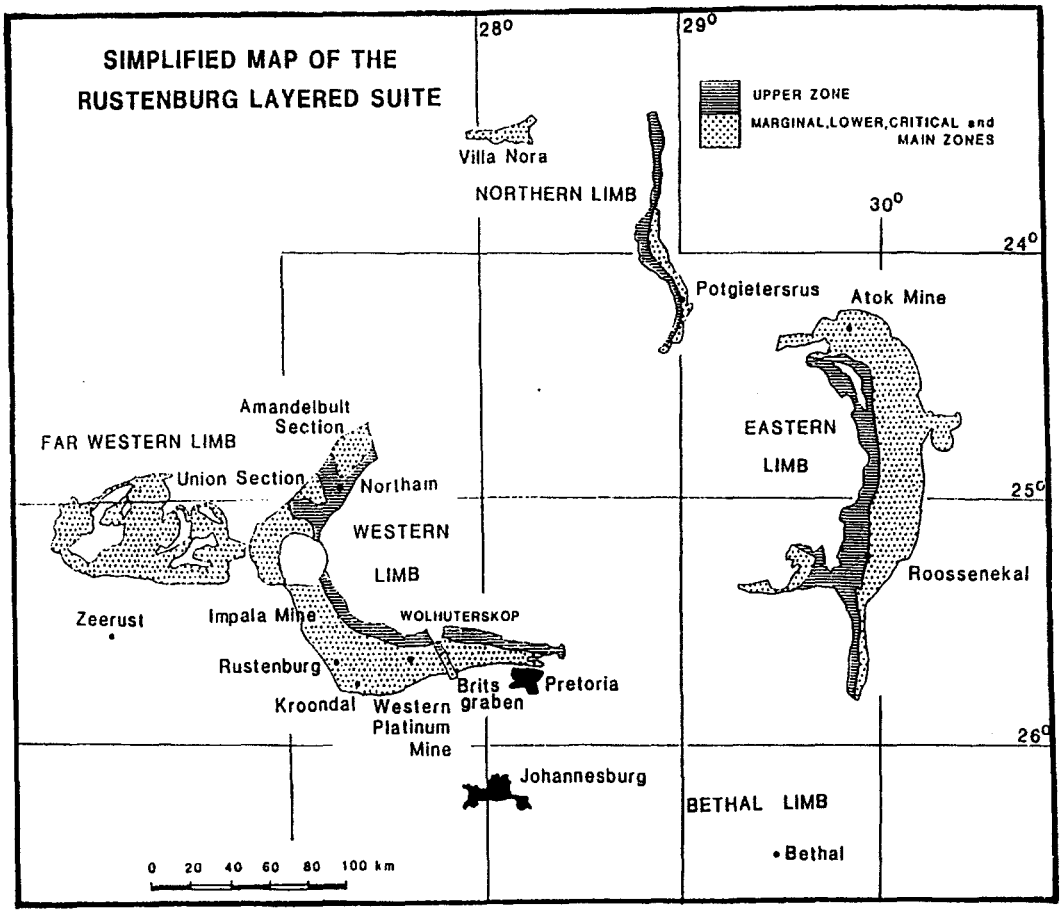

Figure 1.1 Simplified map showing surface exposures of the Bushveld Complex.

transport and precipitation processes is therefore desirable, as it may lead to more successful prediction of mineral distribution.

1.2 Methodology

Only fairly recently has work been done on magmatic fluid and groundwater. All such work has involved very simple one- or two-dimensional models, often producing steady-state solutions only. Antonopoulos and Papazafirou (1990) modelled one-dimensional vertical flow of fluid and solutes in variably saturated porous media. Adler et al (1990) used finite difference techniques to model flow through statistically generated models of porous media to determine permeability. Norton and Knight (1977) and Hayba and Ingebritsen (1997) used two-

dimensional models of permeable magma and country rock. These latter examples model only the thermal characteristics of the magma and the flow characteristics of the water contained in the magma. Thus only a single fluid (water) in the entire magma chamber-country rock system is modelled. However, it is now accepted that at typical intrusive temperatures, some magmas are able to convect. In these cases it is more sensible to model the flow of the magma itself.

The methodology for this thesis was to model the transport of mass and heat in the thermally coupled system of magmatic fluid and groundwater for a range of simple geometries (two- and three-dimensional) and for fluid properties in order to gain a general perspective on the behaviour of such systems. Such a methodology allows the simultaneous study of many of the features of magma chamber-country rock systems considered in previous work, in addition to some aspects not studied previously.

1.3 Content of the Thesis

The models in this work calculate numerical representations of the transient thermal and mechanical behaviour of both the magmatic fluid and the surrounding groundwater. The fluid properties of magma and groundwater have vastly different values. In fact, the software used for modelling (*FLOTRAN*, the computational fluid dynamics part of the *Ansys* package) cannot model such fluids simultaneously and extra code had to be written to couple two separate models. **Chapter 2** describes magmatic fluid and groundwater in terms of transient behaviour and physical properties such as density, viscosity, specific heat and thermal conductivity. Specification of the temperature dependence of density and viscosity is a means of giving the magmatic fluid geological identity. Data from Bottinga and Weill (1972) and Bottinga et al. (1982) were used to fit the density and viscosity curves for modelling. Also described in **Chapter 2** is the physical nature of porous media and the behaviour of groundwater flow within.

Magma and groundwater may both be modelled with the Navier-Stokes equations, the continuity equation and the energy equation for fluids. Certain assumptions (such as incompressibility) can be made to simplify the equations. These equations, and the necessary adjustments required (to model porous media flow for example), are explained in detail in **Chapter 3**.

The common structure to which each equation conforms allows *FLOTRAN* to use only one

solution algorithm. To be made eligible for this algorithm, some of the equations need further adjustment. The common equation and the adjustments required are given in **Chapter 3**. A detailed description of the solution algorithm is given in **Chapter 4**.

Chapter 5, in preparation for the results given in **Chapter 6** (which have been presented at conferences mentioned in all reference listings for Botha et al. (1996 and 1997) and Rice et al. (1997 and 1998) in the References chapter of this thesis), describes the computer models used and the software on which they were run. Finally, discussion of the results and ideas for further development are given in **Chapter 7**.

Chapter 2

The Intrusion-Country Rock System

The physical system that has been modelled is a crustal magmatic intrusion or pluton (molten) with surrounding groundwater in porous country rock. Flow of groundwater in the magma chamber is not modelled and the chamber is considered a closed system containing only magmatic fluid. The model does not deal with eruptions and surface flow, i.e. volcanic systems. A detailed description of the model starts with an examination of the important properties of the fluid in typical magma chambers and their surroundings.

2.1 Behaviour of Magma Melts in Crustal Intrusions

The main processes occurring throughout the active lifetime of a typical magma chamber are the transport of heat (within the melt and across its boundaries) and the precipitation and transport of crystals. These processes determine the position and concentration of economically valuable mineral-rich sequences in geological structures exploited in the present day.

Heat in fluids is transported through space by conduction through the fluid or by the movement of the fluid itself (convection). Much work has been published supporting the hypothesis that magma can convect (Bartlett, 1969; Eichelburger et al., 1976; Elder, 1976; Huppert and Sparks, 1980; Shaw, 1965). The results of this work in fact show that magmatic fluid in an enclosed chamber convects easily and at times can be extremely turbulent.

A group of well known fluid mechanical equations can be used to find a numerical

description of the mass and heat transport of the magma; these are described in the next chapter, but first we look at the physical properties of magmatic fluid.

2.1.1 Behaviour of Magmatic Fluids

Magma in its fluid state is usually (as in the present case) modelled for simplicity as a Newtonian fluid. This means that its stress tensor is a linear function of the velocity gradients (see **Chapter 3**), or

$$\tau = \mu \frac{du}{dy} \tag{2.1}$$

for plane flow in the x-direction where u is the fluid velocity, du/dy is the velocity gradient normal to the direction of shear and μ is the viscosity of the fluid. In fact Robson (1967) found that some lavas have a finite yield strength τ^0 which is a minimum stress that must be applied to the magma before permanent deformation takes place (Bingham fluid). Any stress below τ^0 will cause elastic deformation only. It has been shown by others that the stress applied to certain lavas is proportional to some power of the velocity gradients less than 1 (McBirney and Murase, 1984). Thus we have

$$\tau = \tau^0 + \mu \left(\frac{du}{dy}\right)^n \tag{2.2}$$

where $n < 1$. *FLOTRAN* allows viscosity formulations that simulate fluids with these properties. A viscosity function was used that could mimic most accurately the data available - data that represent the behaviour of laboratory magmas. (Results from experimental work done on lavas and laboratory magmas make up the only available data on such fluids. Experiments of these kinds cannot easily be done on real intrusive systems).

2.1.2 Viscosity

The equation used to model viscosity is a temperature dependent exponential function given by (*FLOTRAN* Manual, 1997)

$$\mu = \mu_n e^{A} \tag{2.3}$$

where

$$A = a_1 \left(\frac{1}{T} - \frac{1}{T_0}\right) + a_2 \left(\frac{1}{T} - \frac{1}{T_0}\right)^2 \tag{2.4}$$

and where μ_n is the nominal viscosity, a_1 and a_2 are constants and T_0 is the temperature at which $\mu = \mu_n$.

Bottinga and Weill (1972) devised a formula for calculating the constants in the equation based on the composition of the parent melt. The choice of initial viscosity (made to adjust the initial Rayleigh number to the desired value) reflects a rhyolitic composition. The exact composition at these early stages of development is unimportant and modelling of a specific intrusion with its own unique composition can be done easily by recomputing the coefficient values in the Bottinga and Weill formula based on the relative abundances of the individual constituents of that system.

Figure 2.1 shows a plot of the log of the viscosity function used in the modelling. The high viscosities at low temperatures serve to model the "cohesive freezing" of the magma as its crystal load increases causing more energy to be dissipated through inter-crystal friction. Such energy loss decreases flow speeds.

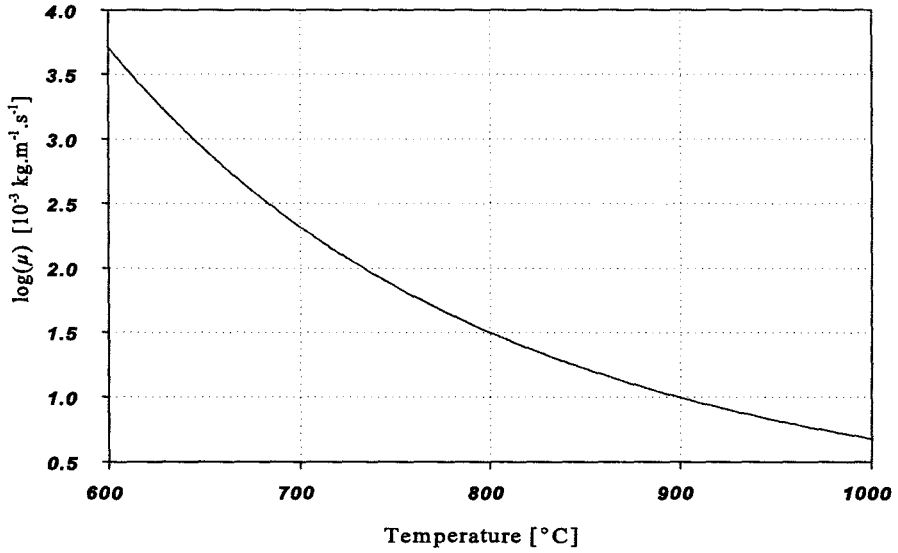

Figure 2.1 Plot of the variation of viscosity with temperature of a rhyolitic melt.

2.1.3 Density

The equations of motion for fluids are greatly simplified by the assumption that density is constant and uniform. However, when a flow is driven by natural convection, variations in temperature (or perhaps solute concentration) cause significant variations in density. Pressure

differences arising from these variations drive the fluid into motion and a non-uniformity in density is therefore fundamental to the processes of mass and heat transfer.

Since temperature and pressure contribute to density variations in thermal problems, density can be expressed as a function of T and p:

$$\rho = \rho(T,p) \tag{2.5}$$

which is simply the thermal equation of state. However, as mentioned in the next chapter, the fluids modelled (magma and groundwater) have, in most instances, been considered incompressible. It is assumed here that variations in pressure will not cause significant changes in density compared to thermal expansion or contraction; hence density can be considered a function of temperature alone.

Another simplification arises from the fact that, because of incompressibility, the gravitational force single-handedly causes instability through density variations. Consequently it is possible to use the Boussinesq approximation which states that density can be considered constant wherever it appears in the equations of motion, except in terms involving the gravitational force.

FLOTRAN allows a fairly general specification of fluid properties. This makes it possible to tailor the properties to match the particular fluid being modelled. The general form of the temperature dependent density is, to second order accuracy

$$\rho(T) = \rho_n + b_1(T - T_0) + b_2(T - T_0)^2 \tag{2.6}$$

where ρ_n is the nominal density, b_1 and b_2 are constants and T_0 is the temperature at which $\rho = \rho_n$. Including the second order term causes the density to increase more rapidly than usual at low temperatures and thus serves to model the increasing crystal load of the magma as it cools (the crystals are usually denser than the remaining fluid). Data from Bottinga et al. (1982) were used to fix the coefficients in the density equation.

2.1.4 Thermal Conductivity and Specific Heat

Thermal conductivity is a function of lattice (phonon) conduction, characterized by propagation vibrations in the lattice, and radiative (photon) conduction. At very high temperatures, radiative conduction becomes predominant and conductivity increases rapidly

(Williams and McBirney, 1979). At lower temperatures, conductivity is in a state of gradual decline as the temperature increases. The present research seeks to model this temperature range where the gradual decline can be considered small enough to treat thermal conductivity as constant. Below (**Figure 2.2**) is a plot of thermal conductivity versus temperature of a basaltic magma, from Williams and McBirney (1979). Although the viscosity function used in this work simulates a rhyolitic rather than a basaltic magma, thermal conductivity does not vary appreciably with viscosity and basaltic values can be used. The region to the left of the broken line indicates the temperature range relevant to the present research . The upper temperature limit of 1000 °C is a relatively high temperature for rhyolitic melts (the choice of a high limit gives breadth to the initial research). A lower value specific to an actual intrusion may be used later. The lower temperature limit is that dictated by the geothermal gradient present in the surrounding country rock before intrusion.

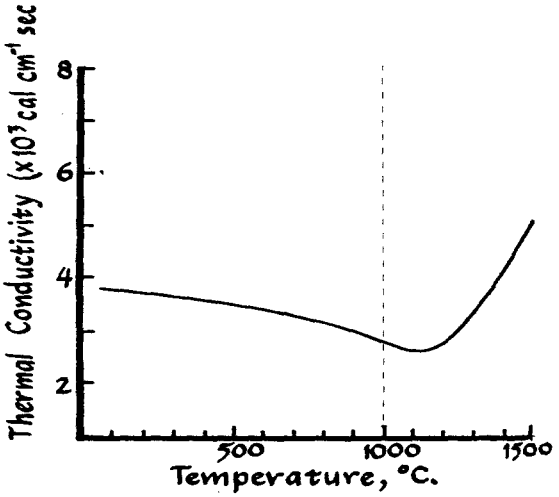

Figure 2.2 Thermal conductivity of a typical basaltic magma.

As the melt cools, the energy required to cool a unit mass by one unit of temperature remains the same, thus the specific heat is constant.

2.1.5 Flow Regime

It is important for modelling purposes to know how vigorous one can expect the flow to be. Convection in a magma chamber may be either laminar or turbulent. Different approaches to solving the equations of motion are required for these different flow regimes. A suitable solution

process for turbulent flow involves the calculation of results which represent a slight averaging of the exact, highly complex flow patterns. It is thus preferable to deal with laminar flow if a numerical solution to the exact flow field is required. Obviously one cannot choose what flow regime will be predominant in a given system, but one should be aware of the requirements for accurate solution and, if possible, optimize the model to comply with the requirements.

The value of the Rayleigh number for a particular system is often the most useful way of predicting the strength of the flow. For confined flow between two flat, parallel plates of different temperatures, the Rayleigh number is given by

$$Ra = \frac{g\beta d^3 \rho^2 c_p \theta}{\mu k} \tag{2.7}$$

where g is the acceleration of a body in free-fall, β is the thermal expansivity, d is the characteristic length of the system (usually the spatial extent of the largest temperature drop), ρ is the density, c_P is the specific heat, θ is the largest temperature difference in the system (initially the temperature difference between the plates), μ is the viscosity and k is the thermal conductivity.

It is difficult to determine a formulation of the Rayleigh number that suits the exact geometry and various fluid property constraints of the model being studied. The formulation given in (2.7) is however useful in many systems for predicting in approximate terms the expected flow regime. Krishnamurti (1970) categorizes flow regimes (between flat, parallel plates heated from below) as follows: if $Ra \leq 1700$, no convection occurs; if $1700 \leq Ra \leq 3 \times 10^6$, flow is laminar and if $Ra \geq 3 \times 10^6$, flow is turbulent. Values of Ra for the models that have been constructed can be found in **Chapter 5**. They imply, for instance, that turbulence can be expected in many cases.

2.2 Porous Media and Groundwater Flow

The system modelled in this work has a magma chamber completely enclosed by the crustal rock into which the invasion of magmatic fluid took place. A full description of the simplifications made to the real physical system for modelling purposes is made in **Chapter 5**. The function of this section is to describe the physical nature of the country rock surrounding the chamber and some properties of the groundwater flow within.

2.2.1 Structure of Porous Media

A porous medium is a solid matrix, such as a rigid conglomeration of soil particles, that does not occupy the total volume V_T defined by its bounding surfaces but has numerous voids or pores that may contain some sort of fluid (liquid or gas). For such a system one can define a porosity which is simply the ratio of the total volume occupied by the voids V_S to the total volume of the medium:

$$n = \frac{V_S}{V_T}. \tag{2.8}$$

Porosity can be determined experimentally using the relationship

$$n = 1 - \frac{\rho_\beta}{\rho_\gamma} \tag{2.9}$$

where ρ_β is the bulk density of a dry rock sample and ρ_γ is the density of the soil grains comprising the sample (Norton and Knapp, 1977). The ratio of the densities is the fraction of the total volume of the sample that is solid, hence its simple relationship to porosity.

The total porosity of a rock can be divided into three different types (Norton and Knapp, 1977). These are flow porosity, diffusion porosity and residual porosity. Flow porosity comprises the well-connected pores and fractures that allow circulation of groundwater, hence advective transport of solutes. Diffusion porosity comprises the poorly connected, smaller pores and fractures in which diffusion is the predominant transport method. Finally, residual porosity comprises those pores not included in the two other types of porosity. Residual porosity is usually predominant so advection and diffusion of solutes in a porous medium is difficult.

The ability of interstitial fluid to flow through the matrix depends on n and particularly on the permeability k which depends on the type and number of connections between pores and also pore size and shape. It is difficult to define permeability mathematically because of its dependence on all these factors but it can be measured experimentally with relative ease.

2.2.2 Behaviour of Porous Media during an Intrusive Event

Although structural changes occur in the country rock during a magmatic intrusion, one of the most important processes that causes variations in the flow pattern and chemical content of the groundwater is a major temperature perturbation. It is assumed here that stresses in the country rock which build up prior to emplacement of the magma are released when the country

rock fails and then accommodates the influx of magma. An increase in the temperature of the groundwater enables minerals to dissolve and be carried away by convection. Once the mineral-rich water cools sufficiently, at some distance from the magma, its load precipitates. Modelling of this hydrothermal system may therefore give clues as to the probable location of mineral deposits.

The real physical behaviour of a porous rock under a high temperature gradient is complex. The configuration of the solid matrix is subject to change given increasing fluid pressure. In return, changes in matrix configuration produce changes in permeability which often substantially increase fluid velocities.

Freeze and Cherry (1979) characterize the stresses in a porous medium in mechanical equilibrium by considering in it a virtual horizontal plane. The total stress applied to the plane is that exerted by the weight of the water and rock above it. This is balanced by fluid pressure and also by the strength of the solid matrix or effective stress. To keep the rock in equilibrium, a decrease in effective stress must be accompanied by an increase in fluid pressure and *vice versa*. However, in an intrusive system, the predominant event is an increase in fluid pressure caused by the large temperature perturbation. This means that the rock opposes the weight upon it with too large a stress so that equilibrium is no longer present and permanent deformation occurs. This may be in the form of fracturing or a rearrangement or reorganizing of matrix particles. A small pressure gradient in the fluid set up by the sudden opening of fractures may cause increases in flow velocity. This effect (in some cases due to seismic pumping) is usually negligible in comparison to the convection caused by thermal perturbations.

In general, tectonic stresses, such as those which cause seismic pumping, are negligible and are not modelled in this thesis. Other effects of the heat of an intrusive event on the country rock is metamorphism which breaks down existing minerals and causes the formation of new mineral assemblages. The effect on permeability and porosity may be substantial but it is not possible at this stage to include the detailed chemistry of such changes in the modelling.

It is interesting to look at the failure criteria of a porous medium in order to estimate the amount of fracturing that one may expect in a given situation. Norton (1990) discusses a simple criterion which involves the balance between confining pressure exerted by the walls of a pore on the fluid p_c, the tensile strength of the walls t and the fluid pressure p_f - quantities similar to

those introduced in the previous paragraph. The criterion for failure is

$$p_f > p_c + t. \tag{2.10}$$

A typical situation in which this might occur is if the fluid is initially in equilibrium with the regional hydrostatic pressure. If it is then locally confined to a group of pores and its temperature raised, the pressure will increase until it reaches p_c. A further increase is required in order to overcome the tensile strength of the rock, whereafter fracturing will occur. Additional deformation may occur due to the pressure gradient set up between the confined fluid and the surrounding fluid, still at the regional hydrostatic pressure.

Fracturing occurs almost instantaneously although elastic deformation may take place over some time preceding this.

2.2.3 Groundwater Flow

The flow of groundwater can be modelled with the same equations of motion that are used for magma, although the fluid properties will have drastically different values (*FLOTRAN* Theory Manula, 1997). Only a small change to one equation (the momentum equation) is needed in order to model the resistance offered by a porous medium to groundwater flow. Before embarking on the detailed description presented in the next chapter, it is of interest to take a brief look at the traditional ways of modelling groundwater flow.

Darcy's Law is used to predict the specific discharge through an aquifer. It is an empirically derived law based on the evidence that discharge is proportional to the hydraulic gradient in the fluid and is given by

$$u = -K\frac{dh}{dl} \tag{2.11}$$

where u is the specific discharge, dh/dl is the hydraulic head and K is the hydraulic conductivity. K is dependent on both fluid and solid properties. To separate the two dependencies we write

$$K = \frac{\rho g \kappa}{\mu} \tag{2.12}$$

where ρ is the fluid density, g is the acceleration due to gravity, κ is the permeability of the porous medium and μ is the fluid viscosity. Properties of the solid matrix are now wholly represented by the permeability. Norton and Knapp (1977) give the following estimate of

fracture-related permeability:

$$\kappa = \frac{ad^3}{12} \tag{2.13}$$

where a is fracture abundance or density (in units of inverse length) and d is fracture aperture (in units of length).

Treatment of fluids with Darcy's Law requires care. Because the exact flow path of each fluid particle is not being calculated (this would be practically impossible), the fluid is treated as a homogeneous substance whose flow differs from that of an unconfined fluid by virtue of the resistance offered by the solid matrix in the real physical system. Darcy's Law can be used, provided the flow through the smallest volume considered can be treated with the law's averaging approach. This strategy ignores the exact paths followed by individual fluid particles and looks at the average flow pattern. The smallest volume to which the law is applicable, also called the critical representative elementary volume, is usually extremely small and its size is dictated by the properties of the solid matrix. Consideration of volumes is important when using a finite element model, as generation of elements smaller than the critical representative elementary volume, such as may happen in high gradient areas, may lead to inaccurate results.

Determination of the flow regime that groundwater can be expected to adopt in a particular situation is again made with the Rayleigh Number. Turcotte and Schubert (1982) present a modified version of the Rayleigh Number given in (2.7) above. The number is derived by considering a saturated porous medium with a vertical temperature gradient just high enough to bring on convection. This means that the degrees of freedom of the fluid can be written in terms of small perturbations from the purely conductive solution. This allows the governing equations to be simplified to such an extent that an analytical solution can be found for the simple problem studied (thermal convection in a saturated porous medium between two impermeable isothermal boundaries). The Rayleigh Number is derived easily from the analytical solution and is given by (Turcotte and Schubert, 1982)

$$Ra = \frac{\kappa g \beta d \rho^2 c_p \theta}{\mu k}. \tag{2.14}$$

All symbols have the same meaning as in (2.7). Note that d is no longer to the third power.

For the physical system described above, there is a minimum Ra for the onset of convection.

This is $Ra = 4\pi^2$. Given this value, (2.14) can be rearranged to give the minimum required temperature gradient for convection in a porous medium:

$$\frac{dT}{dz} = \frac{4\pi^2 \mu k}{\kappa g \beta d^2 \rho^2 c_P} \tag{2.15}$$

where z is the vertical dimension. For the fluid properties used in the models of this work (see **Chapter 5**) a minimum intial temperature gradient of 0.884 °C.m^{-1} is obtained. Over a vertical distance of 1 km, the thickness of the most of the country rock models used, the average temperature difference would have to be 884 °C. Since the initial temperature of the magma is 1000 °C, and the top country rock surface is about 20 °C, the temperature difference is 980 °C. This is sufficient gradient for convection to occur yet not for turbulent flow to develop.

Chapter 3

Equations Governing Magma and Groundwater Flow

For this thesis, *FLOTRAN* is used to solve numerically the time dependent, thermal equations of motion for magma in an enclosed chamber and the groundwater in the country rock surrounding it. The velocity and pressure distributions are found by solving the Navier-Stokes equations and the temperature distributions are found by solving an equation derived by forcing energy conservation. Detailed derivations of these equations are given in **Appendix 1**.

3.1 Magma Flow

The Navier-Stokes equations are obtained by combining the constitutive equation defining the components of the stress tensor (equation (a1.24), **Appendix 1**)

$$\tau_{ij} = -p\,\delta_{ij} + \mu(u_{i,j} + u_{j,i}) \qquad i, j = 1, 2, 3 \tag{3.1}$$

(where p is the hydrostatic pressure, μ is the fluid viscosity and u_i is the ith component of the fluid velocity) with the momentum equation (equation (a1.12), **Appendix 1**)

$$\rho u_{i,t} + \rho u_{i,j} u_j = \rho g_i + \tau_{ij,j}. \tag{3.2}$$

(The summation convention, which operates on indices appearing more than once in a single term, is always used in this work unless otherwise stated. A comma followed by an index

denotes differentiation of the preceding expression with respect to the variable represented by that index.) Substitution of (3.1) into (3.2) gives

$$\rho u_{i,t} + \rho u_{i,j} u_j = \rho g_i + [-p\,\delta_{ij} + \mu(u_{i,j} + u_{j,i})]_{,j}. \tag{3.3}$$

Distributing the main differentiation on the right-hand side to each term in brackets and swapping the order of differentiation in the last term gives

$$\rho u_{i,t} + \rho u_{i,j} u_j = \rho g_i - p_{,i} + \mu(u_{i,j})_{,j} + \mu(u_{j,j})_{,i}. \tag{3.4}$$

Expanding the second term on the left-hand side with the product rule and using the incompressibility constraint to drop one of the resulting terms (and the last term on the right-hand side) gives

$$\rho u_{i,t} + \rho(u_i u_j)_{,j} = \mu(u_{i,j})_{,j} + \rho g_i - p_{,i}. \tag{3.5}$$

The incompressibility constraint (introduced in **Appendix 1**) is

$$u_{i,i} = 0. \tag{3.6}$$

and is a consequence of the assumption that the density of a fluid element does not change appreciably with time. This assumption is valid for most liquids.

Equation (3.6) is in fact obtained from the continuity equation:

$$\rho_{,t} + (\rho u_i)_{,i} = 0 \tag{3.7}$$

(equation (a1.4), **Appendix 1**).

FLOTRAN uses the full version of the continuity equation rather than the incompressibility constraint to maximise the accuracy of non-isothermal models in which the density varies with temperature.

The Navier-Stokes equations and the continuity equation yield numerical solutions to pressure and velocity. A further equation is needed to compute a temperature distribution. This equation is supplied by the principle of the conservation of energy, which is expressed by

$$\rho e_{,t} + \rho u_k e_{,k} = \tau_{ij} u_{j,i} - q_{j,j} \tag{3.8}$$

(equation (a1.32), **Appendix 1**) where e is the internal energy per unit volume. To transform

(3.8) into an equation expicitly dependent on temperature we employ the caloric equation of state $e = c_V T$ where c_V is the specific heat at constant volume. The heat flux q is given by Fourier's Law

$$q_j = -kT_{,j} \tag{3.9}$$

where k is the thermal conductivity. Accordingly (3.8) can be re-written as

$$\rho(c_V T)_{,t} + \rho u_k (c_V T)_{,k} = \tau_{ij} u_{j,i} + (kT_{,j})_{,j}. \tag{3.10}$$

Substituting the constitutive equation gives rise to a pressure term which is eliminated when the incompressibility constraint is applied. The viscosity term that also arises is negligible for low velocities (Knudsen and Katz, 1958). Because of its high viscosity, magma flows very slowly (for the models in this work, maximum velocities of a few millimetres per second are obtained); this factor and the retarding effect of a porous medium on the flow of groundwater, justifies the decision to ignore this term. One thus obtains the slightly simpler energy equation

$$\rho(c_V T)_{,t} + \rho u_k (c_V T)_{,k} = k(T_{,j})_{,j} \tag{3.11}$$

where k is considered constant (see **Chapter 2**).

3.2 Porous Media Flow

Modelling the flow of water through a porous medium requires, like the magma, special treatment of the equations of motion. A porous medium can be defined as a material consisting of a solid matrix containing many small cavities or pores. If the pores are evenly dispersed and well connected it is possible for a fluid to flow large distances through the matrix. Actual paths followed by individual fluid particles are extremely tortuous but the pattern of the overall (average) flow is nonetheless relatively simple and can be modelled to a good degree of accuracy by incorporating into the usual equations a term reflecting the resistance offered by the matrix to the flow. *FLOTRAN* adopts this approach, which it implements as follows.

A hydrostatic pressure gradient exists in any fluid under the influence of gravity which does not cause a fluid in thermal equilibrium to move. Any additional pressure gradient may drive the fluid into motion. This motion will be resisted by the gradient of the fluid's viscous stresses

(a quantity also in units of pressure).

Consider for example a single pore in the matrix of a porous medium. If the pore has width δ and the interstitial fluid has velocity components u_i (i = 1, 2, 3) and viscosity μ, then the viscous stresses in the fluid are proportional to $\mu u_i/\delta$ since

$$\tau_{ij} \propto \mu(u_{i,j} + u_{j,i}). \tag{3.12}$$

Thus the gradient of the stresses must be proportional to $\mu u_i /\delta^2$ and to the driving pressure gradient, i.e.

$$p_{,i} \propto -\frac{\mu u_i}{\delta^2}. \tag{3.13}$$

(The negative sign shows that the gradients are in opposite directions.) It turns out experimentally that the exact relationship is of the form

$$p_{,i} = -\frac{\mu}{\kappa} u_i. \tag{3.14}$$

Here κ is the permeability of the medium as defined by Darcy's Law. The permeability depends on the arrangement and size of the pores (see **Chapter 2**) and is a measure of the ability of the medium to conduct fluid. It has units of length squared and can take any value from 10^{-13} cm^2 for sandstones to 10^{-5} cm^2 for karstic limestones (Freeze and Cherry, 1979). When modelling porous media, *FLOTRAN* simply adds the pressure gradient expression in (3.14) to the existing term in the momentum equation.

Bear (1972) performs a rigorous derivation of flow equations in porous media. He models porous media as systems of flow channels and junctions. Assuming there is no flow normal to the walls of the channels, the channels can be replaced by fixed bundles of stream lines that occupy the same volume as the channels. Equations of motion can be derived for a single small channel, and then averaged over the channel cross-section, thus representing the channels as thin lines. (This averaging procedure can account for the parabolic fluid velocity cross-section typical in laminar channel flow). The equations of flow of the group of channels in a representative volume element are then averaged to arrive at a general description of volumetric flow though a porous medium. The equation for specific discharge (volume of water passing through a given

surface per unit time) is then:

$$u_i + \frac{\rho B}{\mu} u_{i,t} = -\frac{\kappa}{\mu}(p_{,i} + \rho g_i) \tag{3.15}$$

where u_i is the ith component of the Darcy velocity or specific discharge and B is the conductance (a function of the average flow channel cross-section). Bear (1972) drops the second term on the left-hand side because the inertial forces causing the acceleration represented in that term are usually much smaller than the viscous forces. Thus

$$u_i = -\frac{\kappa}{\mu}(p_{,i} + \rho g_i). \tag{3.16}$$

Since the gravity term already appears in the momentum equation, it can be seen that a pressure term the same as in (3.14) remains and is the only type of term that can be added to the momentum equation in order to model porous media flow. The result is an equation that accounts for both viscous stresses in the fluid and the resistance imposed by the solid matrix:

$$\rho u_{i,t} + \rho(u_i u_j)_{,j} = \mu(u_{i,j})_{,j} + \rho g_i - (p_{,i} + \frac{\mu}{\kappa} u_i). \tag{3.17}$$

FLOTRAN requires the value for the permeability to be supplied.

Permeability in geological settings is seldom homogeneous. Heterogeneity can be included in *FLOTRAN* models by meshing each area of the model that has uniform permeability separately. Thus, as the solution algorithm moves through the problem domain, the value of k corresponding to the current node or element in the finite element mesh will be substituted into the momentum equation. Single-direction permeability (that allows flow in one dimension only) and general anisotropic permeability (that allows permeability of a specified magnitude in each dimension) can also be modelled although the momentum equation becomes slightly more complicated.

3.3 Treatment of the Equations by *FLOTRAN*

The manner in which *FLOTRAN* solves the governing equations for fluid flow involves Finite Element Methods which will be discussed in detail in the following chapter. The three equations are solved (sequentially) by the same set of computer instructions. This is possible because of their common structure. This common structure is most easily displayed by writing

each equation in the form

$$(\rho\phi)_{,t} + (\rho\phi u_j)_{,j} = (\Gamma_\phi \phi_{,j})_{,j} + S_\phi \tag{3.18}$$

where ϕ is a mass specific scalar, Γ_ϕ a diffusion coefficient and S_ϕ a source term. **Table 3.1** explains how to identify these symbols in each case with those of the governing equations of fluid motion. It is important to understand that the momentum equation is treated by constructing a separate general scalar equation (as given in (3.18)) for each component of the fluid velocity.

	ϕ	Γ_ϕ	S_ϕ
Continuity Equation	1	0	0
Momentum Equations	u_1	μ	$\rho g_1 - p_1$
	u_2	μ	$\rho g_2 - p_2$
	u_3	μ	$\rho g_3 - p_3$
Energy Equation	$c_P T$	κ	0

Table 3.1 Correspondence between the general scalar transport equation and the five governing equations.

For porous media, the terms $\frac{\mu}{\kappa}u_1$, $\frac{\mu}{\kappa}u_2$ and $\frac{\mu}{\kappa}u_3$ should be added to the three respective pressure terms in the momentum equations.

Chapter 4

Numerical Solution of the Governing Equations by Finite Element Methods

The Navier-Stokes equations have analytical solutions only for a very limited number of simple problems. Certainly no analytical solutions exist for conductive and convective heat transfer and fluid flow in a magma chamber of arbitrary shape, nor for flow in the surrounding country rock. The only option in such cases therefore is to look for numerical solutions which describe the state of the system at various predetermined stages in its evolution.

Finite Element Methods are perhaps the most extensively used methods for solving differential equations numerically. *FLOTRAN* uses the Galerkin Finite Element Method and the Streamline Upwind Method to solve the Navier-Stokes equations, the continuity equation and the energy equation. This chapter describes in detail these methods and their application.

4.1 Finite Element Analysis

Finite Element Methods have traditionally been used as engineering tools to assist in such problems as stress analyses of rigid structures. More recently they have been applied to a wider range of problems, including those involving fluids.

A typical problem in engineering or physics has a number of state variables whose values at a particular time, or times, are desired. These variables are usually related to a set of governing differential equations that have no known analytical solution and must be solved with numerical

techniques. Such techniques convert the governing equations (which are defined continuously) to a set of discretely defined algebraic equations.

Deciding on a mathematical model, i.e. formulating the governing equations, requires abstraction from reality. One must model only those aspects of the problem that contribute significantly to solution accuracy. Including parts of the problem that further refine the solution can be done later if required. A short, self-explanatory synopsis of the process of finite element analysis is shown in **Figure 4.1** (Bathe, 1996).

The primary finite element technique used in this work is Galerkin's method (Wang and Anderson, 1982) which is similar to a variational principle. The aim of such a principle is to minimize a physical quantity over the problem domain. Galerkin's method minimizes instead the error arising from assuming an arbitrary form of solution to the governing partial differential equation. In the governing equations of fluid flow, most terms can be treated satisfactorily with Galerkin's method. There are some terms, however, for which the Galerkin method may produce spurious results in parts of the problem domain. For these terms an Upwind method is used (Rice and Schnipke, 1984).

4.2 Representing the Problem Domain

Consider any differential equation that describes the time evolution of some scalar variable u in a well-defined, finite area in two-dimensional Euclidean space referred to by a set of Cartesian coordinate axes. The derivatives in the equation may be taken with respect to one or a combination of the two Cartesian coordinates, and time.

A complete steady state solution to such an equation consists of a value of u at each point (x, y) in the problem domain. In a numerical solution, however, a lower degree of accuracy is tolerated. A finite number of sample points from the problem domain is selected and the equations are solved at those points only. Thereafter, interpolation techniques are used to estimate the values at intermediate points. This provides an approximate solution over the entire problem domain.

Herein lies the first major problem encountered in practical numerical solution techniques.

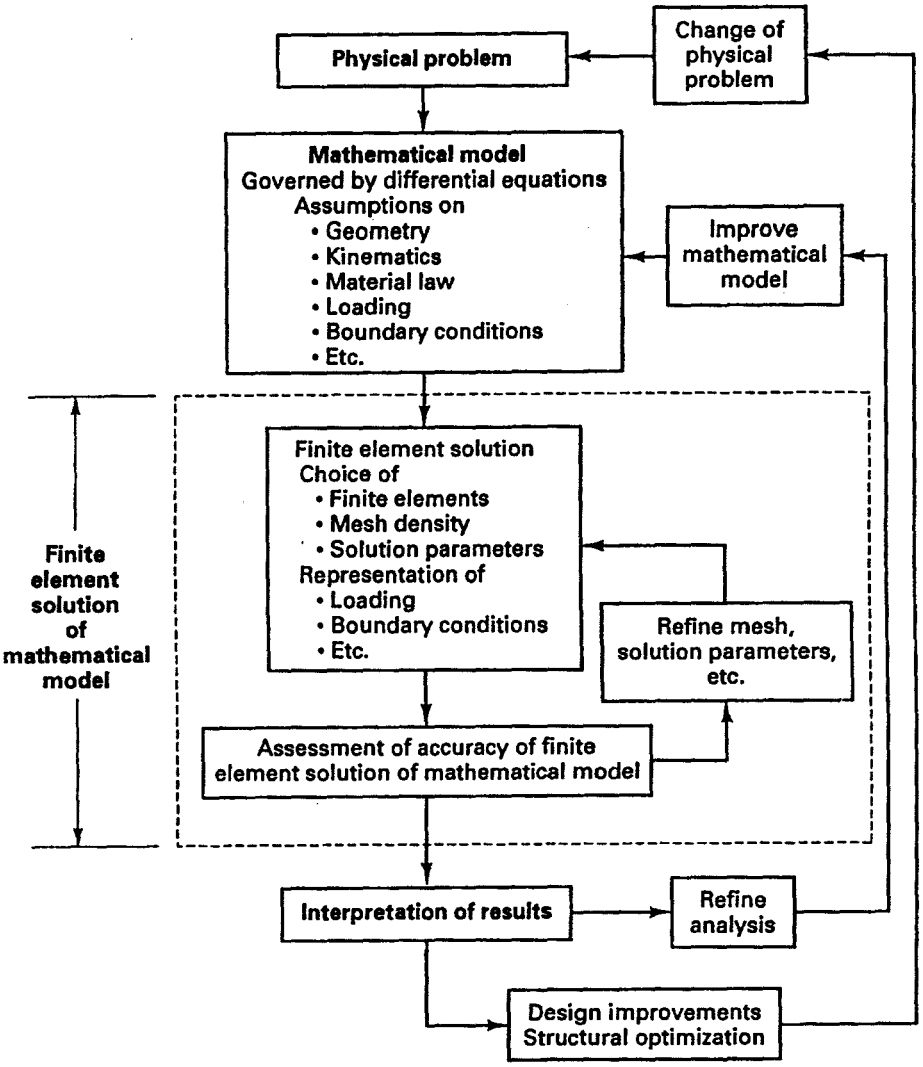

Figure 4.1 A detailed graphical description of the process of finite element analysis introduced in section 4.1.

Which points in the problem domain does one choose? There are several factors that determine this decision. These will be considered later in the discussion. For the moment, the typical form of a finite element mesh, which is the discrete representation of a continuous physical problem domain, is considered. The points (nodes) in the problem domain one wishes to model are connected in such a way as to form the vertices of a system of small, tightly fitting areas (or volumes in a three-dimensional domain) called elements. These are usually triangular

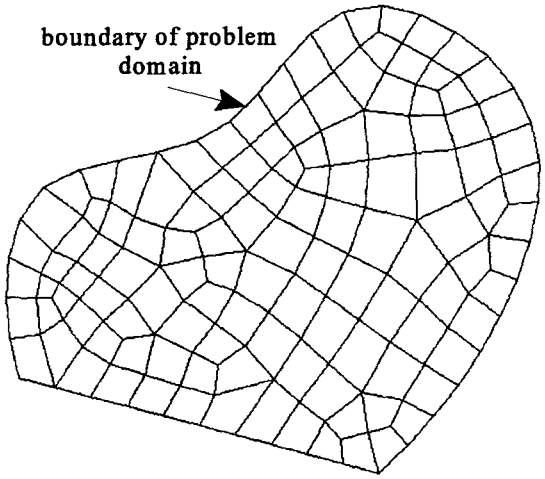

Figure 4.2 A finite element mesh with quadrilateral elements.

or quadrilateral in shape. **Figure 4.2** shows an example of a two-dimensional finite element mesh with quadrilateral elements.

4.3 Representing a Solution

The process of solving for a variable using finite element methods requires manipulation of an initial (often arbitrary) trial solution represented by a set of nodal values. An interpolation function is constructed for each node enabling the discrete trial solution to be transformed into a piecewise continuous solution. For the example described in the previous section, the trial solution could be expressed generally in terms of the nodal solutions u_L and their corresponding interpolation functions $N_L(x,y)$:

$$\hat{u}(x,y) = \sum_{L=1}^{M} u_L N_L(x,y). \tag{4.1}$$

M is the total number of nodes in the problem domain. Simple linear interpolation produces functions of the form shown in **Figure 4.3**. The complex or patch of elements surrounding node L is shaded. N_L is zero along the boundary of the patch and at all points exterior to it. Within the patch, it increases in a linear, piecewise fashion to a maximum of 1 at node L. An algebraic

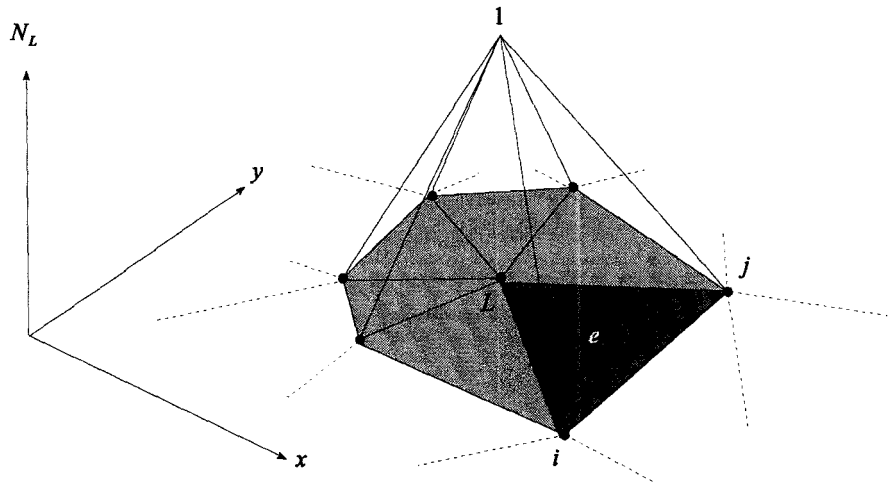

Figure 4.3 The shape of the linear interpolation function $N_L(x,y)$.

expression for $N_L(x,y)$ over one element (e) in the patch about node L is

$$N_L^e(x,y) = \frac{1}{2A^e}\left[(x_i y_j - x_j y_i) + (y_i - y_j)x + (x_j + x_i)y\right] \tag{4.2}$$

where L, i and j are the three nodes (in anticlockwise order) belonging to element e and A^e is the area of the element.

The solution of the problem is found by determining the u_L's in equation (4.1).

4.4 Perfecting the Trial Solution

The Galerkin Finite Element Method and Monotone Streamline Upwind Method are used by *FLOTRAN* to find an approximate solution to the governing differential equations. The Galerkin Method is equivalent to a variational principle whereby a physical property of the system such as energy dissipation is minimized. Instead of using a physical property, however, the Galerkin Method uses the partial differential equations themselves, manipulated to form an expression (called the residual) which is forced to vanish in order to secure a close approximation to the exact solution.

Each point in the problem domain has its own value of the residual. To achieve an exact

solution, the residual would have to be brought to zero everywhere in the problem domain. However, only a finite set of residual values can be handled.

A convenient way of discretizing the residual is to integrate it over the patch of elements around each node. In this way each node produces a single value representing the total contribution of the parts of the problem domain in its neighbourhood. The disadvantage of such a method is that, even if a particular nodal residual is brought to zero, this does not mean that the actual residual is zero over the entire element patch. Hence it is important that elements are small since the residuals then represent a more accurate generalization of the actual residual.

The initial trial solution will usually produce very poor residual values. In order to minimise these to below a prespecified value, a number of passes through all the nodes in order to adjust the trial solution is necessary. This iterative process is the most common method used to achieve a solution once the governing equations have been discretized. The following two sections describe in detail the steps followed.

4.5 Discretizing the Governing Equations

Consider the general scalar transport equation introduced in **Chapter 3**:

$$(\rho\phi)_{,t} + (\rho\phi u_j)_{,j} = (\Gamma_\phi \phi_{,j})_{,j} + S_\phi \tag{4.3}$$

where t is time and j = 1, 2, 3, corresponding to x-, y- and z-components respectively. ϕ represents the variable being solved (e.g. temperature or a component of the velocity). The first term on the left hand side (transient term) is solved using a finite difference technique while the second term on the left hand side (advection term) is solved with the Monotone Streamline Upwind Method and the terms on the right hand side (diffusion and source terms respectively) are solved with the Galerkin Method.

4.5.1 Diffusion and Source Terms

For steady state flow dominated by diffusive transport, the terms on the left hand side of the general scalar equation fall away, giving

$$0 = (\Gamma_\phi \phi_{,j})_{,j} + S_\phi . \tag{4.4}$$

This expression can be used as a residual to test the accuracy of the trial solution of ϕ. As described above, the total contribution to the residual from the patch of elements around each node must be found. This, for node L in a two-dimensional problem is

$$\int \left\{ (\Gamma_\phi \phi_{,j})_{,j} + S_\phi \right\} N_L(x,y)\, dA = 0 \tag{4.5}$$

where $L = 1, 2, ..., M$ and $j = 1, 2$. The interpolation function $N_L(x,y)$ has been used here to ensure that the integration, which is done over the entire problem domain, will be zero for points exterior to the patch of elements about node L. However, instead of unnecessarily integrating over the entire problem domain for each node, the integration can be done over each element separately. In this way, the integrals that do not contribute to the equation for a particular node can be ignored, hence equation (4.5) becomes

$$\sum_{e=1}^{E} \left[\int \left\{ (\Gamma_\phi \phi_{,j})_{,j} + S_\phi \right\} N_L(x,y)\, dA^e \right] = 0 \tag{4.6}$$

for $L = 1, 2, ..., M$. A^e denotes the area of element e and E is the total number of elements in the problem domain. For any particular node, the integrations in the above expression over elements not in the patch about that node are zero. In fact a single element will only contribute to three or four of the above M equations depending on whether it is triangular or quadrilateral. We now consider a single elemental integration as it appears in brackets in (4.6).

The use of a piecewise continuous trial solution implies that first order derivatives of ϕ may be discontinuous in some places, resulting in poorly defined second order derivatives. Hence the second order derivatives in (4.6) must be transformed to first order. This is done by integrating by parts to give

$$\int \Gamma_\phi N_{L,j} \phi_{,j}\, dA^e - \int N_L \Gamma_\phi (\phi_{,1} + \phi_{,2})\, dS^e - \int N_L S_\phi\, dA^e = 0 \tag{4.7}$$

where S^e is the perimeter of element e and L is any node of e.

Discretizations like those of (4.1) are now needed. They are

$$\phi = \sum_{L=1}^{M} \phi_L N_L(x,y), \quad \Gamma_\phi = \sum_{L=1}^{M} \Gamma_{\phi_L} N_L(x,y), \quad S_\phi = \sum_{L=1}^{M} S_{\phi_L} N_L(x,y). \tag{4.8}$$

Substituting these into (4.7) gives, after some manipulation, the matrix equation

$$[K^e]\{\phi^e\} = \{F^e\}. \tag{4.9}$$

Since only three of the total M nodes contribute to it (if the elements are triangular), $[K^e]$ is 3×3 and $\{F^e\}$ and $\{\phi^e{}_L\}$ are 3×1. All element matrix equations such as these are gathered to form a global matrix equation. This is equivalent to doing the summation in (4.6). During the process of assembly it is found that all terms in the element perimeter integral in (4.7) cancel except those including element edges that define the boundary of the problem domain. These terms make up the matrix $\{F^e\}$. The components of this matrix contain first order spatial derivatives of the trial solution and so provide a way of enforcing gradient boundary conditions. (Such boundary conditions that are enforced automatically by the solution method being used are called natural boundary conditions.)

The conductance matrix $[K^e]$ and source vector $\{F^e\}$ need only be constructed once before the solution process begins.

4.5.2 Transient Term

In solving parts of a differential equation one may choose to use finite difference or finite element techniques or both. Finite difference methods for transients are simpler in that the problem domain is represented by discrete points without elements; therefore no attempt is made to produce a time solution to the continuous mathematical model, but rather to the discretized model only.

The simplicity of the transient term in the scalar equation allows it to be treated with a simple backward difference. This is constructed by a discretization process which uses a Taylor Series expansion that is a function of the internodal spacing. In the time domain, internodal spacing is just the time interval (in the physical system) between consecutive applications of the main solution routine.

Consider, for instance, an arbitrary time step n and its immediate predecessor n-1. The

Taylor Series expansion for the value of the general scalar ϕ at time n is

$$\phi_n = \phi_{n-1} + \left.\frac{\partial \phi}{\partial t}\right|_n \Delta t + \frac{1}{2}\left.\frac{\partial^2 \phi}{\partial t^2}\right|_n \Delta t^2 + \ldots \tag{4.10}$$

where Δt is the time interval between times n-1 and n. This gives

$$\left.\frac{\partial \phi}{\partial t}\right|_n = \frac{\phi_n - \phi_{n-1}}{\Delta t} + O(\Delta t^2) \tag{4.11}$$

to first order approximation. The error, denoted by O, is of order Δt^2.

FLOTRAN uses an expression for the time derivative that is a combination of three backward differences involving time steps n, n-1, and n-2 and the three intervals associated with them, giving

$$\left.\frac{\partial \phi}{\partial t}\right|_n = \frac{\phi_{n-2} - 4\phi_{n-1} + 3\phi_n}{2\Delta t} + O(\Delta t^2). \tag{4.12}$$

Since ϕ_n is a quantity that must be solved at the current time level, it is unknown and its coefficient augments the conductance matrix of the global matrix equation. The remaining terms on the right hand side, having been calculated during previous time levels, are known and contribute to the source vector.

4.5.3 Advection Term

The use of Galerkin's Method to solve the advection term is known to produce spatial oscillations in the solution (Brookes and Hughes, 1982). Patankar (1980) describes the source of the problem in detail.

Upwind differencing methods tend to produce better results. These methods make use of forward and backward differences that are dependent on the direction of heat or mass flow through the nodes. Their disadvantage is the production of artificial diffusion, since backward and forward differences are only accurate to first order compared to the second order accuracy of central differences used in the Galerkin Method.

The method described in this section is the Monotone Streamline Upwind Method, used by *FLOTRAN* to solve the Navier-Stokes advection term and is described in detail by Rice and Schnipke (1985). The purpose of the method is to approximate first order derivatives on an element by taking a finite difference along a streamline running through the element rather than between two nodes. The streamline chosen is that which passes through the element's

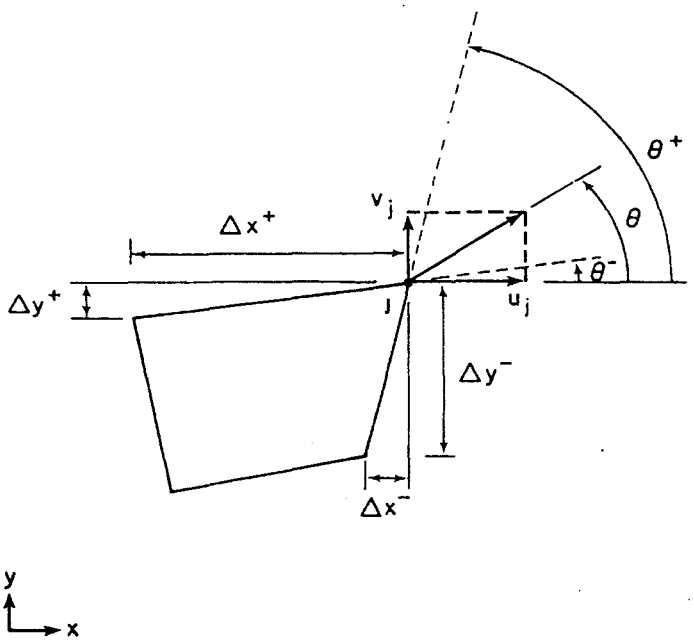

Figure 4.4 A quadrilateral element showing the quantities required to test the top right node (node *j*) for downwindedness.

downwind node. The downwind node is the node whose velocity vector is directed out of the element, which means that fluid passing through the downwind node must emanate from inside the element. **Figure 4.4** (Rice and Schnipke, 1985) shows a quadrilateral element whose top right node (labelled *j*) is to be tested for downwindedness. With reference to this diagram, the criteria for a node being downwind are

$$\tan\theta^- \le \tan\theta \le \tan\theta^+. \tag{4.13}$$

Re-writing in terms of ratios gives

$$\frac{\Delta y^+}{\Delta x^+} \le \frac{v_j}{u_j} \le \frac{\Delta y^-}{\Delta x^-} \tag{4.14}$$

where u_i and v_i are the x- and y-components of the fluid velocity respectively.

These two inequalities are easy to test and the downwind node(s) in the element can be found quickly. *FLOTRAN*'s use of these criteria is somewhat different. It determines first whether the flow through each edge is inward or outward. It then selects the node attached to edges with outward flow only.

The streamline passing through the downwind node must be considered next. It will enter the element upstream of the downwind node through an element edge. An expression for the

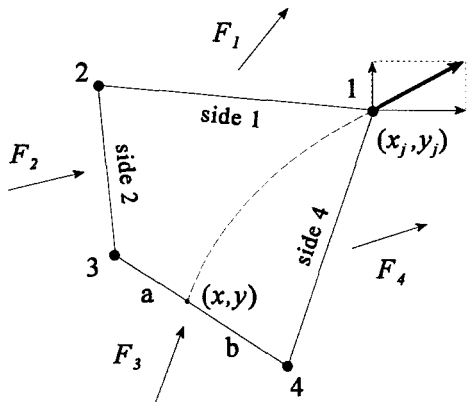

Figure 4.5 Flow rates through the edges of a quadrilateral element with downstream node $j = 1$.

length of this streamline segment is required in order to construct the finite difference that will approximate the advection term. To find the length, the coordinates of the point of entry of the streamline into the element must be calculated, then a simple linear distance formula used as a length estimate. Calculation of the point of entry is done by considering the flow rates through all four element edges. Consider **Figure 4.5** in which an element is shown with the streamline through the downwind node (1) and the flow rates through the edges (F_1, F_2, F_3 and F_4). The streamline enters the element through side 3 splitting it into two segments a and b respectively. All fluid passing through segment b must pass through side 4 since by definition no fluid can cross streamlines; therefore $F_4 = F_b$. The quantity F_b can be expressed in terms of the ratio of b to the total length l_3 of side 3:

$$F_4 = \frac{b}{l_3} F_3 . \tag{4.15}$$

Since the x-components of the lengths appearing above have the same ratio as the lengths themselves, we have

$$F_4 = \frac{b_x}{l_{3_x}} F_3 . \tag{4.16}$$

Re-writing the lengths in terms of their endpoints gives the following expression for the

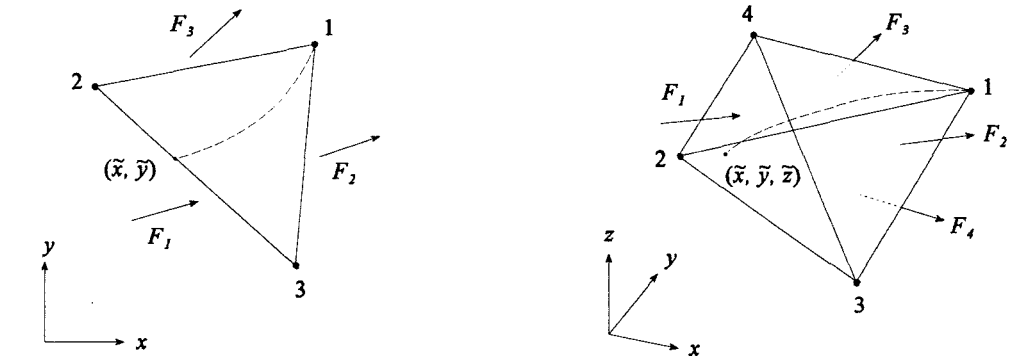

Figure 4.6 (a) Triangular and (b) tetrahedral elements showing the streamline that passes through the downwind node (node 1 in both cases) and its upstream point of entry into the element. Mass flow rates through element edges or faces are also shown.

x-coordinate of the streamline entry point in terms of known quantities:

$$\tilde{x} = x_4 - \frac{F_4}{F_3}(x_4 - x_3). \tag{4.17}$$

The expression for the y-coordinate can be derived in the same way and is identical to the above except for the x's which should all be changed to y's.

If the point of entry of the streamline was on side 2, a manipulation of quantities as done above would give a point of entry x-coordinate of

$$\tilde{x} = x_2 - \frac{F_1}{F_2}(x_2 - x_3). \tag{4.18}$$

As before, replacing x's with y's gives the y-coordinate. The value of ϕ at the streamline's point of entry can be derived easily since it will be in the same ratio to the nodal values as the x- and y-coordinates. The resulting functions (one for a side 2 and one for a side 3 point of entry) are of the same form as above. The relative sizes of the fractions F_1/F_2 and F_4/F_3 will indicate which element edge holds the point of entry so that the correct set of equations can be used.

The *FLOTRAN* Theory Manual (1997) describes the above method as applied to a three-dimensional tetrahedral element. In this case, the streamline through the downwind node must enter the element through the face opposite the downwind node. For a two-dimensional

triangular element this is equivalent to the point of entry being on the element edge opposite the downwind node. The coordinates of the point can again be calculated by using ratios of flow rates. For the element pictured in **Figure 4.6(a)** the x-coordinate of the entry point is just (4.18). This can be simplified by substituting the constraint that $F_1 = F_2 + F_3$ to give

$$\tilde{x} = \frac{F_2}{F_1}x_2 + \frac{F_3}{F_1}x_3. \tag{4.19}$$

For a tetrahedral element as shown in **Figure 4.6(b)** we then have

$$\tilde{x} = \sum_{j=2}^{4} \frac{F_j}{F_1}x_j, \quad \tilde{y} = \sum_{j=2}^{4} \frac{F_j}{F_1}y_j, \quad \tilde{z} = \sum_{j=2}^{4} \frac{F_j}{F_1}z_j, \quad \tilde{\phi} = \sum_{j=2}^{4} \frac{F_j}{F_1}\phi_j. \tag{4.20}$$

If the element is sufficiently small, the length Δs of the streamline from point of entry to the downwind node can be taken as the straight line distance between the two points. Thus

$$\Delta s = \sqrt{(x_j - \tilde{x})^2 + (y_j - \tilde{y})^2 + (z_j - \tilde{z})^2} \tag{4.21}$$

where node j is the downwind node.

It is now possible to approximate the advection term in the scalar differential equation. Steady state flow dominated by advection can be described as follows:

$$(\rho\phi u_j)_{,j} = 0 \tag{4.22}$$

for $j = 1, 2, 3$. This can be written in terms of the distance s along a streamline as

$$\frac{d}{ds}(\rho u_s \phi) = 0 \tag{4.23}$$

where u_s is the fluid velocity tangent to the streamline. Treating the above equation as a residual and performing a weighted integration over a single element e gives

$$\frac{d}{ds}(\rho u_s \phi) \int N_L(x,y)\, dA^e \tag{4.24}$$

where it has been assumed that the derivative is constant over the element. This unchanging gradient can be expressed as a simple average in terms of the quantities derived above:

$$\left[\frac{d}{ds}(\rho u_s \phi)\right]^e = \frac{\rho u_{s_j}\phi_j - \rho \tilde{u}_s \tilde{\phi}}{\Delta s}. \tag{4.25}$$

where j again denotes the downwind node. Substituting into (4.25) the expression for $\tilde{\phi}$ in (4.20) results in an equation in terms of the nodal values ϕ_j. This is then substituted into (4.24) and the resulting coefficients of the ϕ_j's contribute to the element conductance matrix.

4.6 Determining Pressure

The Navier-Stokes equations are discretized in order to solve for the three velocity components and the energy equation is discretized to solve for temperature. The remaining governing equation, the continuity equation, must be used to solve for pressure. However, pressure makes no explicit appearance in the continuity equation so a combination of the momentum and continuity equations must be used.

To avoid this, pressure could be eliminated as an unknown. This can be done with methods such as the penalty function method (Hughes et al, 1979) which sets the continuity equation equal to a penalty parameter times the pressure. The result can then be re-written in terms of pressure alone and substituted into the momentum equation to eliminate pressure. Unfortunately, such a method requires all the governing equations to be solved simultaneously, leading to a poorly conditioned conductance matrix in which the diagonal entries do not dominate. Such a matrix causes a significant increase in solution time.

FLOTRAN does not eliminate pressure but instead derives a Poisson pressure equation. This is done by deriving first an expression for the fluid velocity in terms of the pressure gradient using the momentum equation and then substituting the result for the velocity into a discretized continuity equation. Having an explicit equation for pressure allows the governing equations and the pressure equation to be solved sequentially, resulting in well conditioned matrices that are easier to invert (see *FLOTRAN* Theory Manual). The next few sections describe in detail the *FLOTRAN* pressure solving algorithm.

4.6.1 The Velocity-Pressure Coupling Equations

The discretized momentum equation for velocity component i (over element e) can be written

$$[K_i]\{u_i\} = \{F_i\}. \tag{4.27}$$

for $i = 1, 2, 3$. The row of this set of algebraic equations corresponding to node L of element e is given by

$$\sum_{n=1}^{M} K_i^{Ln} u_i^L = f_i^L - \int p_{,i} N^L(x,y)\, dA^e. \tag{4.28}$$

where M is the total number of nodes in the problem domain and L is any node of element e. (Note that indices representing node numbers have been moved to the superscript position so as not to be mistaken for indices representing x-, y- or z-components).

Here the source vector has been expanded into a pressure gradient term and a remaining source term f_i^L which comprises the buoyancy term and the natural boundary conditions, if any. Solving for u_i^L gives

$$u_i^L = \hat{u}_i^L - \frac{1}{K_i^{LL}} \int p_{,i} N^L(x,y)\, dA^e \tag{4.29}$$

where

$$\hat{u}_i^L = -\frac{1}{K_i^{LL}} \left(\sum_{n=1, n\neq L}^{M} K_i^{Ln} u_i^n + f_i^L \right). \tag{4.30}$$

Treating the pressure gradient over the element as constant (a valid simplification when using linear interpolation functions) simplifies (4.29) to

$$u_i^L = \hat{u}_i^L - A_i^L p_{,i} \tag{4.31}$$

where

$$A_i^L = \frac{1}{K_i^{LL}} \int N^L(x,y)\, dA^e. \tag{4.32}$$

Equation (4.31) is the velocity-pressure coupling equation for the ith component of the fluid velocity at node L in terms of the pressure gradient $p_{,i}$.

4.6.2 The Incompressible Flow Pressure Equation

The next step in the process of solving for pressure is to discretize the continuity equation. The following weighted residual is constructed as per the Galerkin Method:

$$\int [\rho_{,t} + (\rho u_i^L)_{,i}] N^L(x,y)\, dA^e = 0 \tag{4.33}$$

where $i = 1, 2, 3$ and L is any node of element e. The time-dependent term is discretized using the same backward difference formulation as the transient term of the general scalar equation. Considering the steady state continuity equation allows us to concentrate on the other term in (4.33) which, when integrated by parts to remove the velocities from the differential operator gives

$$\int \left(\sum_{i=1}^{3} \rho u_i^L\right) N^L dS^e - \int \rho u_i^L (N^L)_{,i} dA^e = 0. \tag{4.34}$$

The summation in the first term represents the total flow rate across the boundary of element e. As with the diffusion terms of the general scalar equation, all those parts of the integration that involve internal element boundaries cancel. The remaining parts serve as a convenient method of specifying flow rate boundary conditions.

The velocity-pressure coupling equations (4.31) are now substituted for u_i^L in the second term of (4.34) to give the pressure equation:

$$\int \rho A_i^L p_{,i} (N^L)_{,i}\, dA^e = \int \rho \hat{u}_i^L (N^L)_{,i}\, dA^e - \int \left(\sum_{i=1}^{3} \rho u_i^L\right) N^L dS^e. \tag{4.35}$$

The u_i^L 's are left in the last term so that flow rate boundary conditions may be specified.

Development of the above system produces an element matrix equation for pressure:

$$[B^e]\{p^e\} = \{g^e\} \tag{4.36}$$

where $[B^e]$ is a conductance matrix and $\{g^e\}$ a source vector. The element matrices are assembled into a global system which is solved for pressure.

4.7 Solving the Discrete System

4.7.1 General Solution Sequence

The sequence of steps followed by *FLOTRAN* in order to solve for velocity, pressure and temperature in a transient thermal problem is shown in **Figure 4.7**. The figure is mostly self-explanatory although some features require emphasis.

The first of these is the two-way coupling of velocity and pressure solutions. Initial guesses for velocity and pressure are first assembled. The velocity distribution is used to construct the conductance matrix and source vector of the momentum matrix equation ("conductance" and "source" here should be taken in the context of section 4.5.1). Because pressure appears explicitly in the momentum equation, its initial guess must be substituted so that it can be treated as a known. In this way, the momentum equation can be solved for its single remaining unknown, velocity. Once the velocity distribution is known, the $\hat{u}_i^L$'s are calculated and used in the construction of the pressure matrix equation which is then solved for pressure. Herein lies the first of the two links between velocity and pressure. The second link appears after the pressure solution is acquired when the velocities are updated using the velocity-pressure coupling equations (4.31).

The algorithm is a "relaxation" procedure. The loop starting from the construction of the velocity matrices and ending in the query about solution convergence may repeat itself many times before the solution stabilizes and the next time step can be tackled. The number of times this global iteration must be performed depends on the complexity of the system and also on the efficiency of the matrix equation solvers.

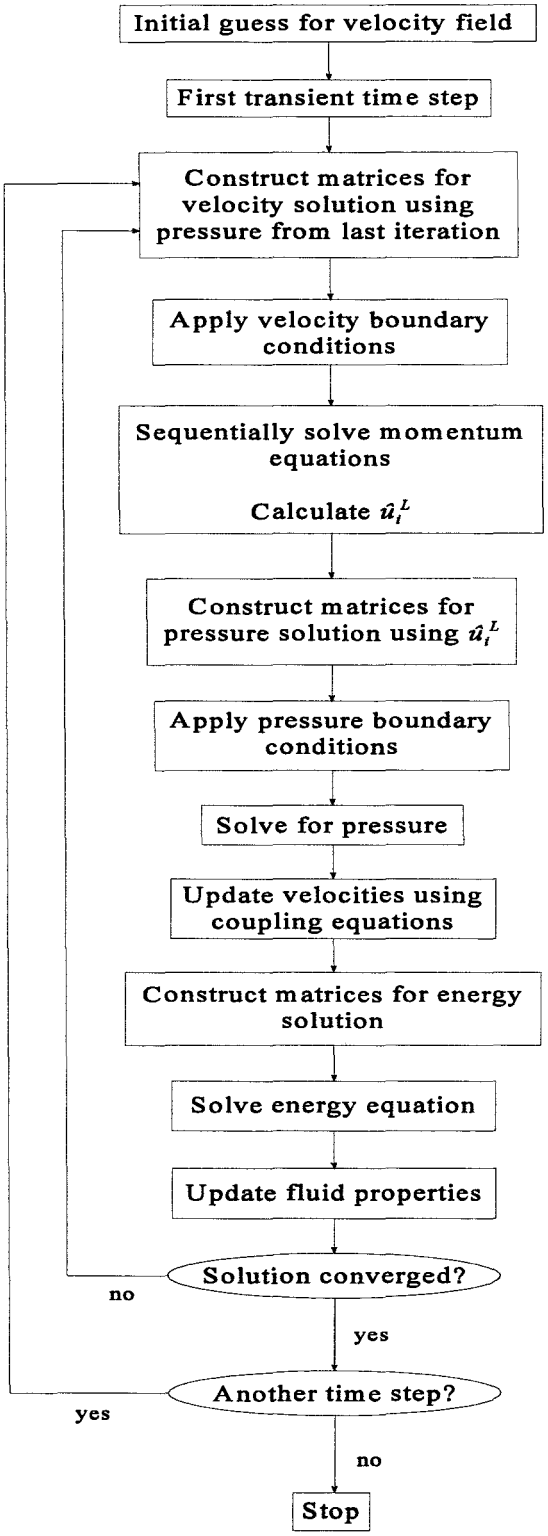

Figure 4.7 Flow chart showing the major steps in *FLOTRAN*'s solution procedure as outlined in section 4.7.1.

4.7.2 The TDMA Matrix Solver

FLOTRAN uses a tri-diagonal matrix method to solve the matrix equations arising from discretization of the governing equations. Wang and Anderson (1982) describe the method which they call the "Thomas Algorithm". It operates on matrices with only subdiagonal, superdiagonal and centre diagonal entries. Entries not falling into these categories are taken to the right hand side of the equation. Their values from the previous iteration are substituted and grouped together with the source terms. What remains on the left hand side is a system of equations with a maximum of three unknowns each. For example, a system of four equations whose coefficients are in tridiagonal form can be written as

$$\begin{aligned} b_1x_1 + c_1x_2 &= f_1 \\ a_2x_1 + b_2x_2 + c_2x_3 &= f_2 \\ a_3x_2 + b_3x_3 + c_3x_4 &= f_3 \\ a_4x_3 + b_4x_4 &= f_4 \end{aligned} \tag{4.37}$$

where the x's are unknowns, the a's are subdiagonal coefficients, the b's are centre diagonal coefficients, the c's are superdiagonal coefficients and the f's are source terms. The first step in the algorithm is to eliminate subdiagonal entries and normalize the coefficients of the centre diagonal entries to 1. The desired end result is

$$\begin{aligned} x_1 + \beta_1x_2 &= y_1 \\ x_2 + \beta_2x_3 &= y_2 \\ x_3 + \beta_3x_4 &= y_3 \\ x_4 &= y_4 \end{aligned} \tag{4.38}$$

Some manipulation of (4.37) and (4.38) would show that for row i,

$$\beta_i = \frac{c_i}{\alpha_i} \tag{4.39}$$

where

$$\alpha_i = b_i - a_i\beta_{i-1} \tag{4.40}$$

and

$$y_i = \frac{f_i - a_iy_{i-1}}{\alpha_i}. \tag{4.41}$$

Once (4.38) is constructed, simple backward substitution of the form

$$x_i = y_i - \beta_ix_{i-1} \tag{4.42}$$

is possible, starting from $i = 4$ or in general $i = n$ where n is the number of equations.

Chapter 5

Model Structure and Control

All the basic equipment necessary to model a transient fluid flow problem has been discussed. The governing equations have been derived and tailored to model magmas and groundwater. A finite element method has been chosen and an algorithm for solution devised. It is fitting now to take a closer look at the actual models used in this work and the software on which they were constructed and run.

5.1 *Ansys* and *FLOTRAN*

The modelling done in this work makes use of the commercial computational fluid dynamics package known as *FLOTRAN* which is part of the *Ansys* finite element analysis software. The first of the most recent suite of *Ansys* products, *Ansys* 5.0, was released in 1992. Since then it has been updated and enhanced several times. Most of the models in this work used versions 5.2 and 5.3, and some used version 5.4.

Ansys offers a wide range of analysis tools. It can perform structural analyses of the following types: static, modal, harmonic response, transient dynamic, spectrum, buckling and nonlinear. Also available are steady state and transient thermal analyses and solution of radiation problems. The electromagnetic analysis section offers two- or three-dimensional static magnetic, two- or three-dimensional static harmonic, two- or three-dimensional transient magnetic, high frequency electromagnetic, far-field electrostatic field and electric circuit

analyses.

FLOTRAN is capable of analysing flow which may be laminar or turbulent, incompressible or compressible, steady-state or transient, and thermal. Version 5.4 also handles multiple species transport.

5.2 The *FLOTRAN* Fluid Element

FLOTRAN supports two fluid elements: one for two-dimensional and one for three-dimensional use. The elements can be used to model only one fluid in a single phase. Modelling of the effect on flow of physical features in the problem domain whose geometry does not appear explicitly in the model (e.g. detailed pore structure) requires the specification of certain element specific properties. The *FLOTRAN* fluid element allows modelling of distributed resistances caused by friction, localized head loss or a porous medium. As discussed previously, a permeability (possibly anisotropic) to be associated with each element must be provided for porous media flow.

The fluid element also supports non-Newtonian viscosity models such as Power Law, Bingham and Carreau models. The Newtonian model however gives one maximum control over the temperature dependent behaviour of viscosity and is the one used for all modelling for the present research (justification for the use of a Newtonian model for magma and groundwater is given in

Chapter 2).

In some of these models, the fluid content of the country rock was ignored and modelled instead as a thermally conducting solid. The *FLOTRAN* fluid element has a special facility which disables solution of the momentum and continuity equations, thus simulating solid material. The physical properties for the "solid" element can be adjusted to mimic the thermal behaviour of rock-type solids.

Models with fluid elements have the velocity, pressure, temperature, kinetic energy and dissipation rate as degrees of freedom. The values of all these properties as well as heat flux may be set initially as required and allowed to change with time or fixed at one value for all time (boundary conditions).

As is clear from discussion in previous chapters, the full chemical development of the

cooling magma including crystallization and differentiation cannot be modelled with the *FLOTRAN* code. What is currently possible is the modelling of the transport of a number of chemical species suspended in the melt. This is obviously an important aspect of the problem that cannot long be ignored. However, some account of it is made by the special set up of the viscosity and density functions which simulate the thickening of the melt where crystallization occurs. Further consideration of chemical effects is being undertaken this year (1998) and this thesis arguably has laid the groundwork to do so.

5.3 The Process Modelled

The process modelled consists of two distinct, although strongly connected parts. The first is the cooling of hot magmatic fluid and the second is the hydrothermal circulation in the surrounding country rock.

Simulation of the convective cooling of an enclosed magma body can be done with a relatively simple model. The geometry of the chamber may be modelled as accurately as time and hardware resources allow. Very complex geometry requires a large number of elements, leading to long solution times depending on the hardware at hand. The aim of this work was to model simple geometries in order to gain insight into the general behaviour of magmatic fluid and groundwater.

After meshing the magma chamber, zero velocity boundary conditions are applied to the exterior nodes in order to prevent fluid from leaving or entering the chamber. The initial intrusive temperature of the melt is applied to all nodes at the beginning of the first time step and allowed to change thereafter. In order to cool models with no surrounding country rock (but nonetheless in a non-extrusive situation), a low temperature boundary condition is applied to all exterior nodes.

The fluid properties of the magma have already been discussed. The actual values used appear in **Table 5.1** below and are calculated from data taken from Bottinga and Weill (1972) and Bottinga et al. (1982). The symbols in parentheses are those used in **Chapter 2**.

In some models it was desirable to have laminar convection only and so the nominal viscosity was adjusted to keep the Rayleigh number small. Since the magma viscosity varies by orders of magnitude with small changes in temperature, adjustments to the nominal viscosity do

not significantly affect the behaviour of the magma.

Fluid Property	Coefficient	Value
Viscosity (μ)	Nominal Value (μ_0)	$\approx 1\times10^{15}$ N.s.m^{-2}
	Temperature of Nominal Value (T_0)	800 °C
	Linear Coefficient (a_1)	93098
	Quadratic Coefficient (a_2)	70089000
Density (ρ)	Nominal Value (ρ_0)	3000 kg.m^{-3}
	Temperature of Nominal Value (T_0)	800 °C
	Linear Coefficient (b_1)	-1.08
	Quadratic Coefficient (b_2)	0.00075
Thermal Conductivity (k)	(constant)	2 J.m^{-1}.s^{-1}.K^{-1}
Specific Heat (c_V)	(constant)	1200 J.kg^{-1}.K^{-1}

Table 5.1 The physical properties used for modelling magmatic fluid.

FLOTRAN by itself can only model a single fluid at once. Since it was important to our studies to model a system involving the thermally coupled flow of magmatic fluid and groundwater, it was necessary to write additional code to do so. Separate models were constructed for each fluid and the solution obtained after a single time step from one model used as the initial or boundary conditions for the next time step in the other model and vice versa. This method of communication between models was implemented through the construction of code written in the *Ansys* Parametric Design Language (APDL). This language is a mixture of common FORTRAN commands and structures together with a substantial group of *Ansys* functions.

The code developed can be executed as a "macro" from the *Ansys* command line. The essence of the program I have written is as follows. From the solution given at the end of a magma chamber time step, record the heat fluxes through the external element faces of the chamber. Apply these as boundary conditions to the corresponding contact surfaces of the country rock model. Run a single time step for the country rock and from its solution record the temperature of all the contact surface nodes. Apply these temperatures as boundary conditions

to the external nodes (which are on the magma chamber boundaries) in the magma chamber model. Run a time step for the magma and record the next set of heat fluxes, and so on.

The final version of the code I wrote to handle a general three-dimensional model with any geometry can be found in **Appendix 2**. The restrictions and initial requirements for running the program are also given.

Convecting groundwater in the porous rock adjacent to a hot pluton is a more complex process geometrically than magma chamber convection and has unique difficulties. The first is the amount of country rock to model. One must correctly predict the spatial extent of the region of rock affected by the intrusion. Computer hardware restrictions place an upper limit on model size and I decided as a rule of thumb to model a shell of country rock as thick as the depth of the magma chamber.

The groundwater fluid properties used in all country rock models appear in **Table 5.2**. The permeability in all models was uniform and homogeneous.

Zero velocity boundary conditions were applied to the inner (magma contact) surfaces, however the choice of boundary conditions to apply to the outer surfaces was somewhat problematic. Most of the models I ran had zero velocity and fixed temperature boundary conditions. The temperatures were chosen to simulate a geothermal gradient which has temperatures rising with depth at a rate of 25 $^{\circ}C.km^{-1}$. See the next section for details on initial and boundary conditions.

An alternative scenario is that used by Hayba and Ingebritsen (1997). They modelled country rock extending from the surface of the earth to the bottom of the magma chamber. Along the surface of the earth they applied typical ambient temperatures (20 $^{\circ}C$) and pressures (1 atm). Along the bottom surface of the magma chamber and country rock they applied zero velocity and constant heat flux boundary conditions simulating an impermeable sequence conducting heat into the model from the warmer, deeper parts of the crust. Because they were modelling only half of the pluton-country rock system, one side edge represented a plane of symmetry and had appropriate boundary conditions. The side representing the outer limits of the country rock had no boundary conditions imposed. Also, the bottom surface only had velocity boundary conditions. Fluid was allowed to cross all other boundaries.

I used these sorts of boundary conditions for some of my later models. However, instead of setting the country rock so that its upper surface coincided with the surface of the earth, I

positioned it at a depth of one kilometre. This was to ensure sufficient groundwater pressure to avoid dealing with phase change.

Fluid Property	Coefficient	Value
Viscosity (μ)	Nominal Value (μ_0)	0.00112 N.s.m^{-2}
	Temperature of Nominal Value (T_0)	60 °C
	Linear Coefficient (a_1)	23.68
	Quadratic Coefficient (a_2)	-7883
Density (ρ)	Nominal Value (ρ_0)	1045 kg.m^{-3}
	Temperature of Nominal Value (T_0)	60 °C
	Linear Coefficient (b_1)	-0.45
	Quadratic Coefficient (b_2)	0
Thermal Conductivity (k)	(constant)	2 J.m^{-1}.s^{-1}.K^{-1}
Specific Heat (c_V)	(constant)	4342 J.kg^{-1}.K^{-1}
Permeability (K)	(constant)	1×10^{-15} m^2

Table 5.2 The physical properties used for modelling groundwater.

For all country rock models, the initial interior temperature of the groundwater was set according to the geothermal gradient.

5.4 The Models

Presentation of the finite element meshes used in this work follows. First is a description of an experiment carried out to determine the impact of mesh refinement on solution accuracy. **Figure 5.1** shows a two-dimensional square of magma and likewise of country rock, each 1 km^2 in area. The two models were coupled in such a way that they made contact along a single edge. A transient thermal analysis was performed on this system for a number of element sizes. Uniform temperature and zero velocity boundary conditions were imposed on both the magma and the country rock. The results of the experiment are given in the next chapter.

The meshes shown have the minimum element size used in the experiment. There are 35 elements along the contact surface. The model was also run for 10, 15, 20, 25 and 30 contact

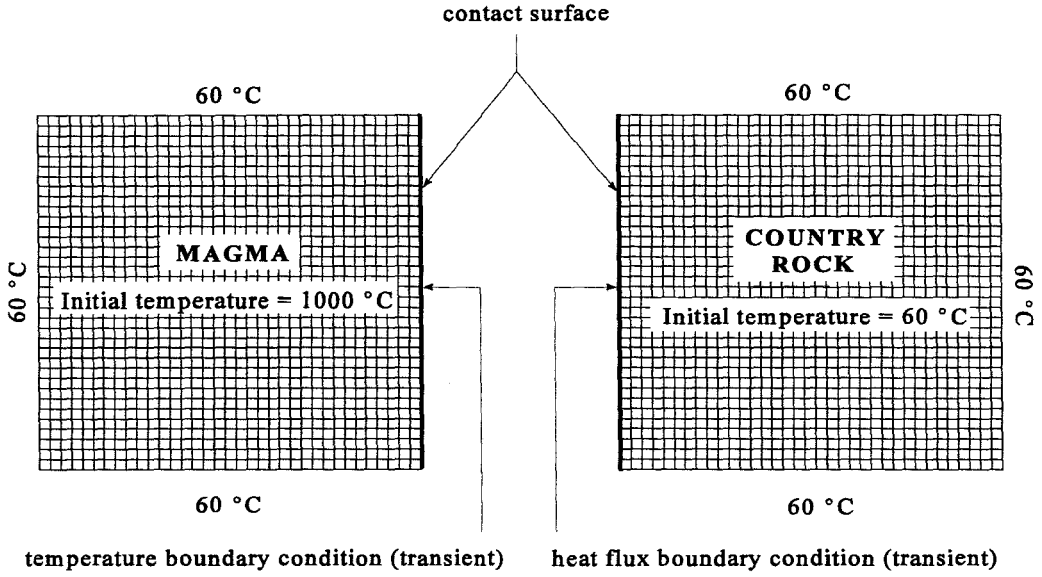

Figure 5.1 Two-dimensional model used to investigate the effects of mesh refinement on solution accuracy.

elements.

The last few pages of the chapter contain pictures of the main models studied in this work. A detailed description of each follows.

5.4.1 Two-dimensional Square Chamber

The first model studied was that shown in **Figure 5.2**. The magma chamber was identical to the one used for the mesh experiment described above, except that it had 40 elements along each edge, making for a more accurate solution than any of those achieved in the mesh experiment. The country rock was 1 km thick and completely surrounded the magma chamber. One of the requirements of the code controlling the coupled solution procedure was that contact surface nodes on the magma chamber and the country rock coincide. Consequently the inner edges of the country rock also had 40 elements each.

In general, meshing was controlled fairly rigorously. The number of elements along every line in the model was specified and only quadrilateral elements were allowed. *FLOTRAN* notifies one of overly distorted elements created during meshing. This enables one to engineer a stable mesh of reliable elements.

The boundary and initial conditions applied to the model are listed in **Table 5.3**. Boundary

conditions followed by "(Transient)" imply that the quoted values are applied for the first time step only. The heat flow between the magma chamber and country rock will cause these boundary conditions to change slightly on each successive time step.

	Magma Chamber	Country Rock
Boundary Conditions	Velocity: 0. Temperature: Geothermal gradient of 30 °C.km^{-1}. (Transient).	*Outer Surfaces* Velocity: 0. Temperature: Geothermal gradient of 30 °C.km^{-1}. Top surface temperature = 20 °C. *Inner Surfaces* Velocity: 0. Heat Flux: 0. (Transient).
Initial Conditions	Temperature: 1000 °C.	Temperature: Geothermal gradient of 30 °C.km^{-1}.

Table 5.3 Boundary and initial conditions applied to the square magma chamber model.

5.4.2 Two-dimensional Wedge-shaped Chamber

The model shown in **Figure 5.3** was constructed in order to study the flow of magma in a confined area of the chamber. A triangle was added onto the right-hand side of the original square chamber. The country rock had to be modified but it retained its 1 km thickness. The higher number of elements in the resulting mesh forced an increase the element size in both models. The final magma chamber mesh had 24 elements per kilometre along its edges. The boundary and initial conditions were the same as those listed in **Table 5.3** for the square chamber model.

5.4.3 Three-dimensional Cylindrical Chamber

Figure 5.4 displays the three-dimensional coupled model used in this work. The magma chamber is a 1 km deep cylinder with a radius of 500 m. The country rock is 500 m thick and

forms a hollow cylinder around the chamber. The number of elements used in a three-dimensional model is vastly greater than in an analogous two-dimensional model. However, the installation of a newer version of *Ansys* allowed me to retain a mesh of 20 elements along the length of the magma chamber and 56 around the circumference.

The boundary and initial conditions for this model were based on Hayba and Ingebritsen (1997) and are listed in **Table 5.4**. The values are such that the top surface of the country rock is at a depth of 1 km below the earth's surface.

	Magma Chamber	Country Rock
Boundary Conditions	Velocity: 0. Temperature: Geothermal gradient of 25 °C.km^{-1}. Offset to match country rock initial temperature distribution. (Transient).	*Outer Surfaces* Velocity: 0 at bottom surface (impermeable layer). Temperature: 45 °C at top surface. Pressure: 333 atm at top surface. Heat Flux: 5 W.m^{-2} through bottom surface, into country rock. *Inner Surfaces* Velocity: 0. Heat Flux: 0. (Transient).
Initial (Internal) Conditions	Temperature: 1000 °C.	Temperature: Geothermal gradient of 25 °C.km^{-1}. Pressure: Gradient of 0.3 atm.m^{-1}. Top surface at 333 atm.

Table 5.4 Boundary and initial conditions applied to the cylindrical magma chamber model.

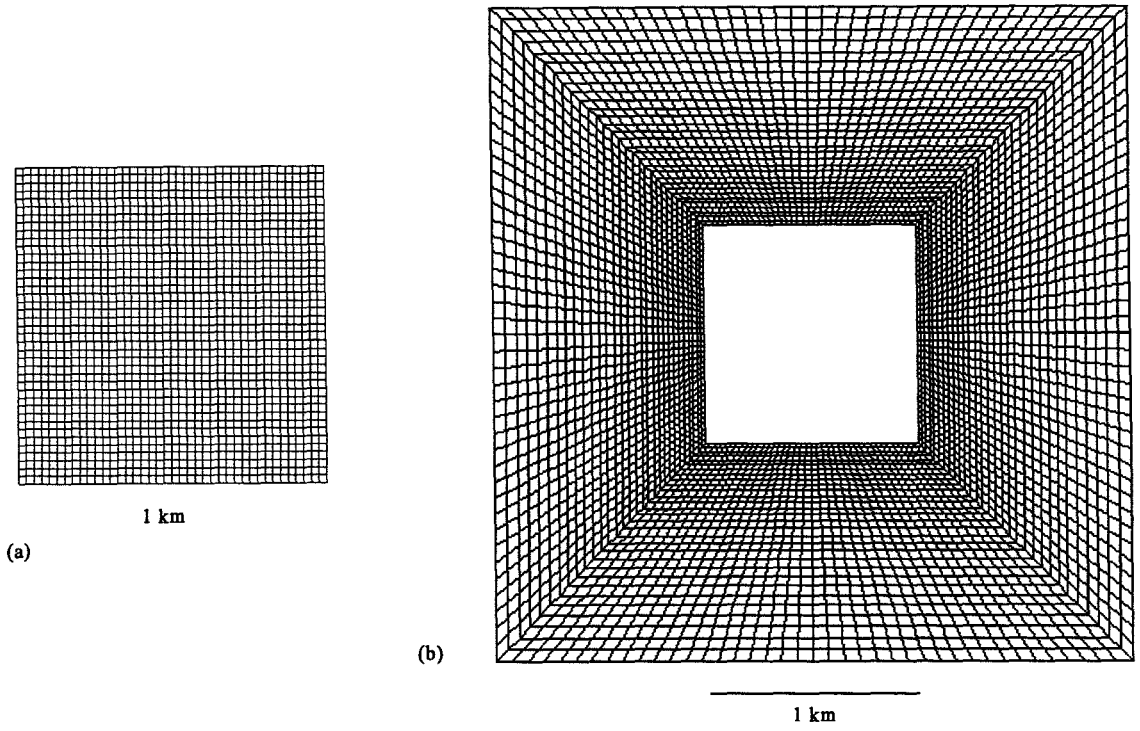

Figure 5.2 (a) Two-dimensional square magma chamber mesh and (b) surrounding country rock mesh. Note that (a) is not to the same scale as (b) and has been enlarged for clarity. With the scales equal, (a) fits exactly into the central cavity in (b) and all nodes along the contact boundaries coincide.

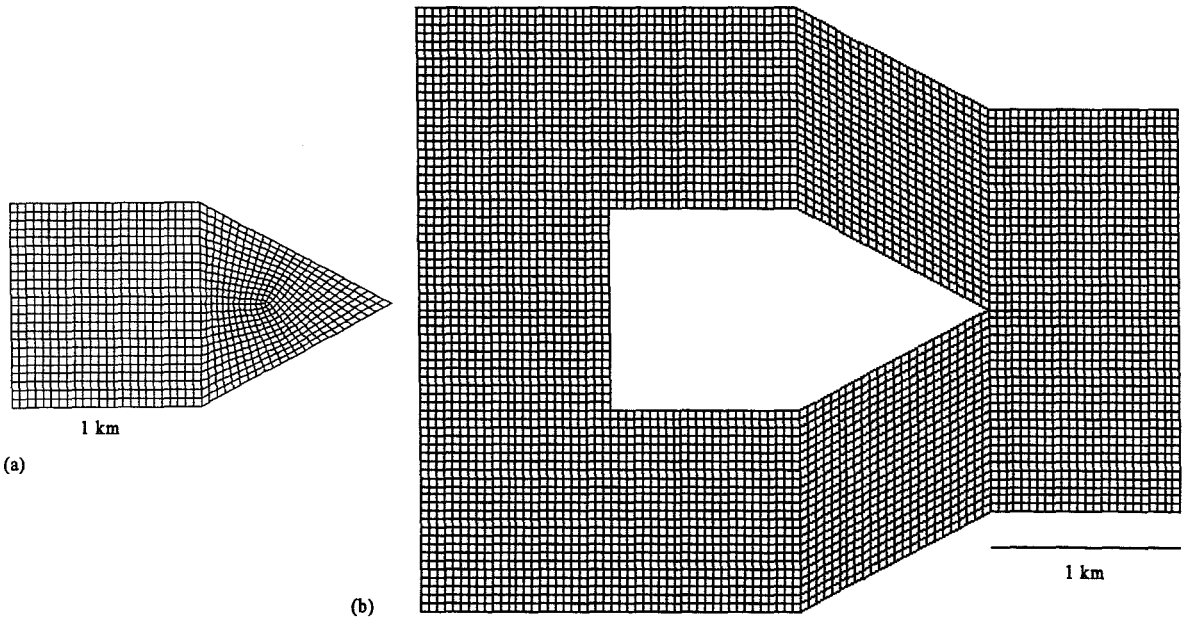

Figure 5.3 Two-dimensional wedge-shaped chamber (a) and surrounding country rock (b).

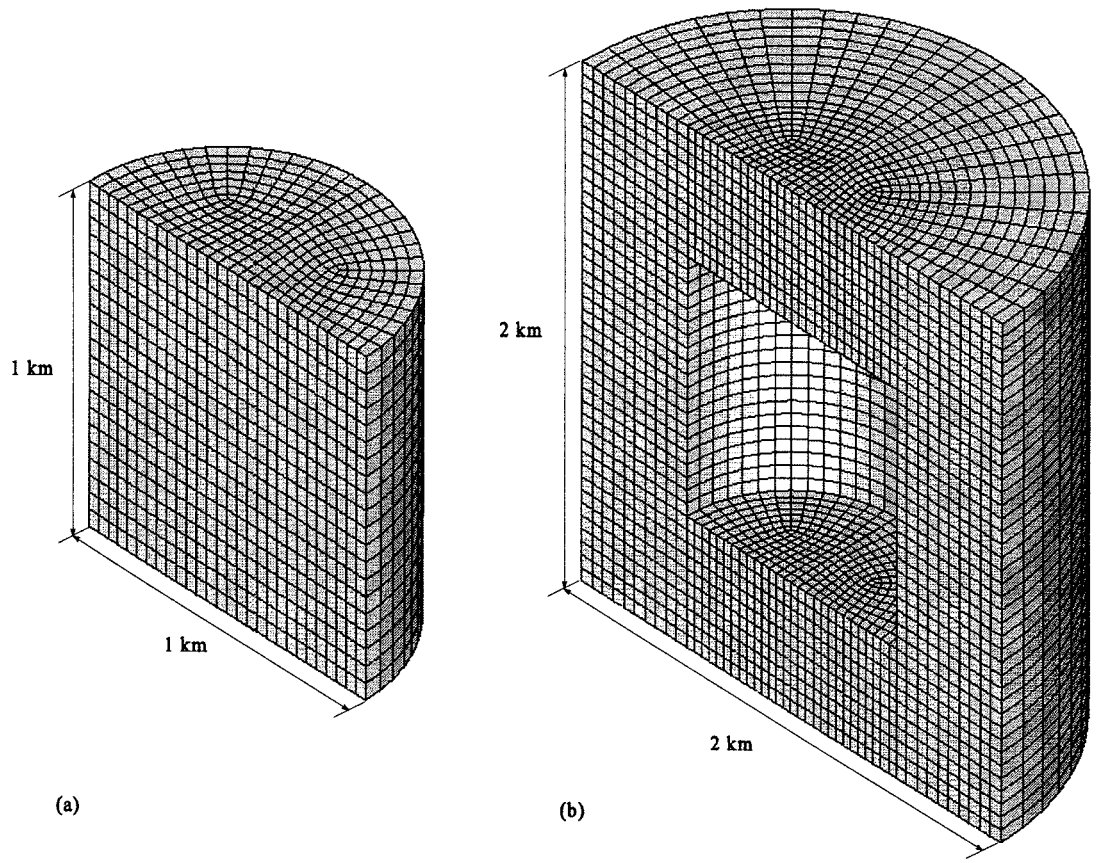

Figure 5.4 Vertical sections through the centres of the three-dimensional cylindrical magma chamber (a) and the surrounding country rock (b).

Chapter 6

Results

Solutions to the governing equations for fluid flow comprise numerical specifications of all degrees of freedom. In particular, velocity and temperature are of primary interest. The *FLOTRAN* graphical user interface makes it possible to visualise numerical solutions in a concise, comprehensive manner.

6.1 Results Displays

6.1.1 Contour Plots

The value of a scalar over a two-dimensional problem domain is best represented by a set of contour lines, each line joining points of equal value. Instead of plotting the contours themselves, *FLOTRAN* plots the intervals between the contours, each with a different colour. The values of the scalar corresponding to a particular colour are given in a legend alongside.

Since degrees of freedom are calculated at the nodes only, *FLOTRAN* uses its interpolation functions (as described in **Chapter 4**), to generate a continuous set of results and therefore contour lines.

Temperature and the individual velocity components may be represented in such a way. The results for any planar cross-section may be viewed.

6.1.2 Vector Plots

Vector quantities may be plotted as arrows with the correct direction and length. Each node in the model will have an arrow of its own. For further clarity, *FLOTRAN* assigns to each arrow a colour related to its magnitude as given in an accompanying scale. As with contour plots, the vectors belonging to nodes in any planar cross-section of the model may be viewed.

6.1.3 Particle Traces

Being able to trace the path of fluid particles may highlight features of the flow pattern that are of interest and may indicate the relative flow speeds of different regions. FLOTRAN is able to plot such paths given a steady-state velocity solution. If the model is transient, each time step may be regarded temporarily as a steady-state solution and a particle trace constructed. While this method does not depict the true transient behaviour of the flow, it allows analysis of individual sets of results.

Particles trace lines may be coloured according to a scale measuring speed, temperature or any other scalar.

Results of transient runs of the models described in **Chapter 5** follow.

6.2 Mesh Refinement Experiment

Results of the simple model described in **Chapter 5** that was used to test the effects of mesh refinement on the accuracy of solution are given in **Figure 6.1**. In **Figure 6.1(a)**, the heat flux through the centre element along the contact edge between magma and country rock is shown for various mesh resolutions. The initial heat flux is zero and as the hot magma is (instantaneously) emplaced, it increases rapidly to a maximum value. The legend gives the total number of elements along the contact edge for each (colour coded) set of data points. The jump in heat flux becomes progressively more sluggish as the mesh becomes more coarse.

In **Figure 6.1(b)** the temperature of the central node along the contact edge is shown. As the magma is emplaced, the temperature of the edge increases rapidly to about half the initial temperature of the magma (1000 °C). Again, the jump in temperature becomes progressively more sluggish as the mesh becomes more coarse.

For the heat flux and temperature plots it can be seen that the solutions do not converge

precisely after the initial jump. Small differences during the first few time steps can lead to major discrepancies later on. (This was particularly evident for temperatures at times greater than those shown on the chart). This emphasises the importance of mesh refinement in transient problems.

6.3 Square Magma Chamber

Figures 6.2(a), 6.2(b) and **6.3** show temperature distributions in the 1 km by 1 km square magma chamber after 90.2, 190 and 385 years respectively. The code written by the author to control the model produced results at specific times. These times are not separated by constant intervals. The intervals are made smaller during the highly transient parts of the analysis in order to obtain a large number of results sets. Conversely, the intervals are made larger during the stable parts of the process so as not to record nearly identical results sets. (This feature of the code saves time and computer resources.) The times chosen in this chapter for the display of results thus correspond to specific sets of results and are not chosen arbitrarily. The displays chosen in this chapter were part of full collections of results. The square magma chamber model (and most others), produced between 100 and 300 sets of results.

Only a short temperature range is plotted in order to display fine detail, hence the uncalibrated grey area on the margins of each plot which in fact correspond roughly to "frozen" magma. Note that the colours in each plot do not correspond to the same temperatures. It is clear that the flow pattern in the chamber is complex and causes asymmetric patterns in the temperature distribution despite the symmetric nature of the model. The accompanying scales give temperatures in degrees Celsius.

Figure 6.4 displays two particle traces, the first calculated at 0.2 years and the second at 90.2 years. (When viewing particle traces, it is important to keep in mind their definition given in section *6.1.3.*) The paths of nine particles, each starting from the horizontal line dividing the chamber in half and placed at 100m intervals along this line, are traced in both plots.

Figure 6.4(a) exhibits double cell convection which predominates the cooling history of the chamber, especially during the last few thousand years (see **Figure 6.17**). In **Figure 6.4(b)** the pattern has changed into one with four cells, a pattern which features during the early cooling stages only. The velocity distribution rapidly cycles through a variety of forms, as shown in

Figures 6.5, 6.6, 6.7 and **6.8**. These figures contain examples of velocity distributions, including those corresponding to the same times as the particle traces in **Figure 6.4**. The other distributions are those calculated after 8.0, 8.5, 10.7, 1083 and 2600 years respectively. Note that the cooling magma freezes resulting in zero velocity regions at the walls of the chamber that thicken with time. In the last picture (**Figure 6.8(b)**) only a small cell of convecting magma remains.

Figure 6.7(b) shows an overlay of the temperature and velocity distributions in the chamber after 90.2 years (the temperature distribution is a reproduction of **Figure 6.2(a)**).

6.4 Country Rock Surrounding Square Magma Chamber

Figures 6.9 and **6.10** together show three temperature distributions (with scales in Kelvin) and one particle trace of groundwater flow. The temperature distributions are calculated after 190, 1083 and 2600 years respectively.

Figures 6.11, 6.12 and **6.13** together show velocity distributions in the country rock after 10.7, 90.3, 1083, 2600 and 15200 years. **Figure 6.13(a)** is an enlarged view of the right hand side of the country rock model and shows an overlay of the temperature distribution after 2600 years and nine particle traces. The traces are of uniform colour so as not to be lost against the coloured background. The groundwater maintains the same flow pattern throughout its history, the only changes being a broadening of the rising columns on either side of the chamber. The maximum velocity is only reached after approximately 1000 years.

6.5 Wedge-shaped Chamber

Figure 6.14(a) shows the temperature distribution in the wedge-shaped chamber after 38.2 years (the length of the chamber is 2 km and the depth is 1 km) . Time did not allow the model to be run beyond this stage, but the results from this short period are still interesting and useful. **Figure 6.14(b)** shows a particle trace calculated after 20.7 years. This makes clear the presence of a number of convection cells.

Figure 6.15 shows the velocity distribution after 20.7 years. Note that the maximum velocities are in the triangular section of the chamber. This section of the chamber experiences

the quickest heat loss because of its geometry.

The groundwater surrounding the wedge-shaped chamber exhibited much the same flow pattern during the short run as the groundwater surrounding the square magma chamber. This pattern consists of upwelling along the left, vertical margin of the chamber and along both oblique edges making up the wedge-shaped right margin of the chamber.

6.6 Transient Results Sequences

Figures 6.16(a)-(f) form a sequence of temperature contour plots of both the square magma chamber and the surrounding country rock. The first plot shows the initial conditions and the remaining plots show subsequent distributions after every 5400 years, with the last plot at 27000 years. It is significant how much cooling takes place in the magma before the second plot. The scale in the upper left corner of the figure applies to all six plots and gives temperatures in Celsius.

Figure 6.17 shows a similar sequence to the first, this time with velocity distributions. The first plot is at the beginning of the model as before, but the interval between successive plots is 1060 years with the last plot at 5300 years. The sequence serves to illustrate the freezing process of the magma chamber and to compare groundwater and magma velocities. For an enlarged view of these plots, which will make the arrows clearer, the reader is referred to the corresponding animation (*anim2.mov* on the compact disc at the back of the thesis).

Figure 6.18 shows a sequence of wedge-shaped chamber velocity distributions. The first plot is at a time of 12.8 years and the others are at 1.8 year intervals thereafter. The convection cells change in strength and position throughout this sequence. Again, the reader should refer to the corresponding animation (*anim3.mov*) for a clearer view of these plots.

6.7 Three-dimensional Cylindrical Magma Chamber and Surrounding Country Rock

Shown in **Figure 6.19** are some preliminary results from this model. Viewing of results in a three-dimensional model is difficult and best done by animation. However, it is possible to display results by plotting a number of sections through the model. **Figure 6.19(a)** shows the temperature distribution in the groundwater for half of the country rock model after 200 years

by means of a number of vertical sections through the model. The same sections are used in **Figure 6.19(b)** to show the velocity vector distribution in the groundwater after 200 years.

Figure 6.19(c) shows a sectioned view of the temperature distribution in the cylindrical magma chamber. The current research may be extended by the production and analysis of more results from this model.

6.8 Animations

On the CD at the back of the thesis may be found nine ".mov" files containing animations of the results described above and of results obtained by my fellow MSc student Andrè Botha who was also part of the project described in this thesis. I have shown these animations as part of oral presentations given at a number of conferences (see all reference listings for Botha et al. and Rice et al.). The last animation is a demonstration of visualisation techniques devised by Soteri Panagou from the Computer Science Department at Rhodes University. Identification of each animation follows. Detailed comment may be found in **Chapter 7**.

1. *anim1.mov*: Temperature contour animation in the square magma chamber and the surrounding country rock.
2. *anim2.mov*: Velocity vector animation in the square magma chamber and the surrounding country rock.
3. *anim3.mov*: Velocity vector animation in the wedge-shaped magma chamber.
4. *anim4.mov*: Particle trace animation in the wedge-shaped magma chamber.
5. *anim5.mov*: Velocity vector animation in a magnified view of the left arm of a sill-shaped magma chamber (with no surrounding country rock).
6. *anim6.mov*: Velocity vector animation in a sill-shaped magma chamber that has been enclosed in purely conductive country rock (i.e. no groundwater flow).
7. *anim7.mov*: Velocity vector animation of a vertical section through a high aspect ratio cylindrical magma chamber with no surrounding country rock.
8. *anim8.mov*: Velocity vector animation of a horizontal section through the high aspect ratio cylindrical magma chamber.
9. *anim9.mov*: Demonstration of sectioning and other visualisation techniques.

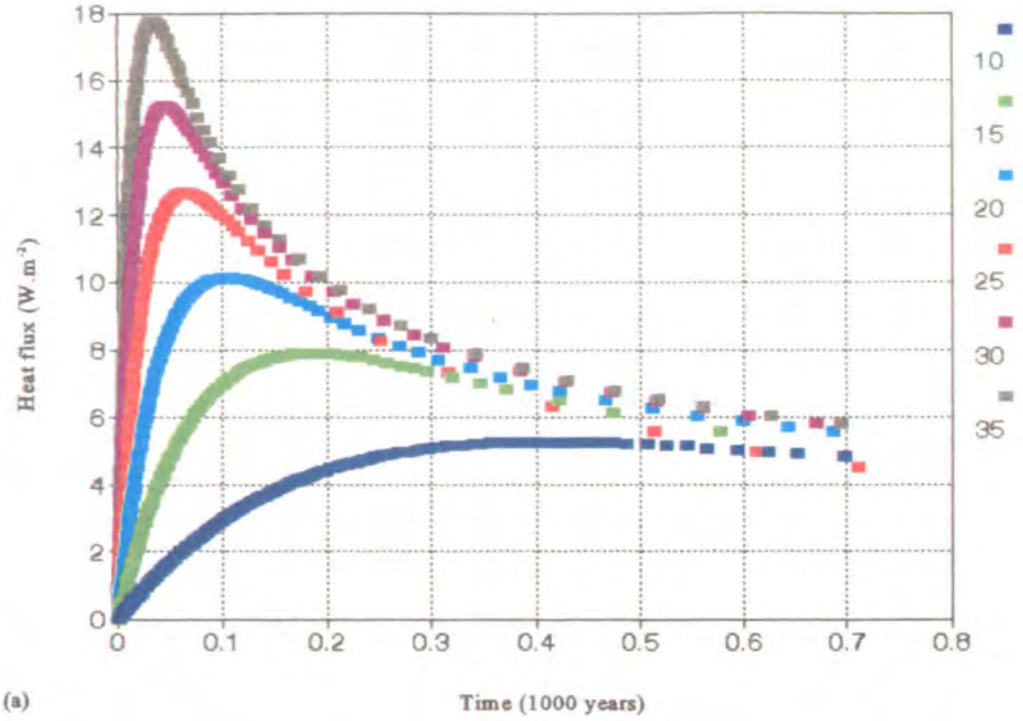

(a)

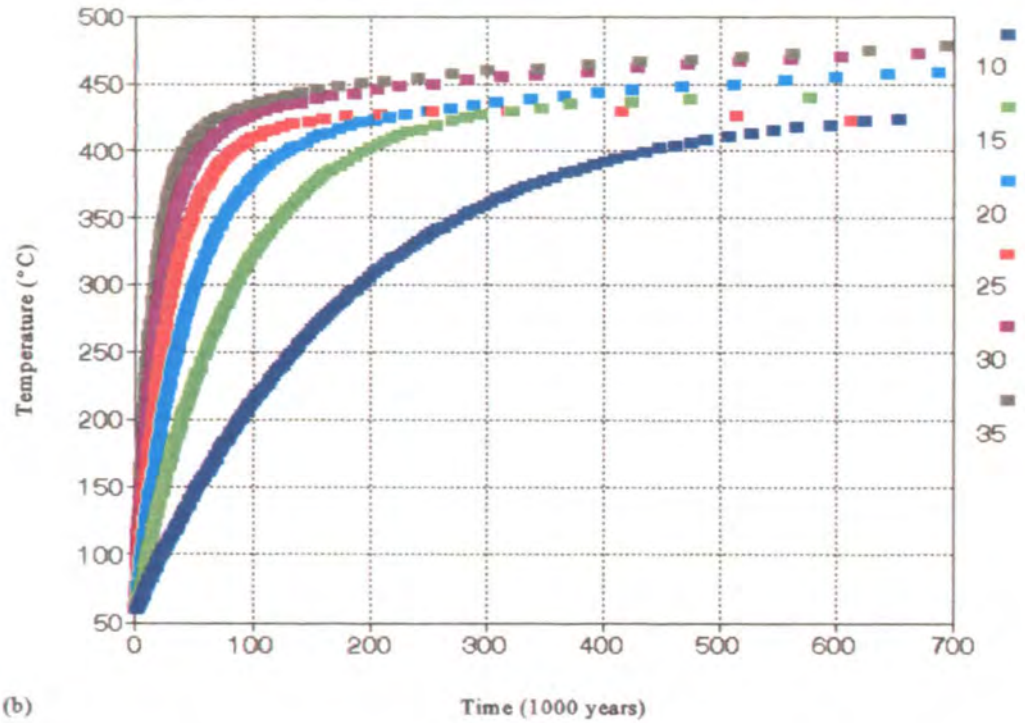

(b)

Figure 6.1 Plot of the heat flux (a) and temperature (b) at the central contact element in the mesh experiment model. The legend gives the total number of elements along the contact edge for each curve.

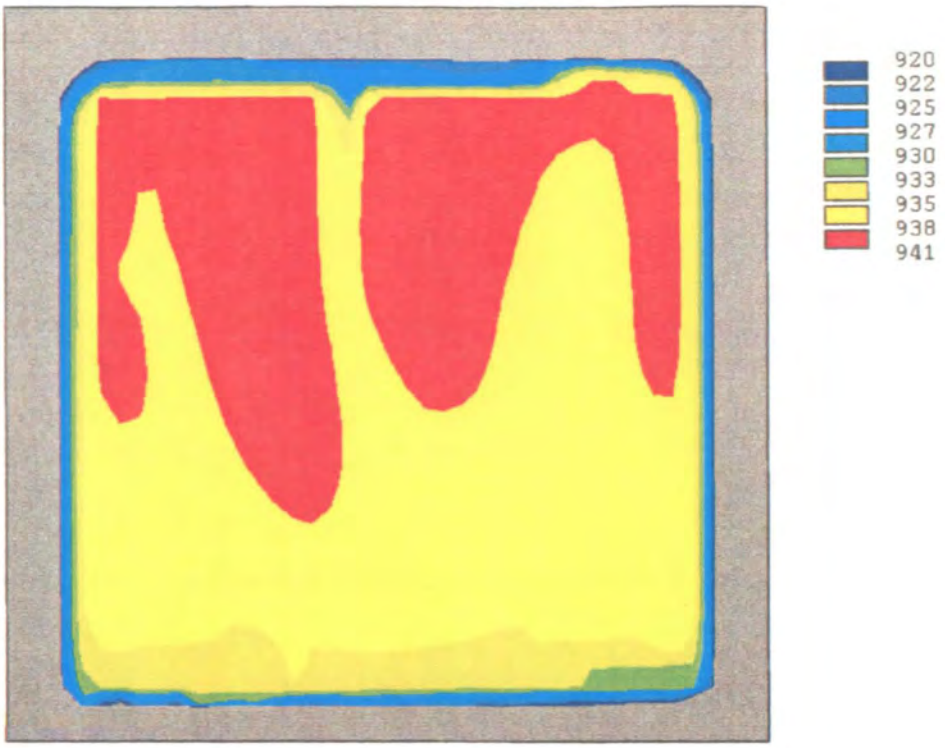

(a)

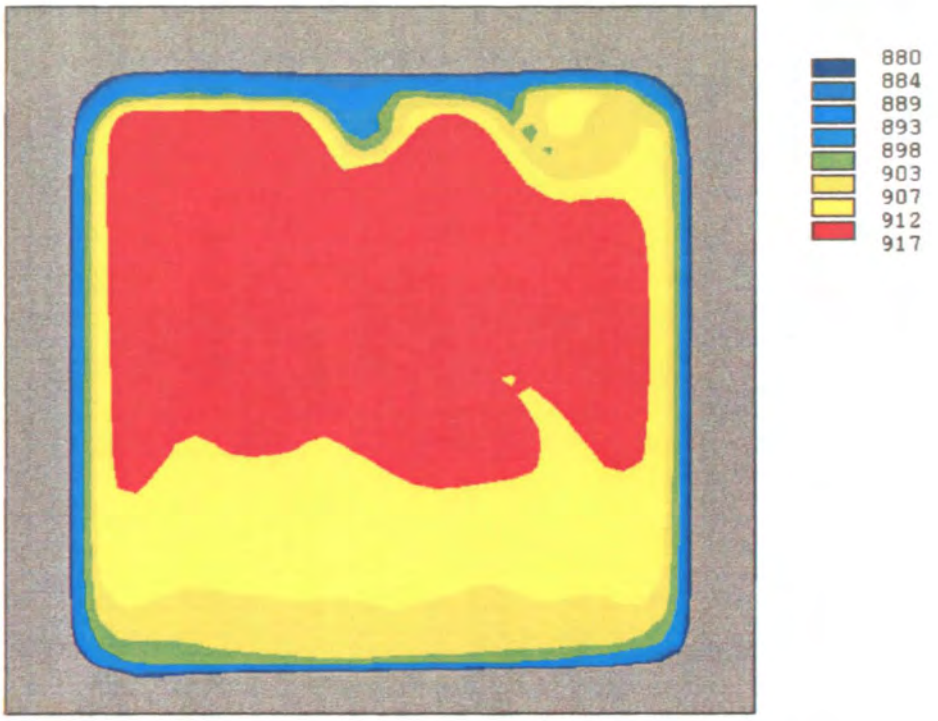

(b)

Figure 6.2 Temperature distributions in the two-dimensional square magma chamber (1 km by 1 km) after (a) 90.2 and (b) 190 years.

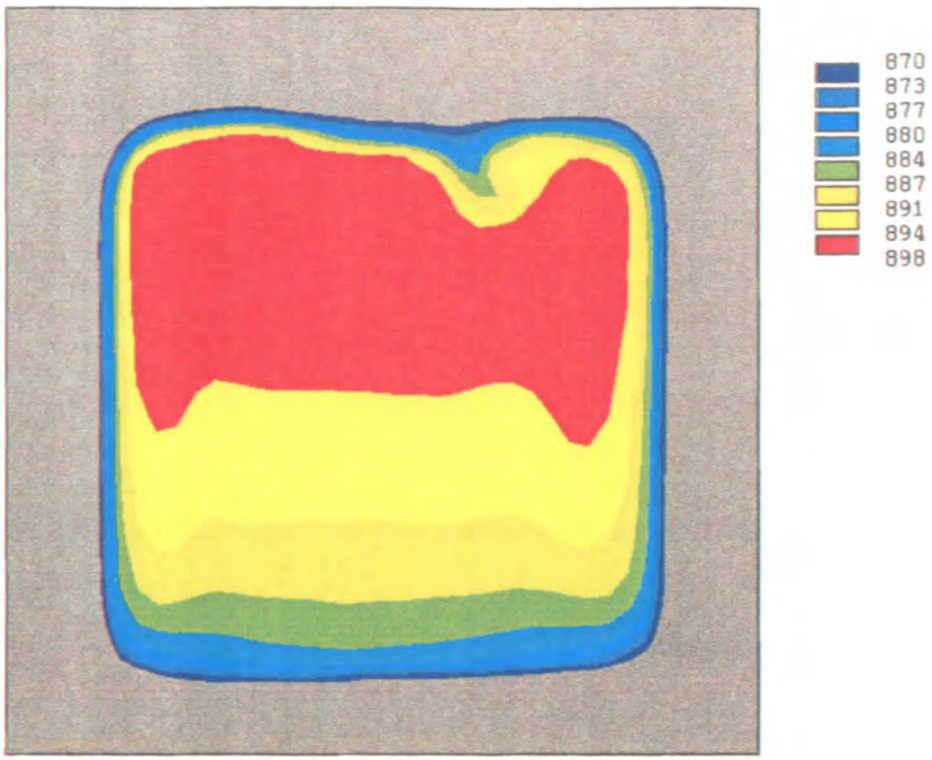

Figure 6.3 Temperature distribution in the two-dimensional square magma chamber (1 km by 1 km) after 385 years.

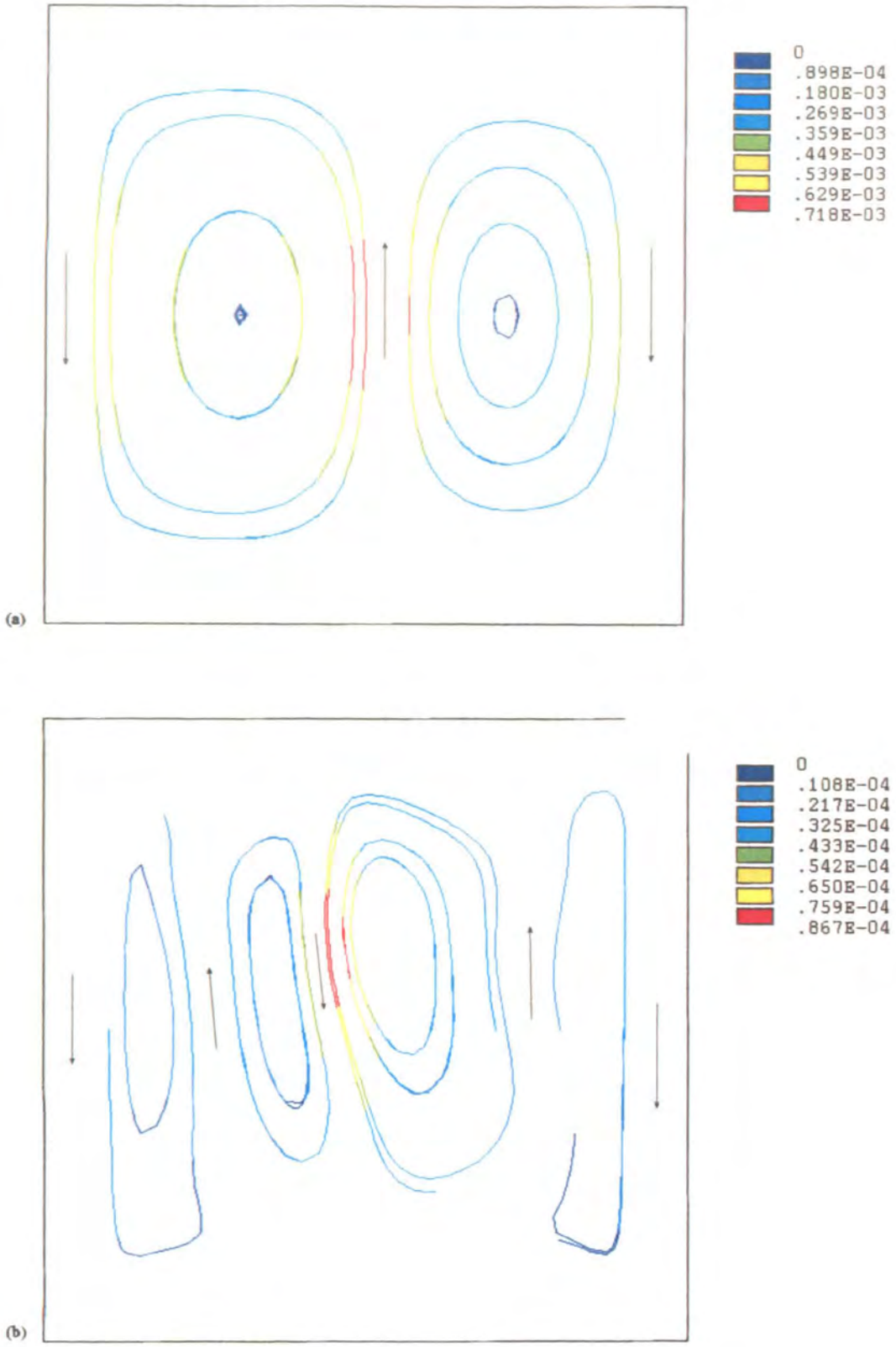

Figure 6.4 Particle traces in the two-dimensional square magma chamber (1 km by 1 km) calculated after (a) 0.2 and (b) 90.2 years. The arrows indicate the direction of flow.

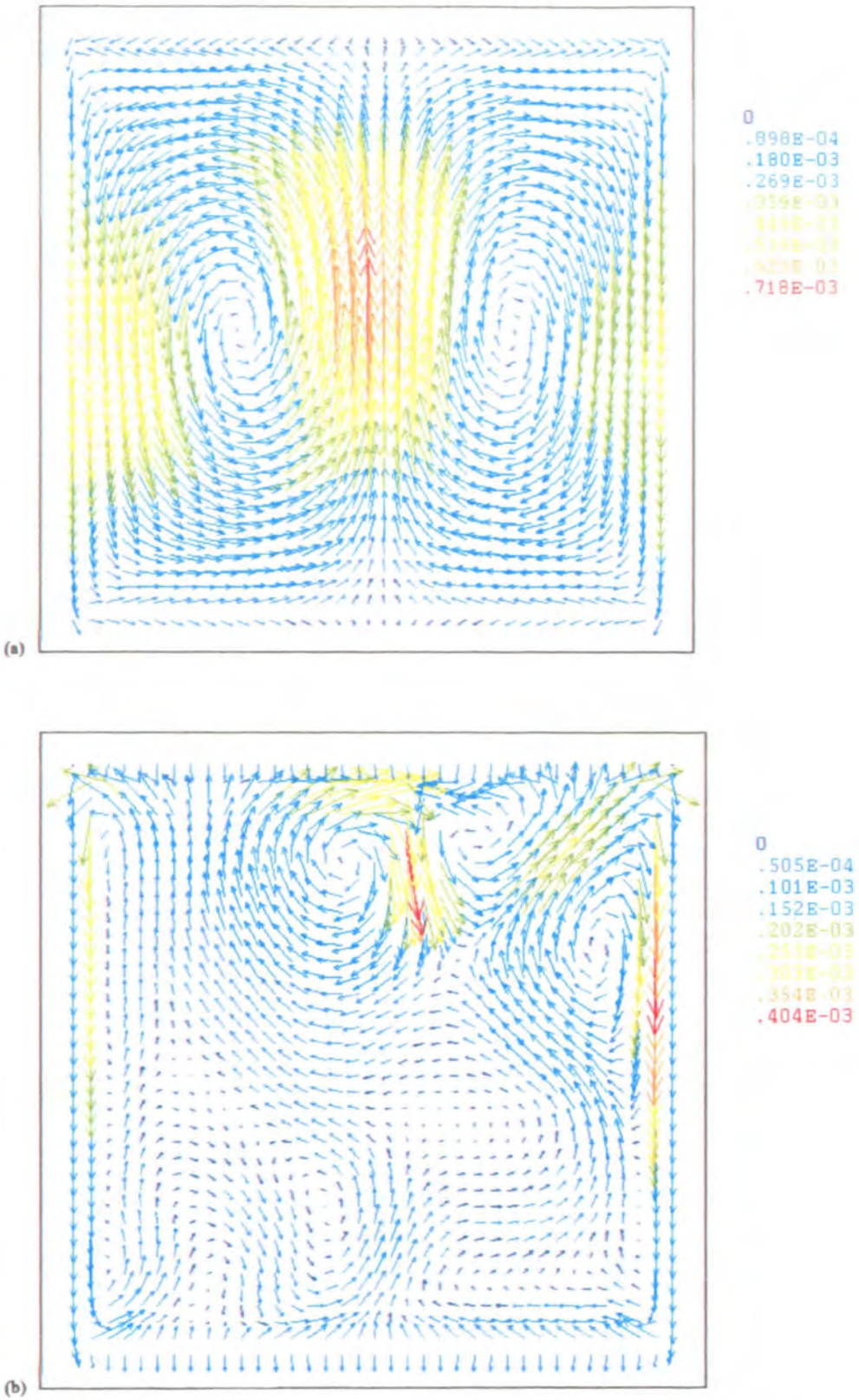

Figure 6.5 Velocity distributions in the two-dimensional square magma chamber (1 km by 1 km) after (a) 0.2 and (b) 8.0 years.

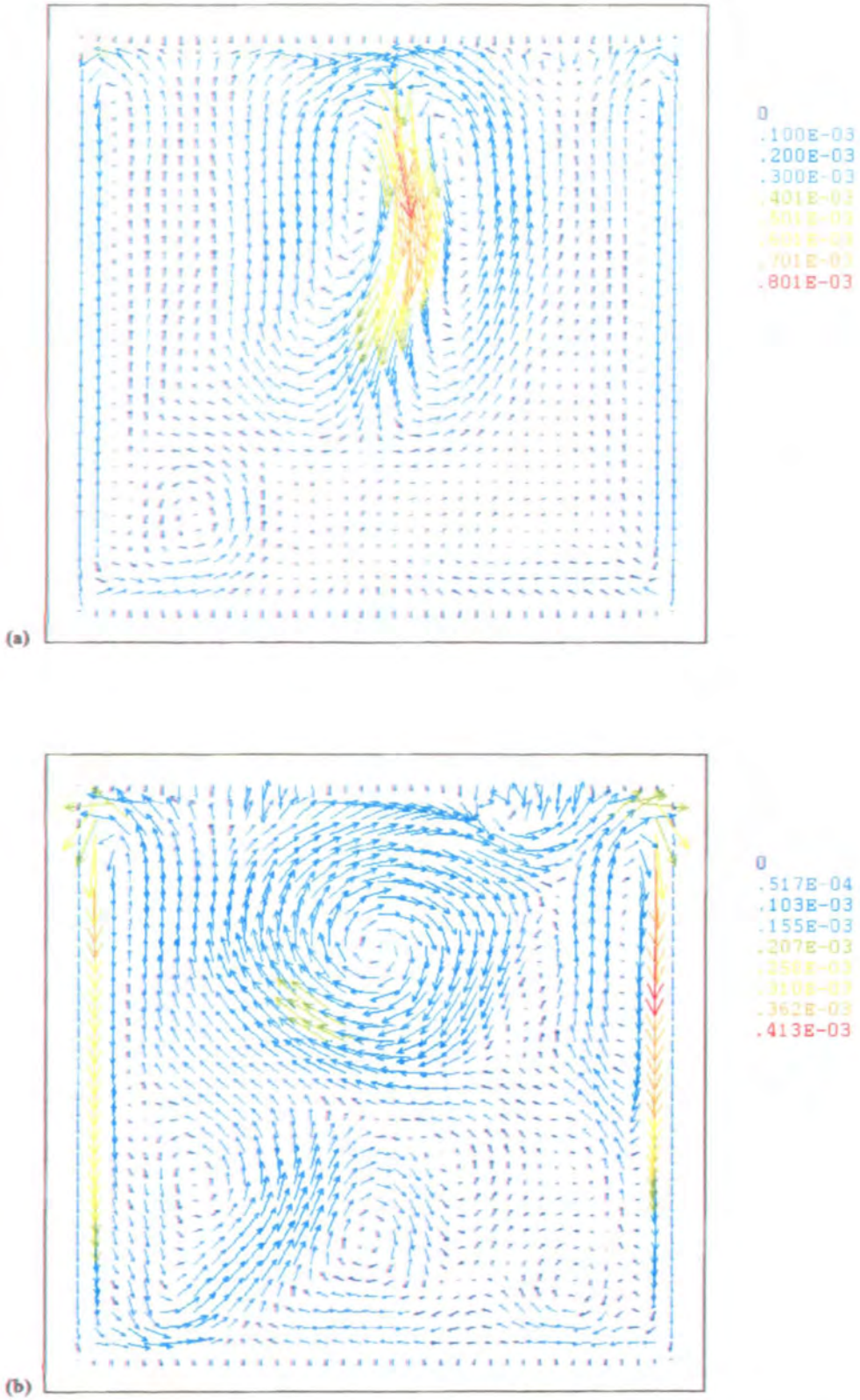

Figure 6.6 Velocity distributions in the two-dimensional square magma chamber (1 km by 1 km) after (a) 8.5 and (b) 10.7 years.

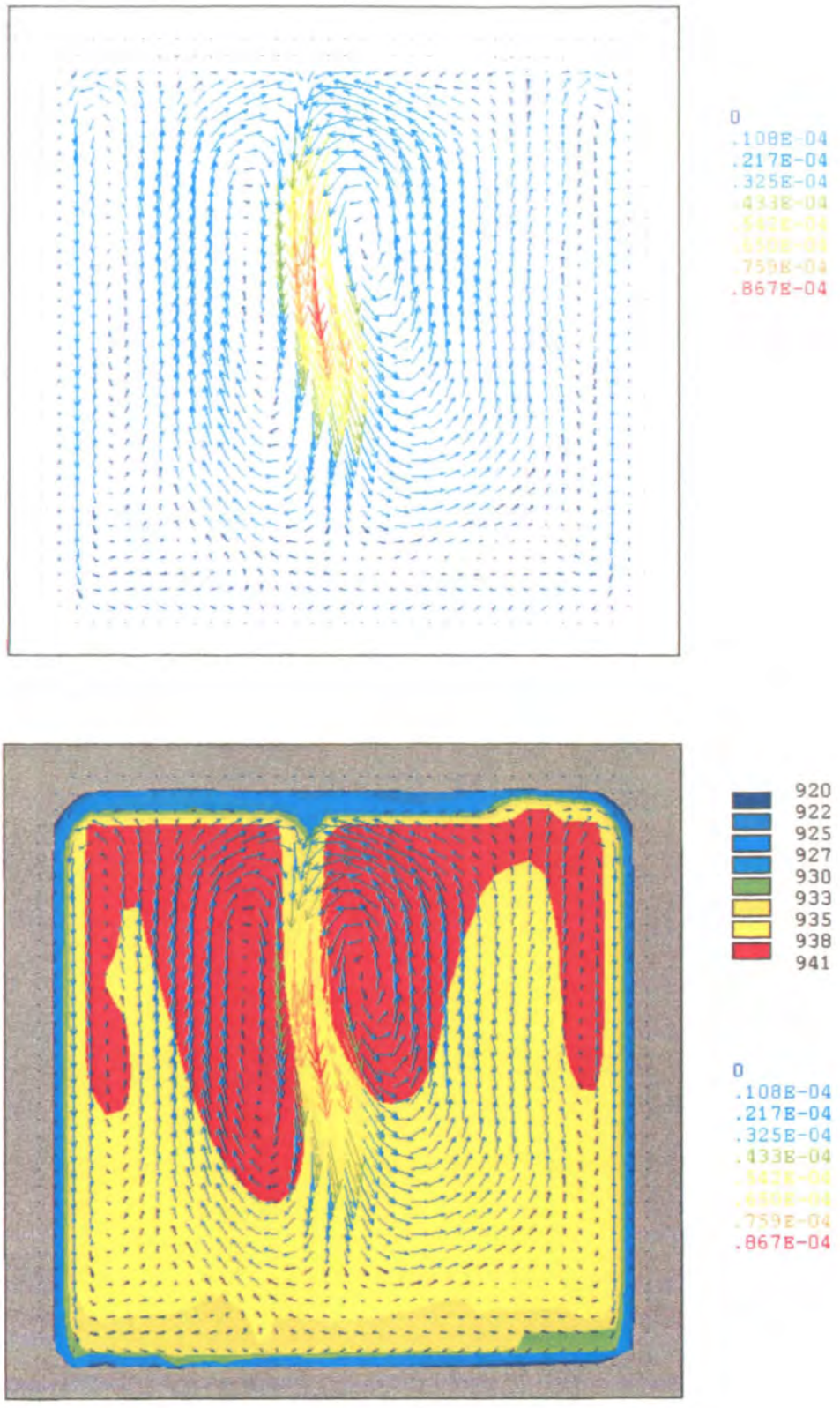

Figure 6.7 (a) Velocity distribution in the two-dimensional square magma chamber (1km by 1 km) after 90.2 years and (b) the same distribution overlayed with the corresponding temperature distribution.

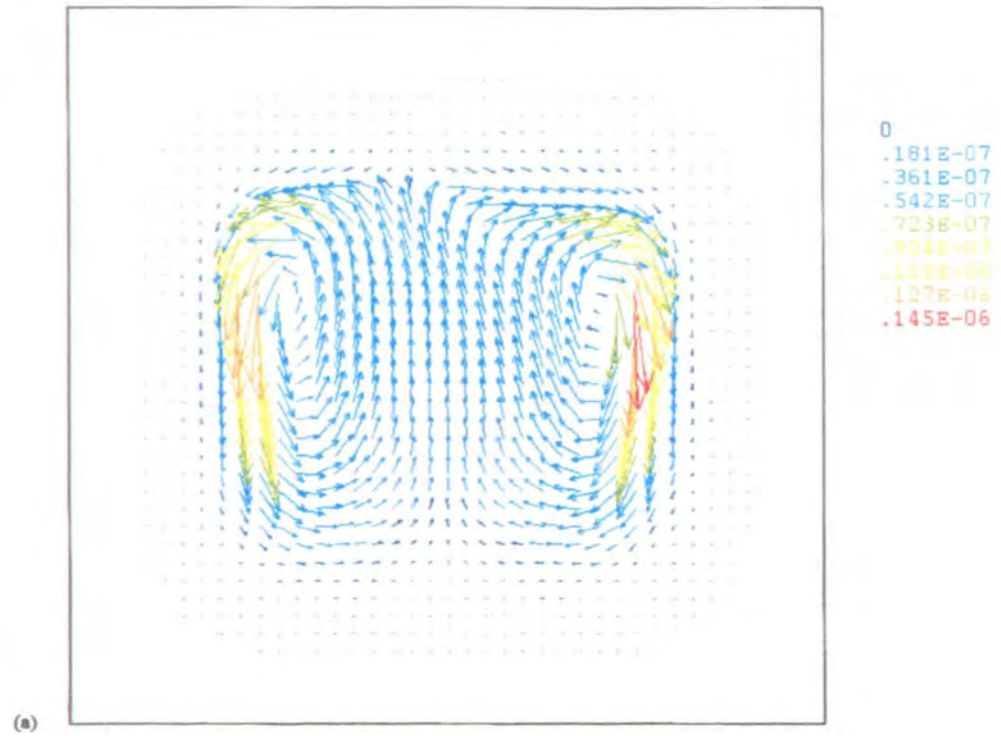

(a)

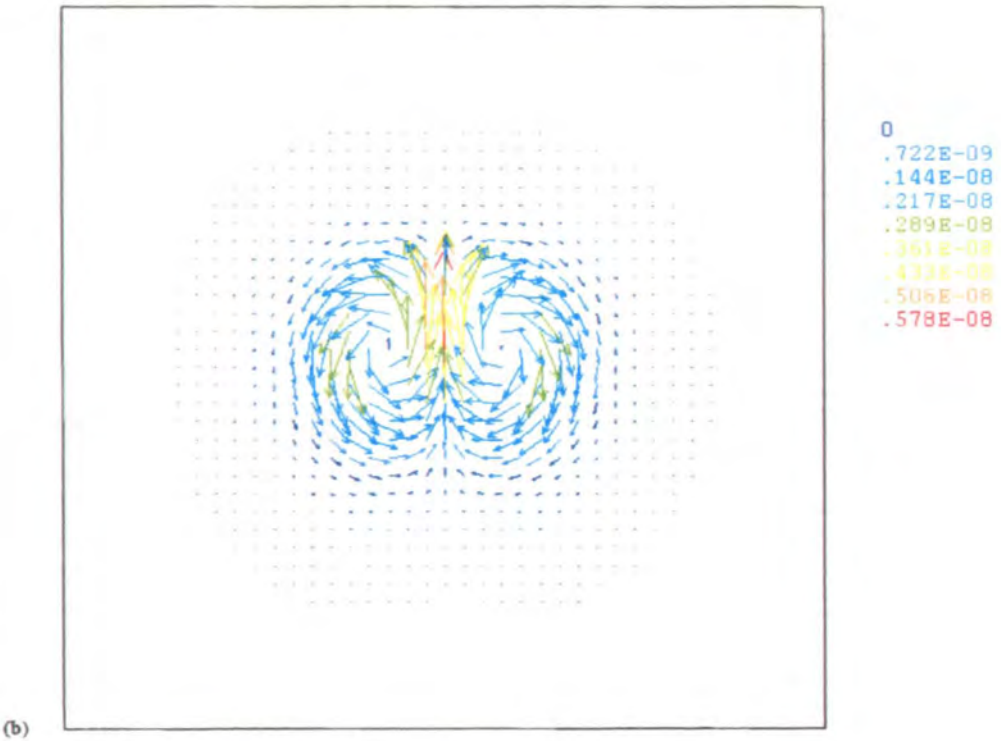

(b)

Figure 6.8 Velocity distributions in the two-dimensional square magma chamber (1 km by 1 km) after (a) 1083 and (b) 2600 years.

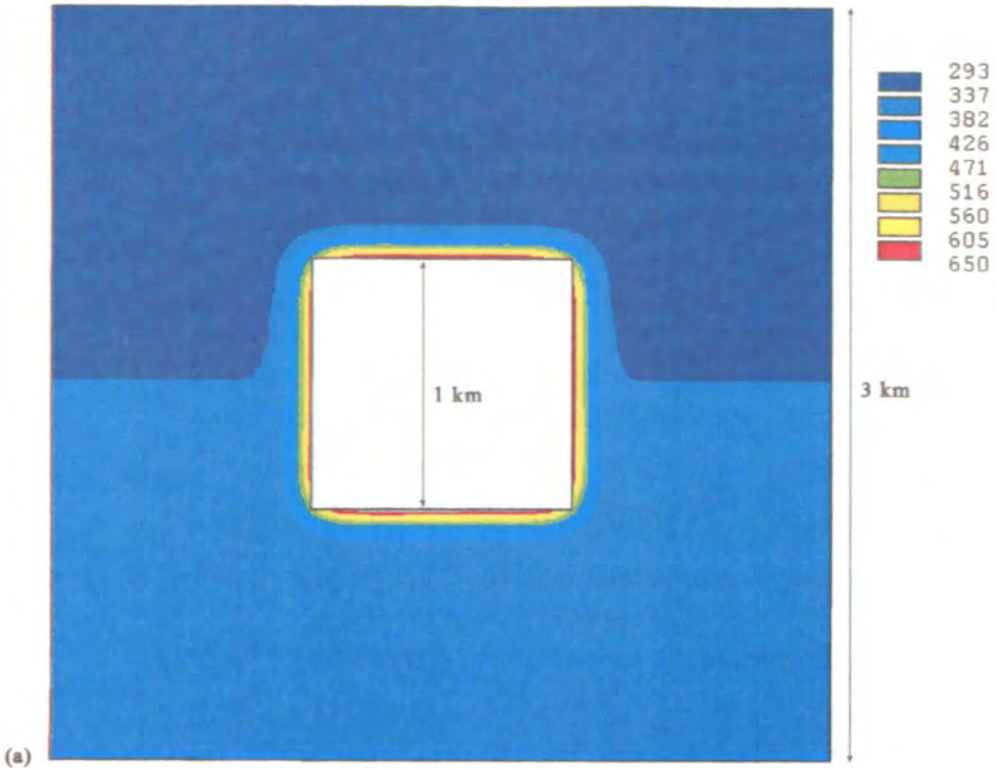

(a)

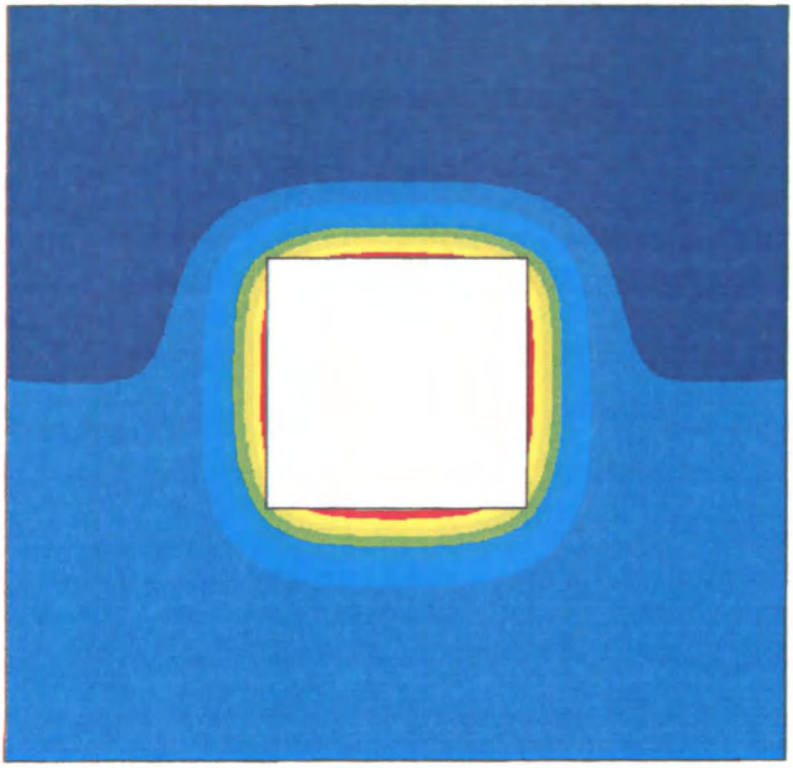

(b)

Figure 6.9 Temperature distributions in the two-dimensional country rock surrounding the square magma chamber after (a) 190 and (b) 1083 years.

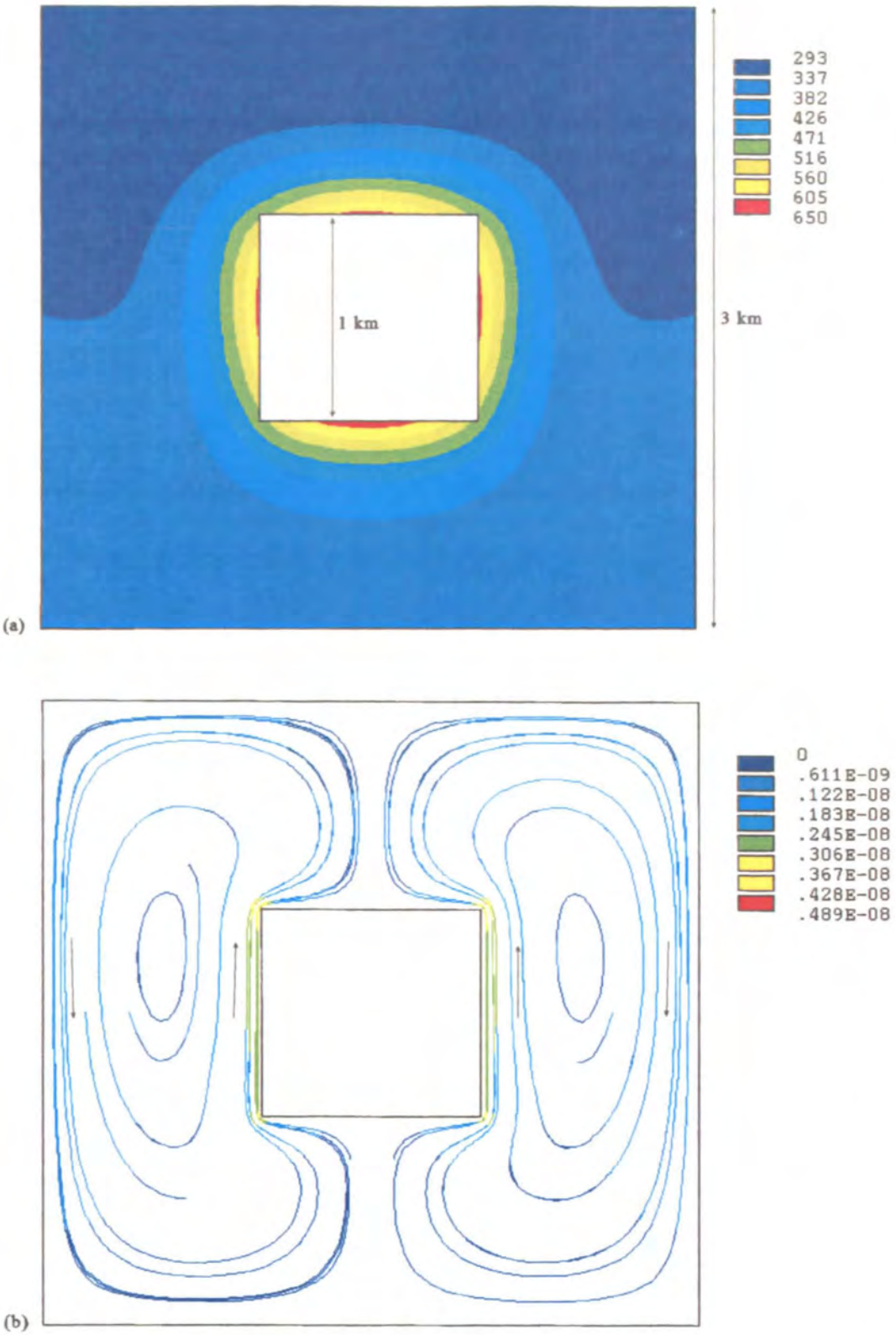

Figure 6.10 (a) The temperature distribution in the two-dimensional country rock surrounding the square magma chamber after 2600 years and (b) particle trace calculated after 15200 years. The arrows in the particle trace indicate the direction of flow.

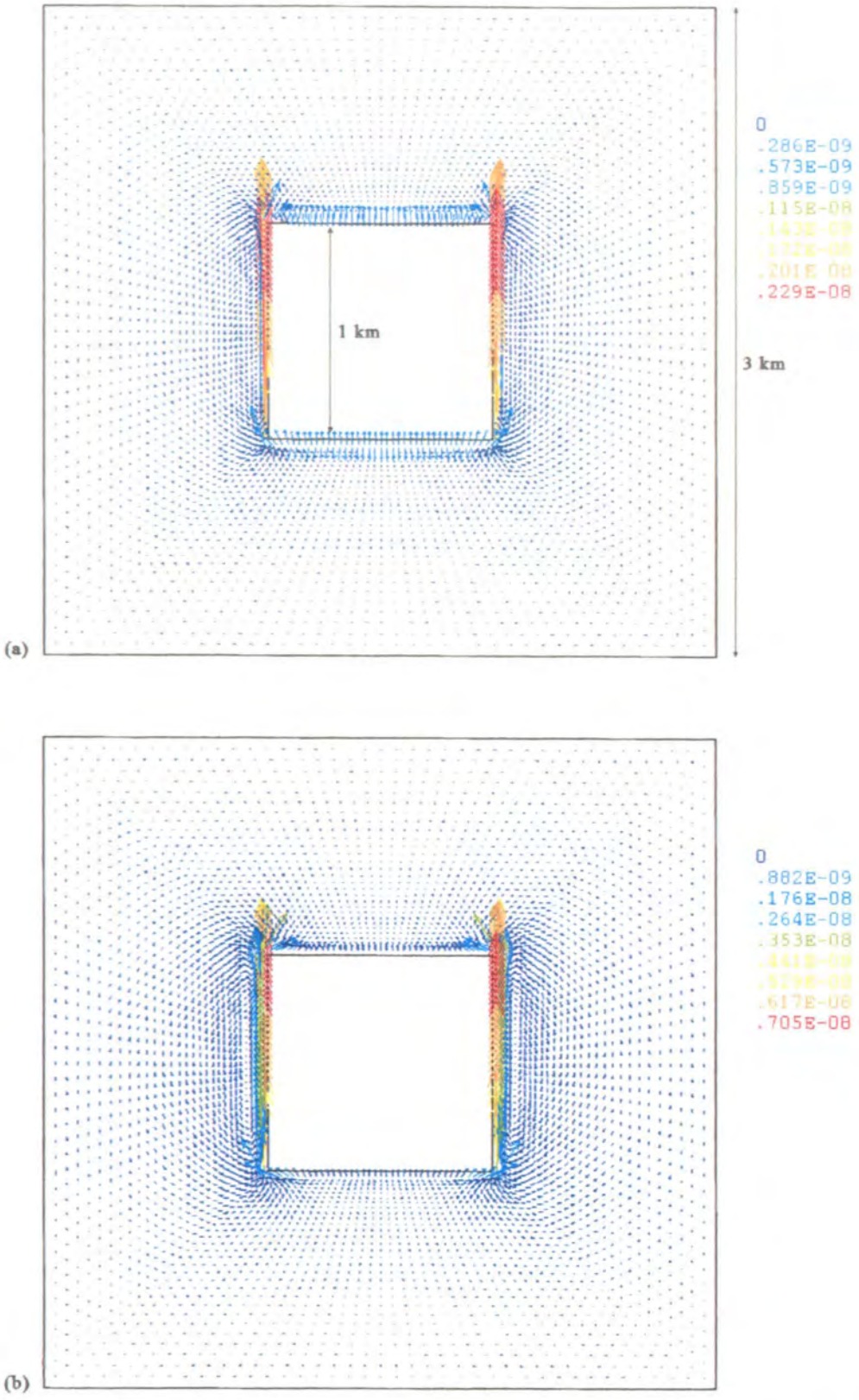

Figure 6.11 Velocity distributions in the two-dimensional country rock surrounding the square magma chamber after (a) 10.7 and (b) 90.3 years.

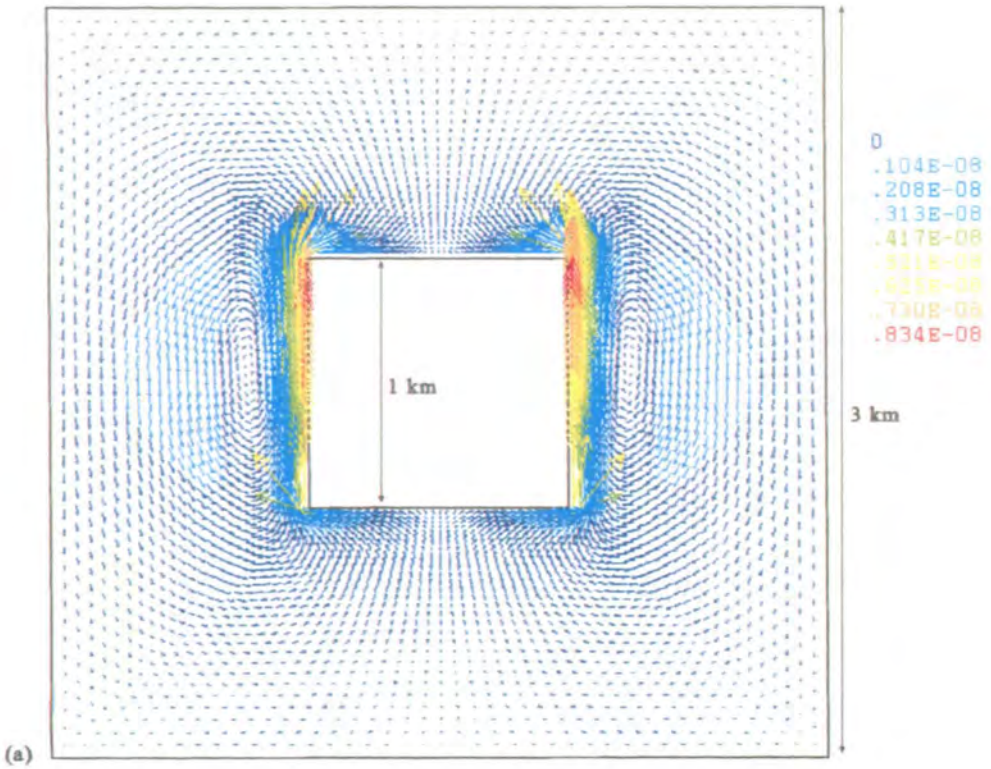

(a)

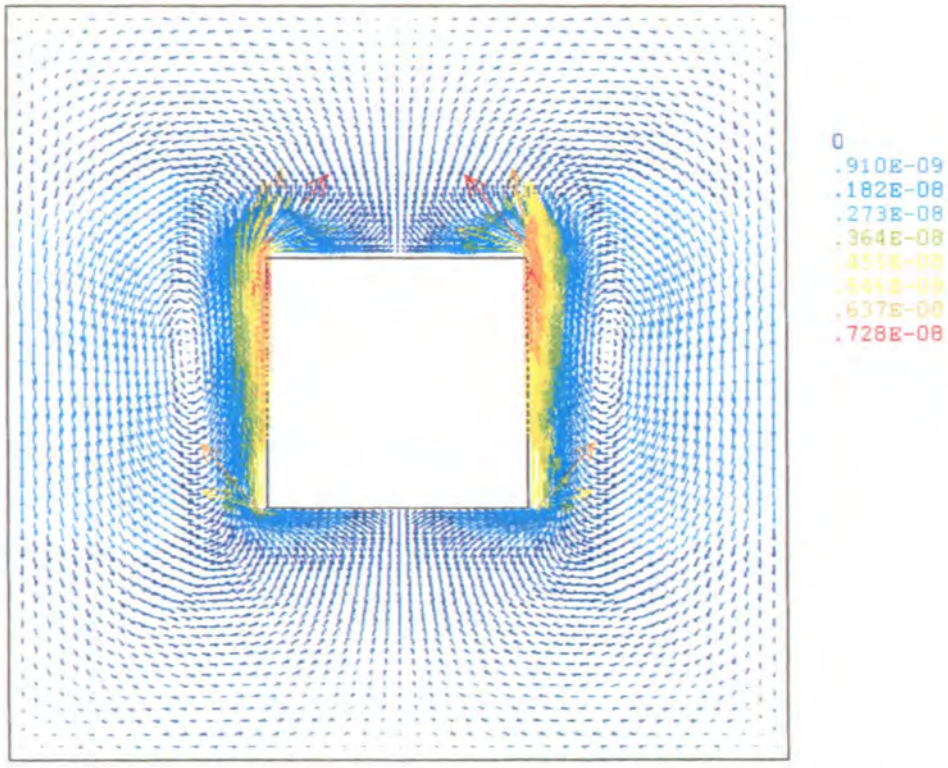

(b)

Figure 6.12 Velocity distributions in the two-dimensional country rock surrounding the square magma chamber after (a) 1083 and (b) 2600 years.

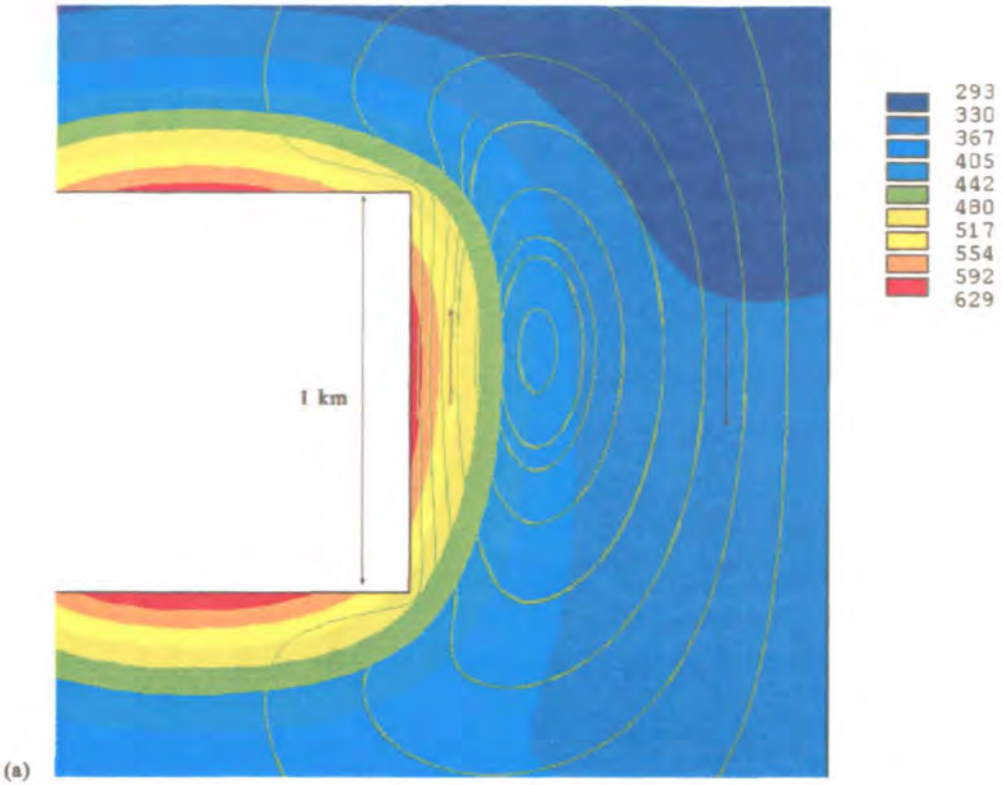

(a)

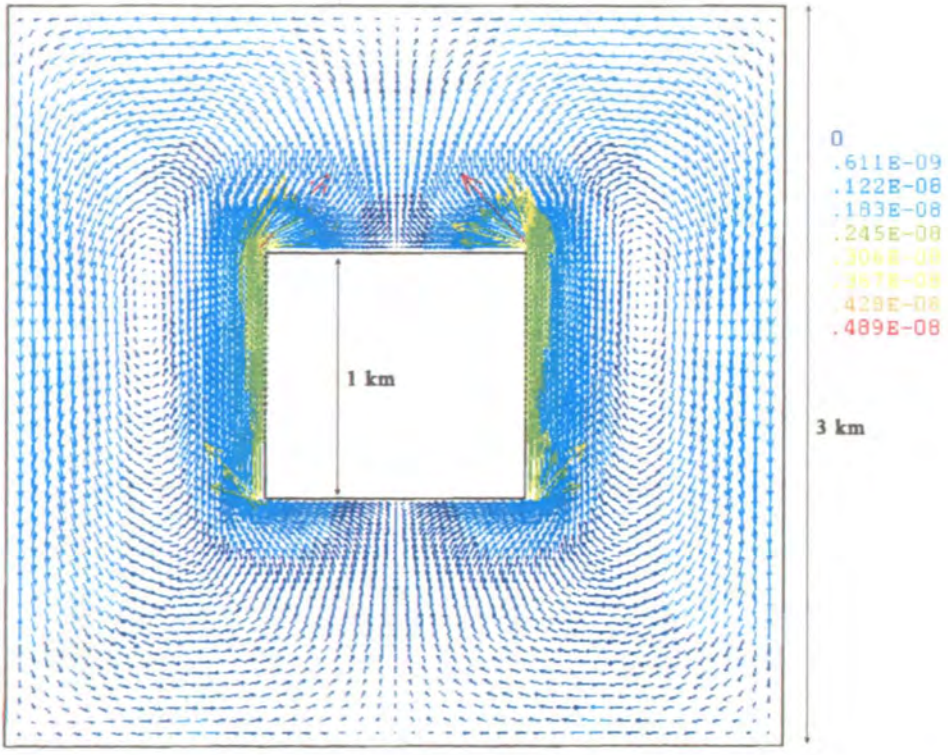

(b)

Figure 6.13 (a) Magnified view of the temperature distribution in the two-dimensional country rock surrounding the square magma chamber after 2600 years overlayed with 9 particle traces (not calibrated in order to be visible against the background colours). (b) Velocity distribution after 15200 years.

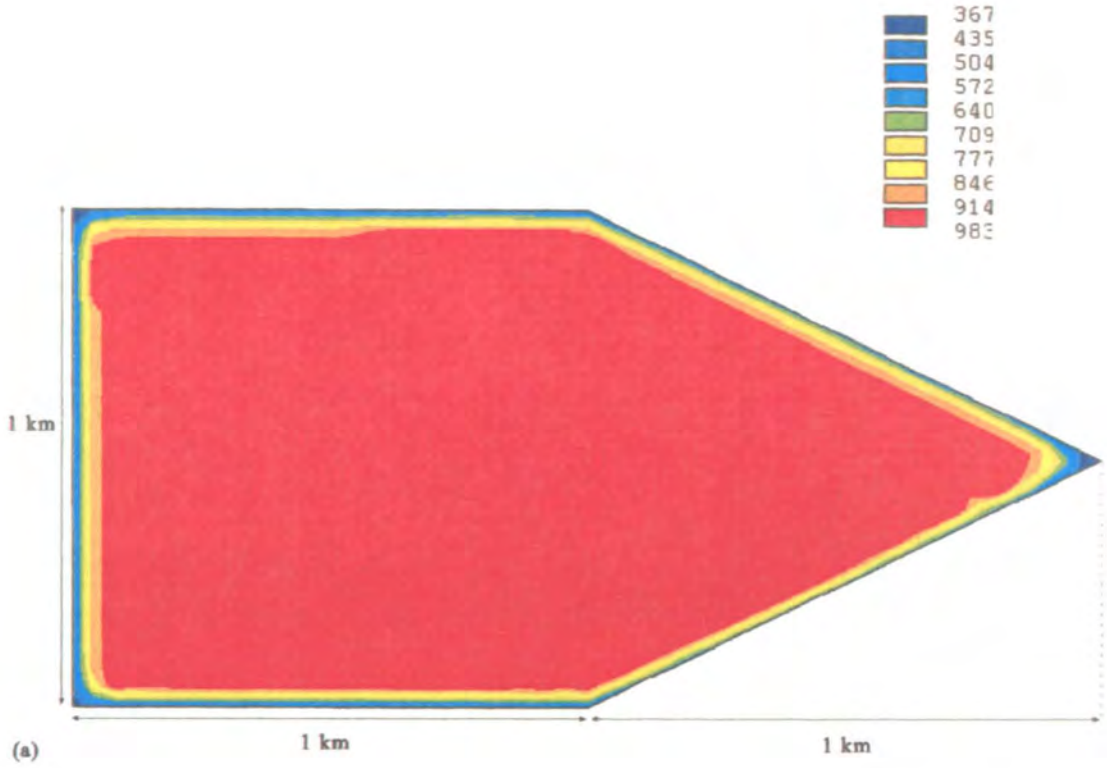

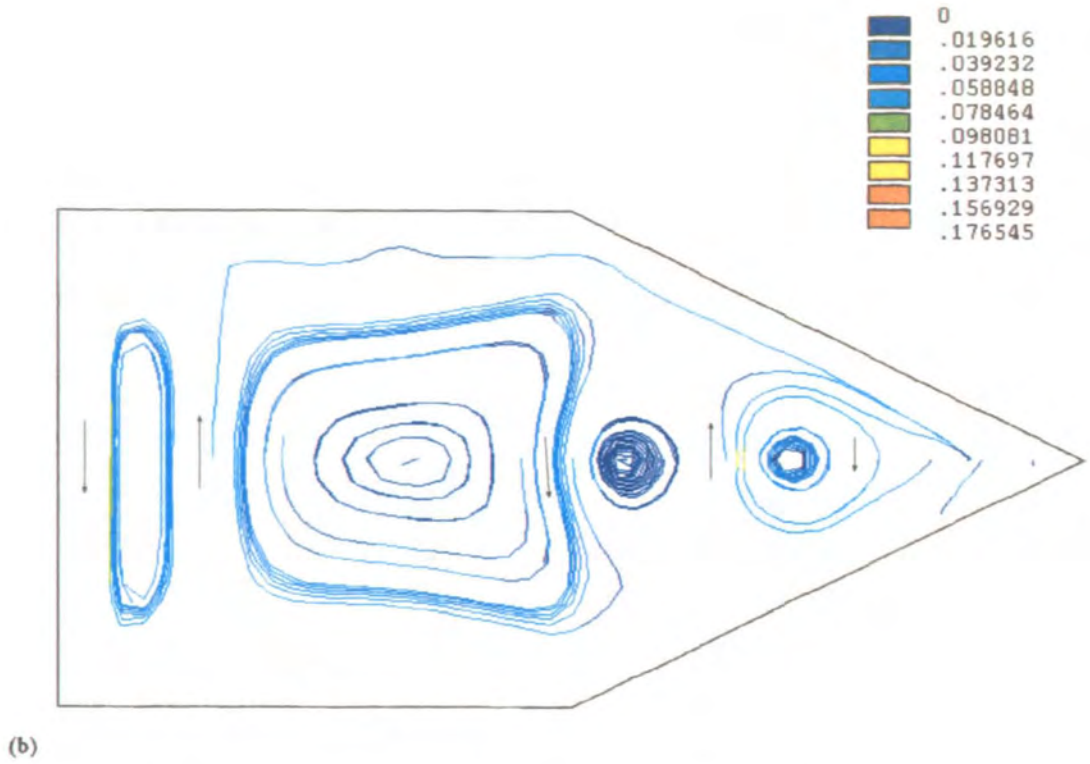

Figure 6.14 (a) Temperature distribution in thetwo-dimensional wedge-shaped magma chamber after 38.2 years. (b) Particle trace calculated after 20.7 years. The arrows indicate the direction of flow.

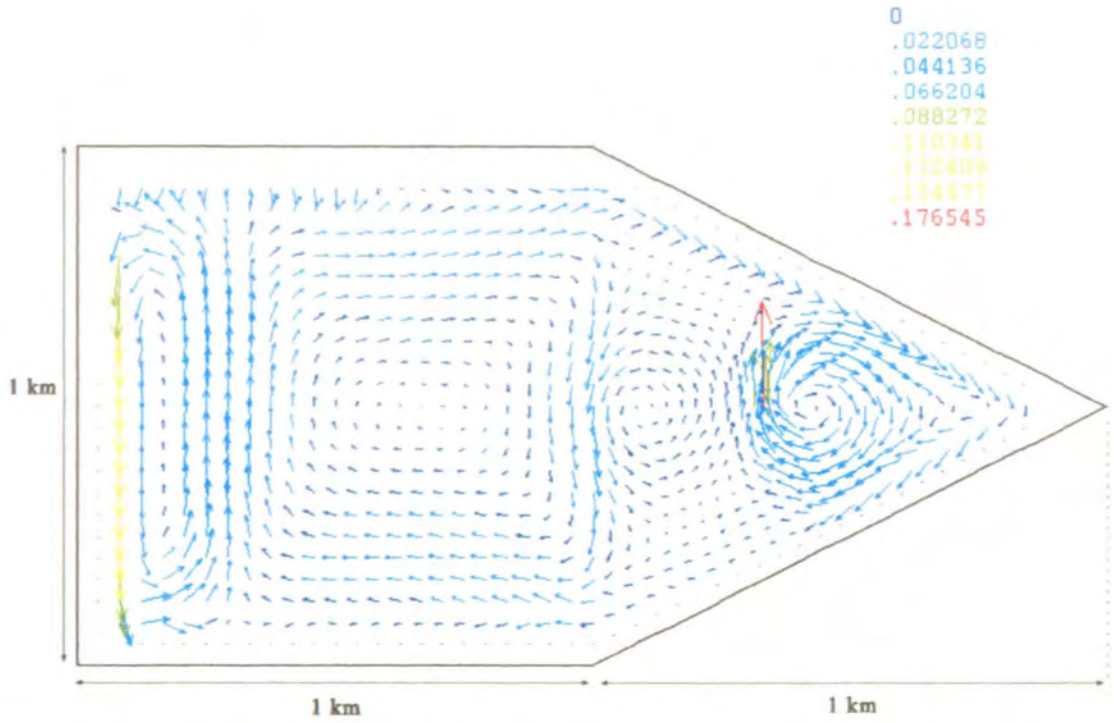

Figure 6.15 Velocity distribution in the two-dimensional wedge-shaped magma chamber after 20.7 years.

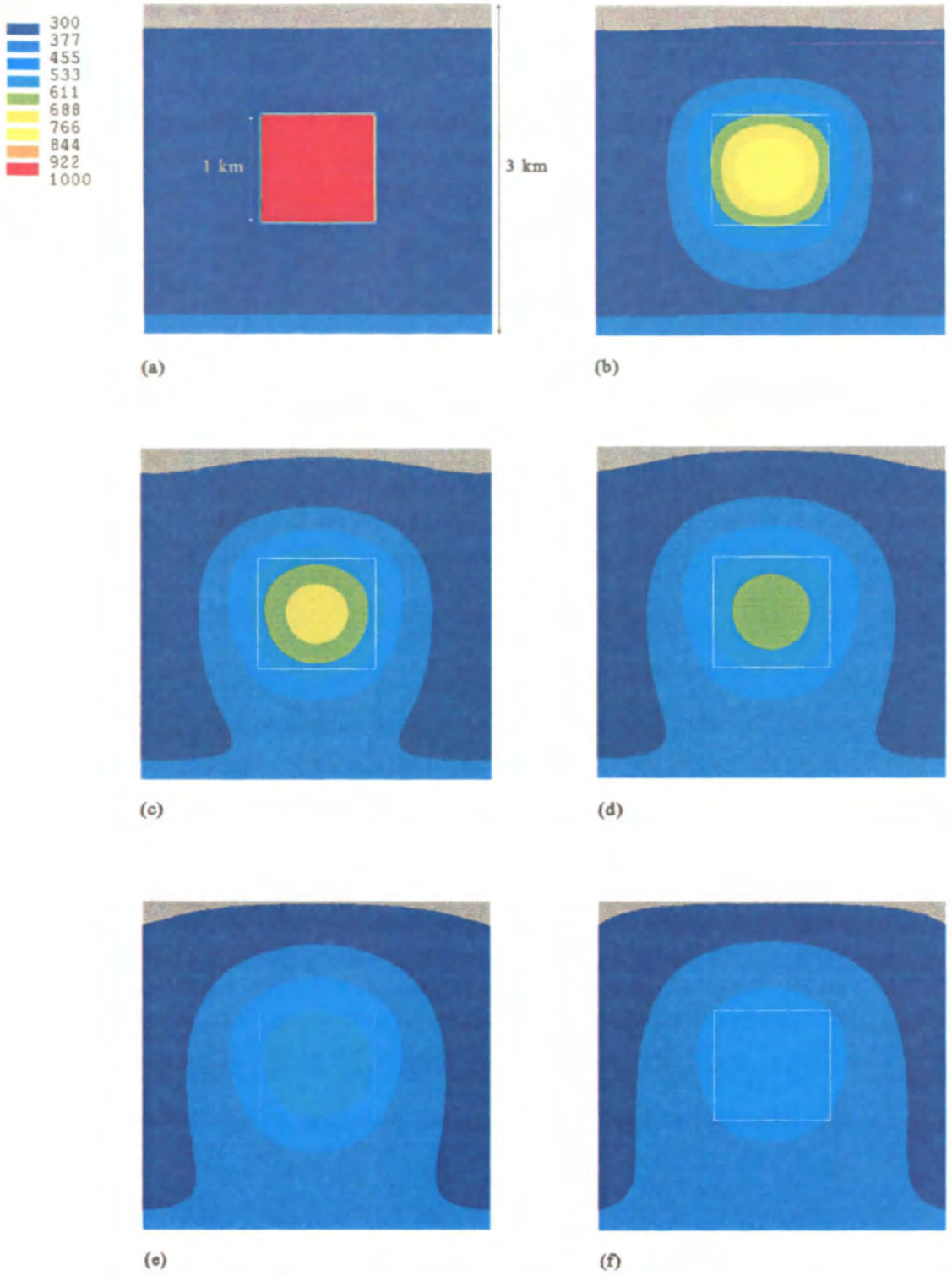

Figure 6.16 Development of the temperature distribution in the two-dimensional square chamber and the surrounding country rock over the first 27000 years with frames approximately 5400 years apart. The gray areas in each plot are uncalibrated.

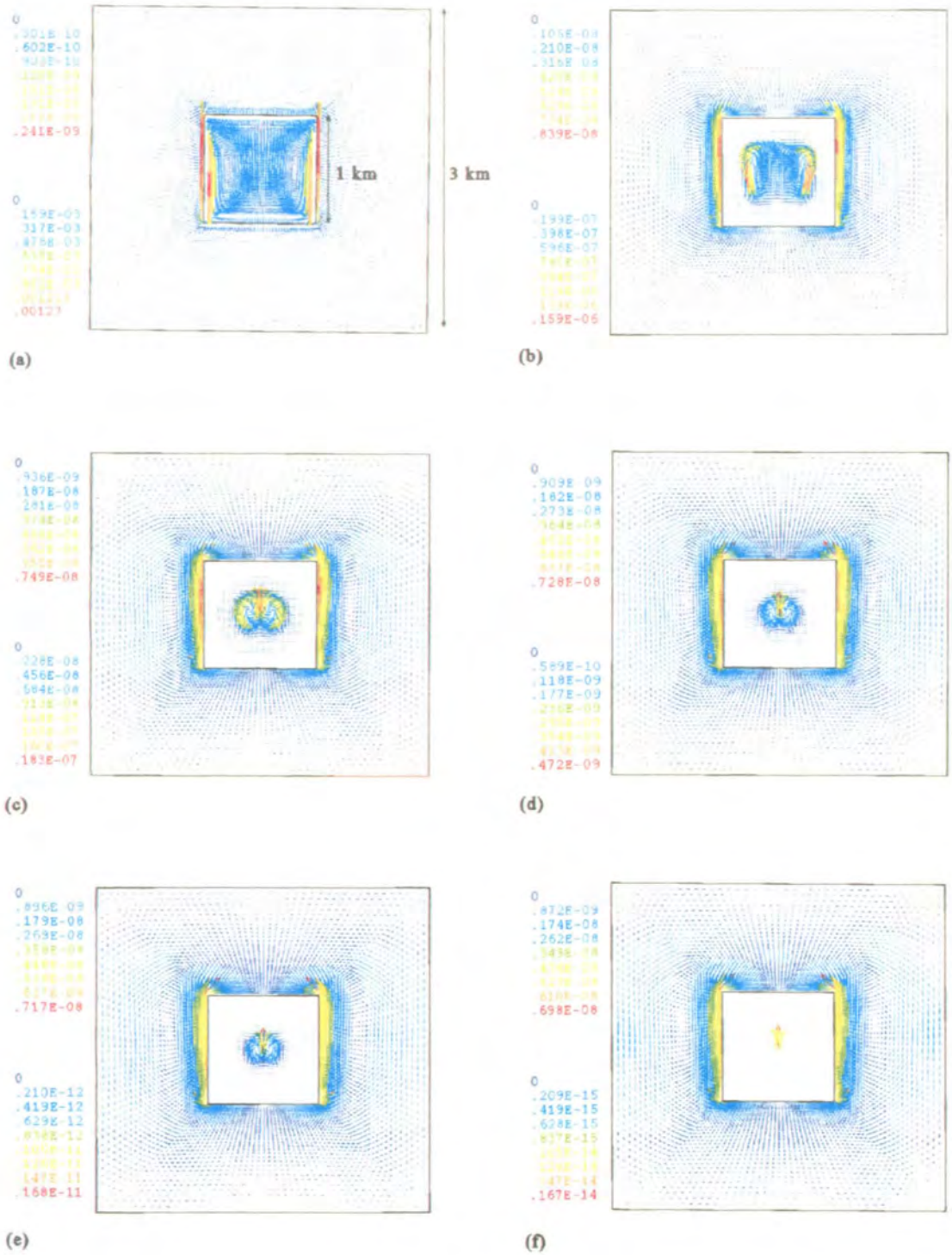

Figure 6.17 Development of the velocity distribution in the two-dimensional square chamber and the surrounding country rock over the first 5300 years with frames approximately 1060 years apart. The upper scale in each picture refers to the country rock while the bottom scale refers to the magma.

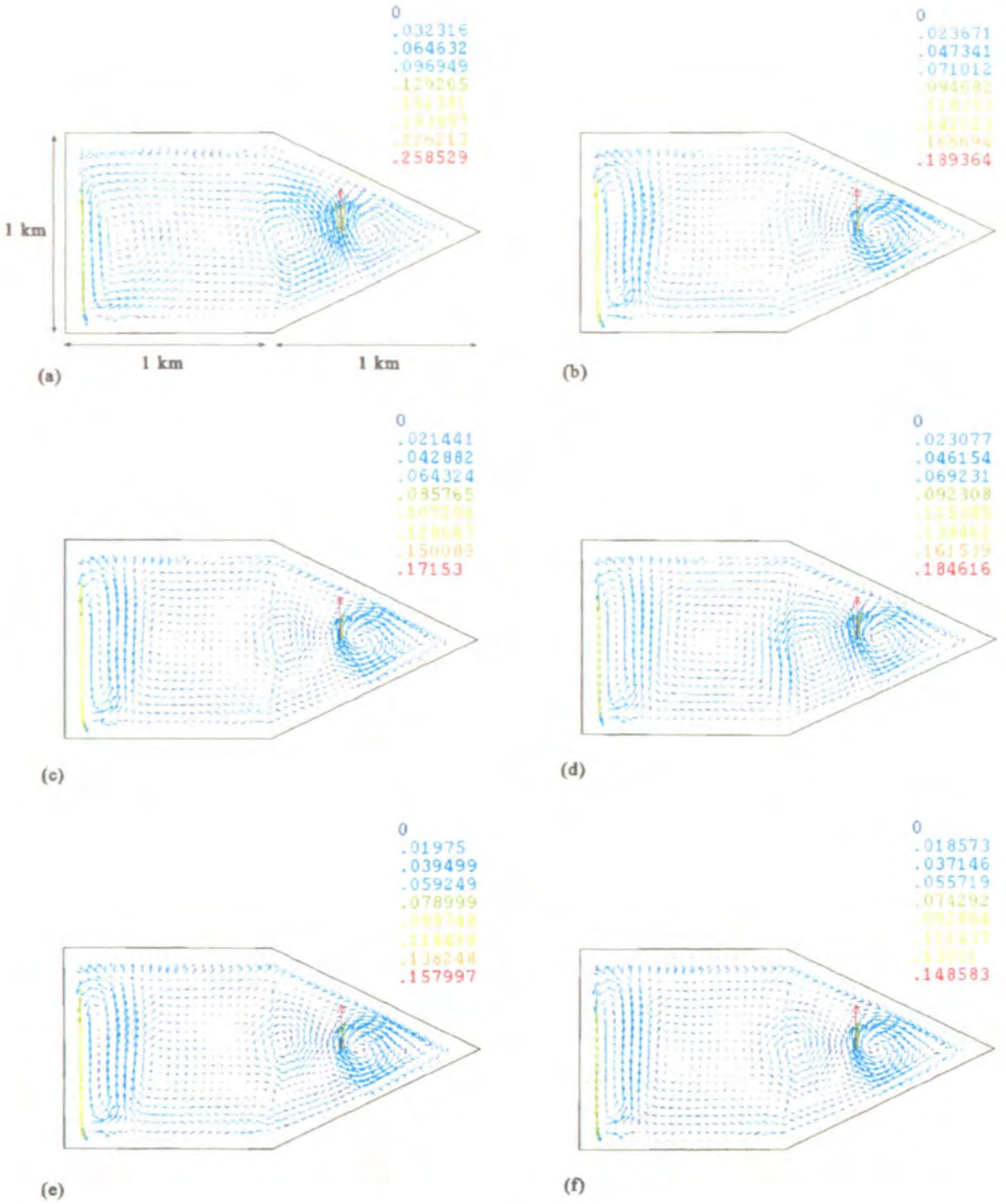

Figure 6.18 Development of the velocity distribution in the two-dimensional wedge-shaped chamber over 9 years, starting from 12.8 years with frames approximately 1.8 years apart.

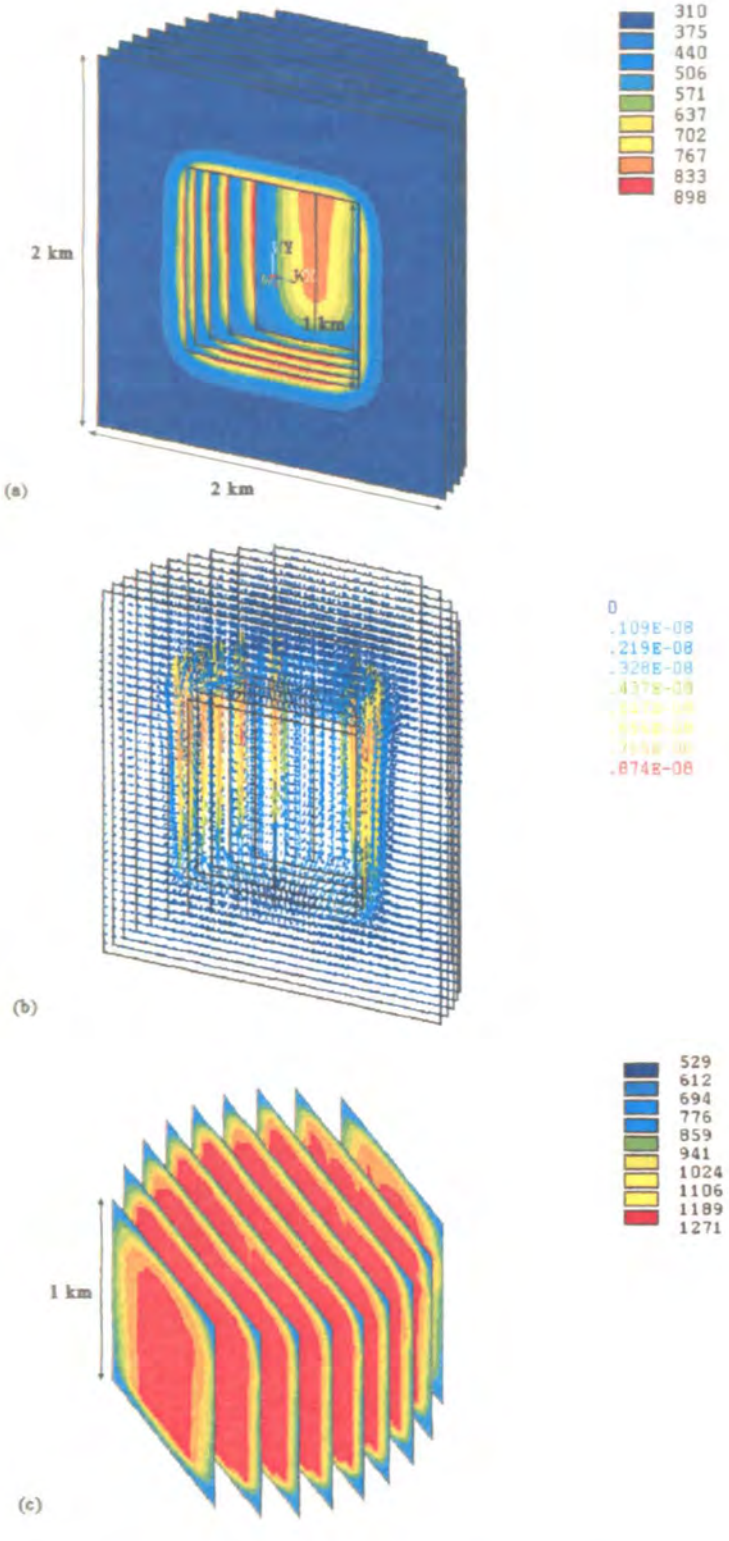

Figure 6.19 (a) Sectioned view of half of the three-dimensional country rock model showing the temperature distribution after 200 years. (b) The same sectioned view showing the velocity distribution after 200 years. (c) Sectioned view of the corresponding three-dimensional magma chamber showing the temperature distribution after 200 years.

Chapter 7

Discussion and Conclusions

7.1 Square Magma Chamber and Surrounding Country Rock

The behaviour of the magma in the square chamber during the first 1000 years is bordering on turbulent which appears consistent with the fact that the initial Rayleigh number is 2.5×10^6. The flow patterns seen in the results are complex and various. Patterns with four or five convection cells are common. The central pair of cells in **Figures 6.6(a)** and **6.7(a)** has a common central downflow rather than an upflow as is the case with double cell convection that dominates the flow for the first few months and again from about 1000 years on (compare **Figures 6.4(a)** and **(b)**). The temperature contour plot in **Figure 6.2(a)** which is at the same time as **Figure 6.7(b)** shows the cooler magma sinking through this central downflow region. Other unique flow patterns are evident in **Figures 6.2**, **6.3**, **6.5**, **6.6** and **6.7**.

After about 90 years, a noticeable region of near-zero velocities along the walls of the chamber appears. This is due to the increased viscosity of the magma because of cooling at the walls. The freezing continues throughout the remaining convection history until the frozen region is so thick that only a very small section of circulating fluid remains. After 5300 years, the magma is solid throughout. The fluid magma that exists during this freezing process also cools gradually. The associated drop in the Rayleigh number indicates a successively more stable, laminar flow, hence the dominant double cell convection pattern during the latter 4300 years of the existence of liquid magma.

Total freezing of the magma occurs a long time before the groundwater ceases convecting.

This is because the freezing temperature of the magma is still higher than the initial temperature of the groundwater. Indeed, the freezing of the magma means that heat passes through it by conduction only. Since conduction is a less efficient means of heat transport than convection, the average rate of heat dissipation into the groundwater will be at a minimum after freezing and convection of the groundwater can be sustained for a very long period.

The extent to which the flow of the groundwater in the country rock outlives the flow of the magma is evident in the particle trace in **Figure 6.10(b)**, calculated after 15,200 years. Velocities here are of the order of 10^{-9} $m.s^{-1}$. The magma has slowed to similar velocities after only 2100 years (see **Figure 6.17**). Furthermore, magma velocities are at their greatest after only 9 years whereas groundwater velocities are at their maximum after 1000 years.

It is worth noting here that an increase in the size of the model could cause significant changes in the results. From the expression given for the Rayleigh number in **Chapter 2**, equation (2.7), it is seen that there is a third order dependence on the characteristic dimension, *d*.

The characteristic dimension is defined in **Chapter 2** as being the distance covered by the largest temperature difference in the system. For the country rock model, the largest temperature difference is initially between the newly intruded magma and the surface of the earth. This difference is vertically orientated. An increase in the Rayleigh number is thus caused by an increase in the depth of the country rock. A similar rule holds for the magma chamber: an increase in the chamber depth increases the Rayleigh number. In both systems, an increase in the Rayleigh number implies a movement of the system from the laminar to the turbulent end of the flow regime spectrum. This causes the flow pattern to become more chaotic and as a result, less predictable.

By the above argument, increasing the horizontal dimensions of the models will not cause a change in the Rayleigh number. It may, however, cause other changes in the flow pattern. For instance, the two-dimensional country rock models used in this thesis have impermeable limits to the left and right. Moving these limits further from the centre of the system better simulates a permeable country rock model that stretches to infinity on either side. (Of course, different boundary conditions may be used to reach this goal rather than changing the model size. This was done for the three-dimensional cylindrical model.)

7.2 Wedge-shaped Magma Chamber and Surrounding Country Rock

Although it was not possible to run the wedge-shaped chamber model for as long a period as the square chamber model, there were some useful results. An example is the particle trace in **Figure 6.14(b)** which shows four very different convection cells. The two cells in the triangular part of the chamber are the fastest rotating cells of the four. The maximum velocities occur mostly at the central upwelling common to this pair of cells as seen in **Figure 6.15**. A sequence of results from this run are shown in the velocity distribution plots of **Figure 6.18**.

Although this model is two-dimensional, the assumption that it be infinite in extent in a direction normal to the page allows comparison of surface to volume ratios of the square portion and the triangular portion to be obtained by perimeter to area ratios.

The perimeter to area ratio of the triangular section of the chamber is $2.236 : 0.5 = 4.472$ (counting only the two external edges of the triangle) and that of the square section is $3 : 1 = 3$ (again counting only the external edges). One would therefore expect more heat to be dissipated from the triangular section. A stronger temperature gradient would thus develop there because hot material moving into the triangular section would mix with the cool magma at the walls, resulting in more vigorous convection.

The computer resources available did not allow for the refinement of the mesh along the chamber boundary as this would require the same refinement along the contact edges (and hence throughout large regions) of the country rock model. (The code I wrote to couple the magma and the country rock assumed matching nodes along the contact edges. See section **7.4**.) Such extensive refinement would increase the number of nodes beyond the available limit.

Despite this drawback, it is still possible to see in **Figure 6.15** that the boundary layer near the tip of the triangular part of the chamber is thinner than along the top and bottom margins of the square part of the chamber and is hence a region of higher shear. The work of Rice and von Gruenewaldt (1995) suggests that mineralisation may be enhanced in regions of high shear. More conclusive evidence for the high shear zone observed in **Figure 6.15** would thus explain the formation of certain deposits (such as platinum) in the Bushveld Complex that occur in narrow, confined parts of the intrusion.

The groundwater flow around the chamber was relatively uninteresting and stable throughout the short run period but may, if run further, exhibit features of greater interest. A similar pattern to the square chamber model, i.e. one with upwelling of groundwater against the side walls of

the chamber was obtained. Velocities were also similar in magnitude to the square chamber-country rock model.

Finally, note the difference in the speed of the flow between the square chamber and the wedge-shaped chamber which has a viscosity two orders of magnitude smaller than the square chamber (to more closely approximate a more mafic environment). This can be seen by comparing **Figures 6.6(b)** and **6.18(a)** that are at approximately the same time (10.7 and 12.8 years respectively). The maximum velocity in the square chamber after 10.7 years is 4.13×10^{-4} $m.s^{-1}$ and in the wedge-shaped chamber after 12.8 years is 0.259 $m.s^{-1}$, about 600 times greater.

7.3 Cylindrical Magma Chamber and Surrounding Country Rock

The flow of magma in the three-dimensional cylindrical chamber is (according to the small set of results - namely 200 years - obtained thus far) highly asymmetric showing that assumptions about symmetry, made in order to save time and computational demand are, in this case, not valid. More results will have to be accumulated before further comment can be made.

The groundwater results obtained thus far do not appear to depart significantly from the two-dimensional models. In the country rock, upwelling of groundwater occurs uniformly along the entire cylindrical magma chamber wall. Again, more results will have to be generated before further comment can be made.

7.4 Animations

The first four animations (*anim1.mov* to *anim4.mov*) on the compact disc at the back of the thesis are of results already described and were identified in **Chapter 6**. Commentary on the remaining animations, constructed from results obtained by Andrè Botha, a fellow physics MSc student working on the same project as set out in this thesis, follows. More information about these animations may be found in the MSc thesis by A. Botha (1998).

7.4.1 Sill-shaped Magma Chamber

The file *anim5.mov* shows a velocity vector animation in the left arm of a T-shaped magmatic intrusion modelled without country rock. The magma is supposed to have intruded upwards

from the mantle and then horizontally to the left and right between two layers of crustal rock. The most interesting feature of the flow pattern in this more basaltic magma chamber (aside from the upwelling through the centre of the chamber and very strong downward return flow along its curved sides) is the wave-like progression of convection cells towards the end of each horizontal limb.

7.4.2 Sill-shaped Magma Chamber with Conductive Country Rock

For this model, the two-dimensional sill-shaped magma chamber of the previous animation was enclosed in purely conductive country rock, i.e. there was no modelling of groundwater flow. The animation of the velocity vector results (*anim6.mov*) serves to indicate the way in which this chamber cools and freezes over long periods of time (thousands of years - see Andrè Botha's MSc thesis for details).

The long, thin foot and limbs of this chamber conduct large amounts of heat into the country rock because of their high surface area to volume ratios (or the two-dimensional equivalent thereof) and are thus the first parts of the chamber to cool, leaving a only a small region of convecting material in the centre of the chamber as was seen in the square magma chamber model.

7.4.3 High Aspect Ratio Cylindrical Chamber

Results of this three-dimensional cylindrical model with a diameter to height ratio of 5 and without an adjacent covering of country rock are in files *anim7.mov* and *anim8.mov*. The files are animations of the velocity vectors in vertical and horizontal sections through the centre of the chamber respectively. The horizontal section animation displays almost perfect four-fold symmetry. The axes of symmetry and the centres of the major convection cells coincide with features in the finite element mesh used to calculate the results.

In particular, the centres of the major convection cells coincide with the most distorted elements in the mesh. Although these elements are not distorted beyond reasonable limits, they could be preferred regions of numerical feeding (S. van Wyk, personal communication, 1998) and hence sites for the development of high velocities and later, convection cells. The extent to which the mesh geometry influenced the observed symmetry could be made clearer by running the model with one or more different meshes.

Despite this problem, the results obtained from the model are not without use. They provide insight into such quantities as the duration of the cooling process, the magnitude of the velocities and the type of flow regime adopted by the magma.

7.4.4 Visualization Techniques

The file *anim9.mov* contains a demonstration of techniques devised by Soteri Panagou, then an honours student in the Rhodes University Computer Science Department, that will make possible an easier visualization of three-dimensional results of the types described in this thesis.

The first part of the animation shows a transient "cat-scan" of a the temperature distribution in a three-dimensional doughnut-shaped magma chamber. Each scan through the chamber, which consists of sectioned views, each section being slightly lower than the last, occurs at the next stage of the cooling history of the chamber. In this way the full three-dimensional data set at every time step may be viewed.

The second part of the animation shows a rotational visualisation technique whereby a transparent three-dimensional view of a magma chamber may be rotated in any direction in real time in order to view it from the desired angle.

7.5 Predicting the Location of Mineral Deposits

The first discovery that came out of the attempted modelling of magma chambers and surrounding groundwater flow in order to predict the location of mineral deposits was the complexity of the system and the extensive demands on computer hardware and time. The project as it stands at the time of writing requires further development and the next section contains some ideas that may be pursued in this regard.

The results so far do suggest areas (of the chamber or of the country rock) in which minerals are likely to appear. For a particular mineral, one could assume a concentration distribution throughout the melt or the groundwater at the start of modelling that varies according to known data or to some hypothetical scenario. Then throughout the modelling process one can identify regions that become hot enough to cause the mineral to dissolve. Consideration of the fluid velocity field in these regions indicates the speed with which the dissolved mineral is transported and the direction in which it flows. Eventually the mineral can be followed into regions in which

the temperature has dropped to a value sufficiently low to cause the precipitation and deposition of the mineral. If one of these regions is the common depositional area of a number of sources in the magma chamber or country rock (as inferred from the numerical results), it will be likely that the mineral will be highly concentrated in that region. Further evolution of the system may lead to repeated cycles of mineral transport and deposition.

Consider the country rock surrounding the square magma chamber. The main feature of the flow pattern is strong upwelling against the walls of the magma chamber. The entire sub-chamber region of country rock contributes fluid to this upwelling. Once fluid reaches the upper regions of the rock, the flow dissipates into a broad, cooler band that slowly returns to the bottom of the model via the outer edges. Such a flow pattern may cause the large scale transfer of dissolved minerals from the hot regions on either side of the chamber into the cooler regions above it on either side.

A more accurate method of prediction uses particle traces. These traces provide one with the exact destination of a small group of fluid particles after a specified amount of time along with information on temperature or any other degree of freedom. In this way they answer questions like "which flow channels are faster?", "which have a greater source area?", "which last the longest?" and "which are hotter or cooler?".

7.6 Problems With the Models and Suggestions for Improvement

The mesh refinement test carried out before the models were run was of great value. Unfortunately, limited resources did not always allow as much refinement of the models as the test suggested was appropriate. A future improvement of primary importance would be to refine meshes in some models, especially at model boundaries.

The mesh refinement test could also be modified to test the suitability of mesh patterns. Some patterns may have regions containing distorted elements that cause instability in the solution and therefore artificial results. This problem was not apparent in the results of this research but it may nonetheless have affected them.

The second problem with the model is that the "freezing" imposed by the increase in the viscosity at low temperatures is cohesive freezing only. No latent heat is drawn from the melt to simulate phase changes.

The models used in this thesis ignore the complex chemical changes that occur in the magma as it cools and in the groundwater as it is heated. The facility offered by *FLOTRAN* that allows multiple species transport could in future be used to incorporate a more accurate chemical behaviour into the model.

The models used in this thesis have simple geometries. This was in order to minimise the complexity of the problem so that the initial results could be interpreted easily and unambiguously. Problems with the model could be easily seen and solved. The models are now ready to be refined with respect to geometry (i.e. realistic, three-dimensional structure), fluid properties and other aspects. Accurate modelling of real physical intrusions should be feasible in the near future.

An improvement to the country rock models that may immediately be made is the introduction of heterogeneous permeability. A common, almost ubiquitous, geological feature of country rock as modelled in this thesis is horizontal layering. Each layer may have a unique permeability. This will affect significantly the flow of groundwater.

The code I have written to couple thermally the groundwater and the magmatic fluid may be improved by discarding the restriction that nodes along the contact surfaces must match.

Other additions to the code may improve the model in the following ways. Cooling of the country rock after heating may cause fracturing. The associated increase in permeability could be incorporated into the model at the appropriate time.

After each time step, the newly frozen regions along the boundary surface of the magma chamber may be made permeable, allowing the flow of groundwater.

Multiple injections of magma may be simulated by periodically increasing the size of the chamber (if necessary) and the temperature of the melt.

References

Adler, P. M., Jacquin, C. G., Quiblier, J. A., "Flow in Simulated Porous Media", International Journal of Multiphase Flow, **16**, no. 4, 691-712, Pergamon Press/Elsevier, Great Britain, 1990.

Antonopoulos, V. Z. and Papazafirou, Z. G., "Solutions of One-dimensional Water Flow and Mass Transport Equations in Variably Saturated Media by the Finite Element Method", Journal of Hydrology, **119**, 151-167, Elsevier Publishers B. V., Amsterdam, 1990.

Bartlett, R. W., "Magma Convection, Temperature Distribution and Differentiation", American Journal of Science, **267**, 1067-1082, 1969.

Bathe, K., "Finite Element Procedures", Prentice Hall, New Jersey, 1996.

Bear, J., "Dynamics of Fluids in Porous Media", Dover Publications Inc., New York, 1972.

Botha, A., Frescura, F., Harrison, K., Moore, J., Rice, A., "Mathematical Modelling of Magma", 39th Annual Congress of the South African Mathematical Society, Cape Town, November 1996.

Botha, A., Rice, A., Harrison, K., Moore, J. M., Bangay, S., Clayton, P., Panagou, S., "Three-dimensional Calculations of Convecting Freezing Magma Chambers and Attendant Hydrothermal Circulation in Surrounding Country Rock", Abstracts, American Geophysical Union Annual Meeting, San Francisco, California, December 1997.

Bottinga, Y. and Weill, D. F., "The Viscosity of Magma Silicate Liquids: a Model for Calculation", American Journal of Science, **272**, 438-475, 1972.

Bottinga, Y., Weill, D., Richet, P., "Density Calculations for Silicate Liquids. I. Revised Method for Aluminosilicate Compositions", Geochimica et Cosmochimica Acta, **46**, 909-919, 1982.

Brookes, A. N. and Hughes, T. J. R., "Streamline Upwind/Petrov-Galerkin Formulations for Convection Dominated Flows with Particular Emphasis on the Incompressible Navier-Stokes Equations", Computer Methods in Applied Mechanics and Engineering, **32**, 199-259, North-Holland, 1982.

Currie, I. G., "Fundamental Mechanics of Fluids", McGraw-Hill Inc., New York, 1993.

Eales, H. V., Botha, W. J., Hattingh, P. J., de Klerk, W. J., Maier, W. D., Odgers, A. T. R., "The

Mafic Rocks of the Bushveld Complex: a Review of Emplacement and Crystallization History, and Mineralization in the Light of Recent Data", Journal of African Earth Sciences, **16**, 55-76, 1993.

Eichelburger, J. C., Gooley, R., Nitsan, U., Rice, A., "A Mixing Model for Andesitic Volcanism", EOS Transactions, American Geophysical Union, **57**, 1024, 1976.

Elder, J., "The Bowels of the Earth", Oxford University Press, London, 1976.

FLOTRAN Theory Manual, Ansys Theory Reference - Chapter 7, *Ansys*, Canonsburg, PA, USA.

Freeze, R. A. and Cherry, J. A., "Groundwater", Prentice-Hall Inc., New Jersey, 1979.

Hayba, D. O. and Ingebritsen, S. E., "Multiphase Groundwater Flow Near Cooling Plutons", Journal of Geophysical Research, **102**, no. B6, 12235-12252, 1997.

Hughes, T. J. R., Liu, W. K., Brooks, A., "Finite Element Analysis of Incompressible Viscous Flows by the Penalty Function Method", Journal of Computational Physics, **30**, 1-60, 1979.

Huppert, H. E. and Sparks, R. S. J., "The Fluid Dynamics of a Basaltic Magma Chamber", Contr. Min. Pet., **75**, 279-289, 1980.

Knudsen, J. G. and Katz, D.L., "Fluid Dynamics and Heat Transfer ", McGraw-Hill Inc., New York, 1958.

Krishnamurti, R., "On the Transition to Turbulent Convection", Journal of Fluid Mechanics, **42**, 309, 1970.

McBirney, A. R. and Murase, T., "Rheological Properties of Magmas", Ann. Rev. Earth Planet. Sci., **12**, 337-357, 1984.

Norton, D. L., "Pore Fluid Pressure Near Magma Chambers", from "The Role of Fluids in Crustal Processes", Geophysics Study Committee, Commission on Geosciences, Environment and Resources and National Research Council, National Academy Press, Washington D.C., 1990.

Norton, D. and Knapp, R., "Transport Phenomena in Hydrothermal Systems: the Nature of Porosity", American Journal of Science, **277**, 913-936, 1977.

Norton, D. and Knight, J., "Transport Phenomena in Hydrothermal Systems: Cooling Plutons", American Journal of Science, **277**, 937-981, 1977.

Ockendon, H. and Ockendon, J. R., "Viscous Flow", Cambridge University Press, Cambridge, 1995.

Patankar, S. V., "Numerical Heat Transfer and Fluid Flow", Hemisphere, New York, 1980.

Rice, A., "Are Stringers a Manifestation of Solute Banding?", Minerology and Petrology, **54**, 137-147, 1995.

Rice, A., Botha, A., Harrison, K., Moore, J. M., Bangay, S., Clayton, P., Panagou, S., "Solidifying Magma Chambers and the Mobilisation of Hydrothermal Circulation in Country Rock", Second South African Conference on Applied Mechanics, Cape Town, January 1998.

Rice, A., Botha, A., Harrison, K., Moore, J. M., Bangay, S., Clayton, P., Panagou, S., "Three-dimensional Calculations of Transport Processes Associated with Convection in Freezing Magma Chambers and Attendant Hydrothermal Circulation in Country Rock", Abstracts, South African Geophysical Association Fifth Technical Meeting, Swakopmund, Namibia, September 1997, 77-80.

Rice, J. G. and Schnipke, R. J., "A Monotone Streamline Upwind Finite Element Method for Convection-dominated Flow", Computer Methods in Applied Mechanics and Engineering, **48**, 313-327, North-Holland, 1985.

Rice, A. and von Gruenewaldt, G., "Shear Aggregation (Convective Scavenging) and Cascade Enrichment of PGEs and Chromite in Mineralized Layers of Large Layered Intrusions", Minerology and Petrology, **54**, 105-117, 1995.

Robson, G. R., "Thickness of Etnean Lavas", Nature, **216**, 251-252, 1967.

Shaw, H. R., "Comments on Viscosity, Crystal Settling and Convection in Granitic Magmas", American Journal of Science, **263**, 120-152, 1965.

Turcotte, D. L. and Schubert, G., "Geodynamics. Applications of Continuum Physics to Geological Problems", John Wiley & Sons, New York, 1982.

Wang, H. F. and Anderson, M. P., "Introduction to Groundwater Modelling: Finite Difference and Finite Element Methods", W. H. Freeman & Company, San Francisco, 1982.

White, F. M., "Viscous Fluid Flow", Second Edition, McGraw-Hill, New York, 1991.

Williams, H. and McBirney, A. R., "Volcanology", Freeman, Cooper & Co., San Francisco, 1979.

Appendix 1

Derivation of Equations Governing Fluid Flow

Three governing equations evolve from the consideration of a fluid's motion subject to the conservation of mass, momentum and energy respectively. General derivations of the equations follow. Simplifications and adjustments that must be made in order to model magma and groundwater are discussed in **Chapter 3**.

A1.1 The Continuity Equation

The continuity equation is derived from the principle of the conservation of mass. Consider the small, fixed volume of space, cubic in shape, in **Figure a1.1**. For convenience, the origin of the Cartesian coordinate axes used to refer to points on the cube is placed at the centre of the cube.

The entire volume and the region immediately around it are filled with fluid which moves with some given but arbitrary velocity field. The velocity of the fluid at the origin is given by the vector (u,v,w). Consider the mass transported by the flow through shaded faces X^- and X^+ in the x-direction. The mass flow rate through X^- into the cube is $[\rho u - \frac{\partial}{\partial x}(\rho u)\frac{\Delta x}{2}]\Delta y \Delta z$ where ρ is the fluid density. Similarly, the mass flow rate through X^+ out of the cube is $[\rho u + \frac{\partial}{\partial x}(\rho u)\frac{\Delta x}{2}]\Delta y \Delta z$. Hence the net mass leaving the cube along the x-direction per unit time is $\frac{\partial}{\partial x}(\rho u)\Delta x \Delta y \Delta z$.

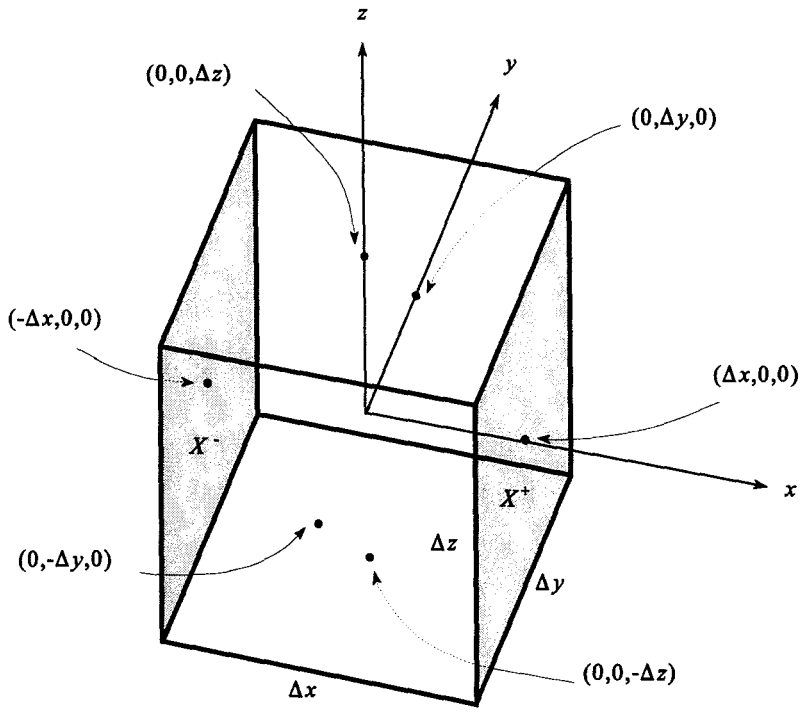

Figure a1.1 Flow through a small cubic volume.

Consideration of the two remaining pairs of opposite sides gives similar expressions for the net mass loss per unit time along the y- and z- directions. Hence the contribution to the total efflux of mass from the volume per unit time due to the mass flow across all surfaces is

$$\frac{\partial m}{\partial t} = -\left[\frac{\partial}{\partial x}(\rho u) + \frac{\partial}{\partial y}(\rho v) + \frac{\partial}{\partial z}(\rho w)\right]\Delta x\,\Delta y\,\Delta z \qquad \text{(a1.2)}$$

Now $m = \rho\Delta x\Delta y\Delta z$, thus

$$\frac{\partial \rho}{\partial t} + \frac{\partial}{\partial x}(\rho u) + \frac{\partial}{\partial y}(\rho v) + \frac{\partial}{\partial z}(\rho w) = 0. \qquad \text{(a1.3)}$$

The continuity equation, (a1.3), can be written in index notation as

$$\rho_{,t} + (\rho u_i)_{,i} = 0 \qquad \text{(a1.4)}$$

where $i = 1, 2, 3$ (corresponding to x-, y- and z-components respectively) and the commas denote differentiation. From this point forward if the same index appears more than once in one term of an equation (such as i above), the index is summed (Einstein summation convention).

A1.2 The Momentum Equation

To use the conservation of momentum principle a group of fluid particles is chosen and their flow through the problem domain is considered. To this body of particles (called a fluid element) is applied Newton's Second Law, which states that the total rate of change of momentum of a body is the sum of the external forces acting on it.

The *i*th component of the resultant force per unit volume acting on a small fluid element is

$$f_i = \rho a_i \qquad i = 1, 2, 3. \tag{a1.5}$$

The acceleration a^i is the first temporal derivative of the particle velocity. Since the velocity

$$a_i = \frac{du_i}{dt} = \frac{\partial u_i}{\partial t} + \frac{\partial u_i}{\partial x^1}u_1 + \frac{\partial u_i}{\partial x^2}u_2 + \frac{\partial u_i}{\partial x^3}u_3 \tag{a1.6}$$

depends on both time and position, this can be written more simply as

$$a_i = u_{i,t} + u_{i,j}u_j. \tag{a1.7}$$

Note that (a1.6) can also be written

$$a_i = \frac{Du_i}{Dt}. \tag{a1.8}$$

The operator *D/Dt* is called the particle derivative or substantial derivative and is useful when an Eulerian reference frame is being used. It is given by

$$\frac{D}{Dt} = \left(\frac{\partial}{\partial t}\right) + u_j\left(\frac{\partial}{\partial x^j}\right). \tag{a1.9}$$

The forces acting on the fluid element can be categorised as either body forces (forces whose point of application is distributed throughout the volume of the fluid) or surface forces (applied to the bounding surface of the body, e.g. shear stress). It is assumed here that the only body force acting on the fluid is gravitational, i.e.

$$f_i^{body} = \rho g_i \tag{a1.10}$$

and that the surface forces can be expressed in terms of the stress tensor τ_{ij}. White (1991) in fact

shows that

$$f_i^{surface} = \tau_{ij,j}. \qquad \text{(a1.11)}$$

Equation (a1.5) can now be re-written as

$$\rho u_{i,t} + \rho u_{i,j} u_j = \rho g_i + \tau_{ij,j} \qquad i = 1, 2, 3 \qquad \text{(a1.12)}$$

which is the momentum equation.

The nature of the fluids modelled allows the use of the incompressible form of the Navier-Stokes equations. In fact compressibility is usually only important in the treatment of gases. Incompressibility of a fluid implies that a parcel of fluid as it flows with time will not change its density. By using the particle derivative, one can express this as follows

$$\frac{D\rho}{Dt} = 0. \qquad \text{(a1.13)}$$

This simplifies the continuity equation to

$$u_{i,i} = 0. \qquad \text{(a1.14)}$$

This incompressibility condition allows the other governing equations to be simplified also (see **Chapter 3**).

To develop the momentum equation completely, the components of the stress tensor must be found. First it is shown that the tensor is symmetric as this reduces the number of unique components from 9 to 6.

Consider torques about the centre of a small, two-dimensional fluid element as shown in **Figure a1.2**. The total torque is the sum of the four torques shown and is

$$\tau = 2(\tau_{21}\Delta y)\frac{\Delta x}{2} - 2(\tau_{12}\Delta x)\frac{\Delta y}{2}. \qquad \text{(a1.15)}$$

However, the total torque must be equal to $\rho\Delta x\Delta y I\alpha$ where I is the moment of inertia and α is the resultant angular acceleration of the element. Thus

$$\tau_{21} - \tau_{12} = \rho I\alpha. \qquad \text{(a1.16)}$$

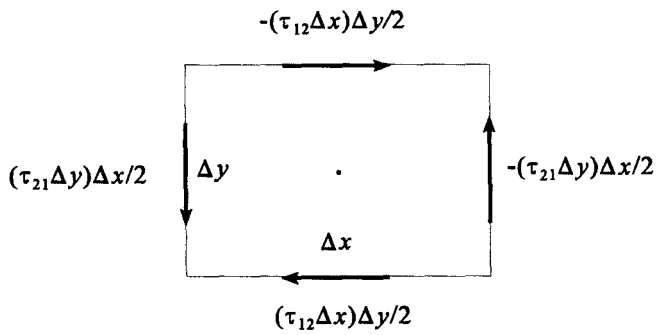

Figure a1.2 Torques about the centre of a small fluid element.

If the area of the element shrinks to zero but a finite angular acceleration is maintained then I (which depends on the spatial distribution of mass around the axis of rotation) tends to zero giving

$$\tau_{21} = \tau_{12}. \qquad \text{(a1.17)}$$

Similar calculations can be done for a three-dimensional element giving the general symmetry relation

$$\tau_{ij} = \tau_{ji} \qquad i, j = 1, 2, 3. \qquad \text{(a1.18)}$$

An initial guess at the form of the stress tensor arises from the consideration of the viscosity of the fluid. For example, an inviscid fluid offers no resistance to shearing thus only normal stresses have effect and result in an isotropic pressure in the fluid (Lamb, 1972). Thus the stress tensor components should be $-p\delta_{ij}$ where p is the hydrostatic pressure. For a viscous fluid, something must be added to this expression to account for the fluid's capacity to resist shear stresses. Therefore a deviatoric stress term d_{ij} is added giving

$$\tau_{ij} = -p\delta_{ij} + d_{ij}. \qquad \text{(a1.19)}$$

From experimental observations (Ockendon and Ockendon, 1995) it is argued that the

deviatoric term usually varies linearly with velocity and inversely with the length scale of the apparatus. Therefore d_{ij} must be a linear function of the velocity gradients. This defines a Newtonian fluid. A discussion on the suitability of the Newtonian model for magma and groundwater can be found in **Chapter 3**. The most general form of the deviatoric term is a linear combination of the velocity gradients, expressed mathematically as

$$d_{ij} = A_{ij\alpha\beta} u_{\alpha,\beta} \tag{a1.20}$$

where $A_{ij\alpha\beta}$ is a rank-4 tensor and the greek indices are summed. There is no physically preferred direction in either d_{ij} or $u_{\alpha,\beta}$ so $A_{ij\alpha\beta}$ must be the same in all sets of rotated Cartesian axes, i.e. must be isotropic. This permits the reduction of the 81 independent components of $A_{ij\alpha\beta}$ to only 3. A further condition, namely

$$A_{ij\alpha\beta} = A_{ji\alpha\beta} \tag{a1.21}$$

which arises from the symmetry of τ_{ij}, reduces the number of independent components to 2. Using a Euclidean basis, it is now possible to write

$$A_{ij\alpha\beta} = \lambda\delta_{ij}\delta_{\alpha\beta} + \mu\delta_{i\alpha}\delta_{j\beta} + \mu\delta_{i\beta}\delta_{j\alpha} \tag{a1.22}$$

where λ and μ are scalars. Substituting back into (a1.20) and then (a1.18) gives

$$\tau_{ij} = -p\delta_{ij} + \lambda\delta_{ij}u_{k,k} + \mu(u_{i,j} + u_{j,i}) \tag{a1.23}$$

which is the constitutive equation of a Newtonian fluid. λ is the bulk viscosity and measures the response of the fluid to changes in volume (the term containing λ will become zero for incompressible flow); μ is the dynamic viscosity and measures the response of the fluid to shearing and extension.

A1.3 The Energy Equation

The first law of thermodynamics states that the change in the intrinsic (internal) energy of a system as a result of its evolution from one equilibrium state to another is equal to the sum of the total work done on the system during the change and any heat which was added.

A parcel of fluid is a well-defined thermodynamic system yet it is seldom in true equilibrium

since it is never at rest. Thermodynamically however it can be considered close to equilibrium provided that its instantaneous energy in an equilibrium state is regarded as the sum of its intrinsic and kinetic energies (per unit mass). In view of this modification, Currie (1993) thus rephrases the first law as follows:

"The rate of change of the total energy (intrinsic and kinetic) of the fluid as it flows is equal to the sum of the rate at which work is being done on the fluid by external forces and the rate at which heat is being added by conduction."

External forces can be categorized as before into surface stresses and body forces. The rate at which surface stresses do work on a surface S is

$$\int_S \boldsymbol{u}.\boldsymbol{P}\,dS \tag{a1.24}$$

where $\boldsymbol{P}$ is the force vector whose jth component is given by $P_j = \tau_{ij}n_i$ where n_i is the ith component of the normal vector to the surface. By applying Gauss's theorem, (a1.24) can be written in index notation in terms of the volume V enclosed by S as

$$\int_V (u_j\tau_{ij})_{,i}\,dV. \tag{a1.25}$$

The rate at which the body forces do work is

$$\int_V \boldsymbol{u}.\rho\boldsymbol{f}\,dV = \int_V u_j\rho f^j\,dV \tag{a1.26}$$

where $\boldsymbol{f}$ is the force (vector) per unit mass.

Finally we consider heat added to the system. The expression for the rate at which heat is conducted *out* of the system is

$$\int_S \boldsymbol{q}.\boldsymbol{n}\,dS = \int_S q_j n_j\,dS = \int_V q_{j,j}\,dV \tag{a1.27}$$

using Gauss's theorem in the last step. The above formulations allow the first law of thermodynamics to be expressed mathematically as

$$\frac{D}{Dt}(\rho e + \tfrac{1}{2}\rho u_j u_j) = (u_j\tau_{ij})_{,i} + u_j\rho f_j + q_{j,j} \tag{a1.28}$$

where the operator D/Dt is again the particle derivative and e is the intrinsic energy. The particle derivative can be written out in terms of the usual (Eulerian) derivatives and the result expanded further using the product rule. Some of the terms cancel giving the following

expression for the left hand side of (a1.28):

$$\rho e_{,t} + \rho u_k e_{,k} + \rho u_j u_{j,t} + \rho u_j u_k u_{j,k} \tag{a1.29}$$

and it can be seen that the first term on the right-hand side of (a1.28) is equivalent to

$$u_j \tau_{ij,i} + \tau_{ij} u_{j,i}. \tag{a1.30}$$

When the above expressions are substituted back into (a1.28), some of the terms form the product u_j multiplied with the momentum equation. These terms must balance independently of the others and so drop out of the equation. What remains is a general form of the energy equation for a viscous fluid:

$$\rho e_{,t} + \rho u_k e_{,k} = \tau_{ij} u_{j,i} - q_{j,j}. \tag{a1.31}$$

The terms on the left-hand side represent the rate of change in internal energy. The first term provides for temporal changes and the second term for changes due to local convection of fluid. The terms on the right-hand side represent the internal energy change. The first term allows for the dissipation of mechanical energy (provided by surface forces) into thermal energy and the second term for the heat conducted into the fluid.

Appendix 2

APDL Macros for the Coupled Solution of Magma Chamber and Country Rock Models

Ansys uses a simple programming language called the *Ansys* Parametric Design Language (APDL). It follows a FORTRAN-like style and includes some basic structures such as *if* and *do* loops and also a wide range of special commands. *Ansys* will execute programs that make use of APDL constructs and standard *Ansys* commands (such as those that are executed when using the graphical user interface).

The macros used to aid modelling in the ways described in the body of the thesis contain a number of commands whose functions are not immediately obvious. A list of definitions thus appears below, followed by the macros themselves.

***cfclos**

Closes the file opened with the ***cfopen** command.

***cfopen,** *filename*, *ext*

Opens a text file *filename.ext*. Data may be written to this file with the ***vwrite** command and read with the ***vread** command.

d, *nodenum*, *property*, *num*

Applies a value of *num* to the *property* (e.g. temp, vel) of node *nodenum*. Used to apply

boundary conditions as the applied value remains constant during a transient analysis.

***dim**, *array-name*, array, *number-of-columns*, *number-of-rows*

Initialises the array *array-name*.

/filname, *%filename%*

Changes current database file name to the string of characters that is the value of parameter *filename*. The file name extension is assumed to be "db".

***get**, *parameter*, *entity*, *entity-number*, *property*, *sub-property*

The value of the *property* (e.g. temp, vel) of the *entity* (e.g. node, line) of number *entity-number* is assigned to *parameter*. Occasionally a *sub-property* is required (e.g. if *property* = loc, a *sub-property* of either x, y or z must be given to specify which component of the location of *entity* is required).

ic, *nodenum*, *property*, *num*

Similar to the **d** command except the value assigned serves only as an initial value for the node and may change during analysis.

lsel, *type*, , *min*, *max*

Selects all lines with numbers between *min* and *max*. If *type* = s, then the selected lines replace the previously selected line set (if one exists). If *type* = a, then the selected lines are added to the previously selected set. If only a single line is to be selected, the *max* argument can be omitted and the command takes the following form:

lsel, *type*, , *line-num*

where *line-num* is the number of the line to be selected.

***msg**, *type*, *parameter-list*

message

Writes *message* in a dialogue box. The parameters in *parameter-list* are included in the message according to format codes in *message*.

nint(*real-number*)

Returns the nearest integer to *real-number*.

nsel, *type*, , *min*, *max*

Node selection command. Arguments have similar meanings to those of the **lsel** command.

nsll, *type*, *range*

Used to select all nodes associated with the selected lines. *type* has the same meaning as the **nsel** argument of the same name. If *range* = 1, nodes at the line's endpoints are included in the selection; if **range** = 0 they are not.

set, last

Opens the most recent set of results for processing.

sf, *node-list*, *property*, *num*

Applies a value of *num* to the *property* (e.g. heat flux) of the surface formed by connecting the nodes in *node-list*. At least two nodes must appear in node-list; however if *node-list* is replaced by the argument "all", then all currently selected nodes are included in the list.

***use**, *macro-name*, *argument1*, *argument2*, ...

Runs the user-defined macro *macro-name* that takes arguments *argument1*, *argument2*, ...

***vread**, *arg*, *filename*, *ext*, , *maximum-dimension*
(*format*)

Reads data from *filename.ext* according to the *format* specification that follows and assigns data to *arg*. If *arg* is an array, a starting array element index must be given. Reading will proceed one line at a time, each line's value being assigned to the next array element until the array is full or the end of the file is reached. If the array has a dimension greater than one, ***vread** can be made to fill the array by cycling through one dimension index at a time until the specified *maximum-dimension* is reached.

***vwrite**, *arg*

(format)

Writes *arg* to the file opened with the ***cfopen** command according to the given **format** statement. If *arg* is an array, a starting array element index must be given. Each array element will be written on a new line until the array is exhausted. If the array's dimension is greater than one, ***vwrite** will always cycle through the first dimension index.

The macros I wrote for control of magma and country rock models follow. The main code is found in *master_ini.mac* and *master_loop.mac*. The subroutines called by the main code follow these master macros.

master_ini.mac

```
! Part 1: Executes the coupled solution of a magma chamber and a country rock model. Once
! this has run successfully, execute the main solution loop (master_loop.mac).
!
! Requirements and Restrictions:
!
! Two arguments must be given: magma chamber database file name then country rock database
! file name, in single quotes, without extensions.
!
! Initial requirements prior to execution are as follows:
! 1. Magma chamber and country rock database files exist and are meshed. The contact surface
!    nodes for both models must coincide.
!
! 2. All model settings must be correctly configured for solution except all thermal boundary and
!    initial conditions. Conditions for other degrees of freedom, such as velocity and pressure,
!    must be applied prior to execution. The execution controls should be set such that the
!    solution to only one time step is calculated during a single run.
!
! 4. A component consisting of the outer boundary areas of the country rock model must exist
!    and be named "extareas".
!
! 5. The correct value of "elfaces" must appear in the code below. The location of the relevant
!    assignment statement is marked clearly with the line:
!    "------------------------! Adjust elfaces !-------------------------"
!
! 6. This macro stores (in a file or as a component) the various initial structures and settings. !
     Since the magma and country rock database files are saved after creation of these objects, !
     this macro need not be executed again if another run of the model is required. The last line
!    of this code calls the main solution loop macro (master_loop.mac). If you do not wish the
!    solution algorithm to run then delete the last line or convert it into a remark.

*cfopen,fnames,cmd   ! Recall the two database file names.
*vwrite,arg1,arg2   ! magma file, country rock file
(A)
*cfclos

! Retrieve magma chamber:
finish
*use,getnames.mac
/filname,%outfile%
```

```
resume

! Select exterior elements:
nsel,s,ext   ! First select all exterior nodes.
esln,s,0   ! Select elements with (some) nodes in the selected set.
cm,elemset,elem   ! Store them in a component called 'elemset'.
save   ! Save the file so that 'elemset' can be used later.

asel,all   !
nsel,all   ! Select everything.
esel,all   !

!-----------------------------------------! Adjust elfaces !-----------------------------------------
elfaces = 2296
!-----------------------------------------------------------------------------------------------------

elnodes = 4*elfaces   ! "elnodes" must be the number of external element faces multiplied by
                      ! four, thus representing groups of four nodes per face.
elfaces=   ! Delete "elfaces".

! Write the value of "elnodes" to file.
*cfopen,geometry,cmd
*vwrite,elnodes
(F5.0)
*cfclos
save

! Initialise "nodeinfo": Node numbers on the contact surface are stored in groups of four values
! which are the nodes belonging to a particular element face. (This makes flux application
! easier.) There are 2 rows: 1 for the magma contact nodes and another for the country rock
! contact nodes.

nodeinfo=
*dim,nodeinfo,array,elnodes,2

! Initialize three 2-D arrays which will store coordinates of each magma nodeinfo node so that
! the corresponding country rock nodeinfo nodes can be found easily.
xinfo=
yinfo=
zinfo=
*dim,xinfo,array,elnodes
*dim,yinfo,array,elnodes
*dim,zinfo,array,elnodes

! Construct and store magma node information.
*msg,ui   ! Display a message.
```

Filling magma node array...

```
! Record a list of the external area numbers.
asel,s,ext   ! Select exterior areas.
*get,numareas,area,0,count
exareas=
*dim,exareas,array,numareas   ! Construct an array to store the area numbers.

*do,k,1,numareas
    *get,areanum,area,0,num,max   ! Select the area with maximum area number.
    exareas(k) = areanum   ! Store in "exareas" array.
    asel,u,,,areanum   ! Discard used area from the current set.
*enddo

esel,all
index = 0
nodes=
*dim,nodes,array,4
*do,k,1,numareas   ! Loop through the external areas.
    *msg,ui,exareas(k),k,numareas   ! Display a progress report.
    Area number %G  ( %G out of %G ).
    asel,s,,,exareas(k)   ! Select an exterior area.
    cmsel,s,elemset   ! Select all exterior elements.
    nsla,s,1   ! Select nodes attached to the currently selected area.
    *get,numelems,elem,0,count
    *do,i,1,numelems   ! Cycle through the exterior elements.
        *get,elemnum,elem,0,num,max
        count = 0
        *do,m,1,8   ! Loop through "elemnum's" eight nodes:
            nodenum = nelem(elemnum,m)   ! Select node at position j of 'elemnum'.
            *if,nsel(nodenum),eq,1,then
                    ! Is it one of the selected (exterior) nodes? If so, it belongs to the exterior
                    ! face of the element and it must be stored in the temporary array "nodes".
                count = count + 1
                nodes(count) = nodenum
            *endif ! nsel...
        *enddo ! m
        *if,count,eq,4,then   ! The element is part of the current area.
            *do,m,1,4
                index = index + 1
                nodeinfo(index,1) = nodes(m)
                xinfo(index) = nx(nodes(m))   ! Store its coordinates.
                yinfo(index) = ny(nodes(m))
                zinfo(index) = nz(nodes(m))
            *enddo   ! m
        *endif   ! count...
```

```
        esel,u,,,elemnum   ! Discard used element.
    *enddo   ! i
    save
*enddo   ! k


nsel,all
esel,all
asel,all
lsel,all


! Write accumulated information to file.
*cfopen,nodestore,cmd
*do,i,1,2
    *vwrite,nodeinfo(1,i)
    (F7.0)
*enddo
*cfclos

*cfopen,coordstor,cmd
*vwrite,xinfo(1)
(F10.5)
*vwrite,yinfo(1)
(F10.5)
*vwrite,zinfo(1)
(F10.5)
*cfclos
!xinfo=
!yinfo=
!zinfo=
save

! Create initial temperature boundary conditions for magma chamber and initial flux boundary
! conditions for country rock.
*msg,ui   ! Display a message.
Setting up boundary condition arrays...
fluxes=   ! Delete if already defined.
temps=
*dim,fluxes,array,elnodes
*dim,temps,array,elnodes
! Assign initial values:
*do,i,1,elnodes
    temps(i) = 293 + (1000 - ny(nodeinfo(i,1)))*0.025
        ! T0 = TS + (yS - ny)ΔT
        ! where TS = temperature of top country rock surface
```

```
        !          y_S = depth of top country rock surface
        !          n_y = node's y-coordinate
        !         ΔT = geothermal gradient in °C.km-1
    fluxes(i) = 0
*enddo   ! i

! Write these to file.
*use,savebcs.mac
save

! Set initial temperature of interior of magma chamber.
*msg,ui
Applying magma's initial conditions...
/solu
nsel,all
*get,totnum,node,0,count
*do,i,1,totnum,1
    ic,i,TEMP,1273   ! Apply initial temperature of 1273 K.
*enddo
save
finish

! Finished with magma.  Now open country rock database file.
*use,getnames.mac
/filname,%infile%
resume

! Restore all the required information.
*dim,a,array,1   ! Temporary array for reading in "elnodes".
*vread,a(1),geometry,cmd
(F5.0)
elnodes = a(1)
a=

*msg,ui
Initializing country rock node array...
nodeinfo=
*dim,nodeinfo,array,elnodes,2
*vread,nodeinfo(1,1),nodestore,cmd,,2
(F7.0)
xinfo=
yinfo=
zinfo=
*dim,xinfo,array,elnodes
*dim,yinfo,array,elnodes
*dim,zinfo,array,elnodes
```

```
*dim,coords,array,elnodes,3
*vread,coords(1,1),coordstor,cmd,,3  ! Recall node coordinate information into temporary array
                                     ! "coords".
(F10.5)
*do,i,1,elnodes
    xinfo(i) = coords(i,1)  ! Copy into permanent arrays.
    yinfo(i) = coords(i,2)
    zinfo(i) = coords(i,3)
*enddo
coords=
save
nsel,all



! Set up "nodeinfo" entries for country rock.
*do,i,1,elnodes
    nodenum = node(xinfo(i),yinfo(i),zinfo(i))  ! Find the node with matching coordinates.
    nodeinfo(i,2) = nodenum
*enddo
!xinfo=
!yinfo=
!zinfo=
save

! Set the country rock temperature initial conditions according to the geothermal gradient.
*msg,ui
Applying country rock temperature initial conditions (with geothermal grad.)...
/solu
nsel,all
*get,totnum,NODE,0,count
*do,i,1,totnum
    ic,i,TEMP,293 + (1000 - ny(i))*0.025,   ! Apply temperature initial conditions.
    ic,i,PRES,(1000-ny(i))*30405,  ! Apply pressure initial conditions according to a gradient
                                   ! of 0.3 atm.m-1 = 30405 N.m-3.
*enddo

! Set outer surface boundary conditions for country rock.
*msg,ui
Applying country rock outer temperature boundary conditions (with geothermal grad.)...

cmsel,s,extareas   ! Select the component that contains the external areas. This component must
                   ! created in FLOTRAN before execution of this macro.
nsla,s,1   ! Select nodes attached to those areas.
*get,totnum,node,0,count
```

```
*do,i,1,totnum
    *get,maxnode,NODE,0,NUM,MAX   ! Select maximum node number in currently selected
                                  ! set.
    d,maxnode,TEMP,293+(1000-NY(maxnode))*0.025,   ! Apply appropriate boundary
                                                   ! condition.
    nsel,u,,,maxnode   ! Remove node from currently selected set.
*enddo
lsel,all
nsel,all
save
finish

!------------------------- Following line optional:  calls main solution loop. -------------------------
*use,master_loop.mac
```

```
! Part 2: main control program for general 3-D magma chamber and country rock coupled
! model.
!
! This macro takes no arguments.
!
! The section of code below that appears before the main solution loop must be executed if the
! solution is being started from time = 0. If results already exist and the solution is to be
! continued from the last of these, the section of code before the main solution loop must be
! converted to remarks.

! Create initial temp. boundary conditions for magma chamber and initial flux boundary
! conditions for country rock.
finish
*use,getnames.mac
/filname,%outfile%  ! Open magma chamber database in order to retrieve the value of "elnodes".
resume
*msg,ui
Setting up boundary condition arrays...
fluxes=   ! Delete if already defined.
temps=
*dim,fluxes,array,elnodes
*dim,temps,array,elnodes
! Assign initial values.
*do,i,1,elnodes
    temps(i) = 293 + (1000 - ny(nodeinfo(i,1)))*0.025
    fluxes(i) = 0
*enddo  ! i
! Write these to file.
*use,savebcs.mac
save


!========================== Main Solution Loop ==========================

*msg,ui
Starting main solution loop...
finish
*do,i,1,10000
    *use,getnames.mac
    /filname,%outfile%    ! Open magma chamber database.
    resume
    *use,getbcs.mac   ! Retrieve the saved parameters "temps" and "fluxes".
    *use,newtemp.mac   ! Do a magma run with "temps" boundary conditions.
    /post1
```

```
set,last  ! Select the last set of results.

*do,j,1,elnodes  ! Record from these results the external fluxes.
    *get,fluxes(j),NODE,nodeinfo(j,1),HFLU  ! Store the values in "fluxes".
*enddo
*use,savebcs.mac  ! Save for later use.

finish
save
*use,getnames.mac
/filname,%infile%  ! Open country rock database.
resume
*use,getbcs.mac
*use,newflux.mac  ! Do a country rock run with "fluxes" boundary conditions.

! Termination test...
*get,testtemp,node,node(0,510,0),temp  ! Test the temperature of a node just above the
                                       ! chamber.
*if,testtemp,LE,330,then  ! If the country rock has cooled sufficiently, stop.
    finish
    *exit
*endif
testtemp=

oldtemps=
*dim,oldtemps,array,elnodes
/post1
set,last
! First plot the velocity vectors so that you can assess the progress of the run.  Manual
! termination, if required, can be done through the "stop.cmd" file as described below.
plvect,v,,,,vect,node,off  ! Velocity vector plot.
*do,j,1,elnodes
    oldtemps(j) = temps(j)  ! Remember old temperature boundary conditions for future
                            ! comparison.
    *get,temps(j),NODE,nodeinfo(j,2),TEMP  ! Store latest results in "temps".
*enddo
*use,savebcs.mac  ! Save the new boundary conditions.
save


!---------- Time Step Checking Routine. ----------

! Find the contact node with the biggest temperature change.
maxdT=0

*do,j,1,elnodes
```

```
        --->> Program abandoned manually. <<---
        *exit
    *endif
    a=
*enddo
finish
```

newtemp.mac

```
! Executes a single magma chamber solution time step with updated temperature boundary
! conditions.

/solu
nplot,0
*msg,ui
Applying new temperatures to magma...
*do,m,1,elnodes
    d,nodeinfo(m,1),temp,temps(m),   ! Apply new boundary condition.
*enddo
m=
nsel,all
save
*msg,ui
Solving magma...
solve   ! Run the FLOTRAN solution procedure.
```

newflux.mac

```
! Executes a single country rock solution time step with updated heat flux boundary conditions.

/solu
esel,all
nsel,all
nplot,0
*msg,ui
Applying new fluxes to country rock...
*do,m,1,elnodes,4   ! Loop through the external nodes in groups of four.  Each group was
                    ! initially !arranged in "master-ini.mac" to contain the nodes attached to a
                    ! single element face.
    value = -(fluxes(m)+fluxes(m+1)+fluxes(m+2)+fluxes(m+3))/4
```

```
                    ! Find the arithmetic mean of the four corner fluxes.
   nsel,s,,,nodeinfo(m,2)  ! Select the four nodes.
   nsel,a,,,nodeinfo(m+1,2)
   nsel,a,,,nodeinfo(m+2,2)
   nsel,a,,,nodeinfo(m+3,2)
   sf,all,hflux,value  ! Apply the new flux to all of them.
*enddo
nsel,all
save
*msg,ui
Solving country rock...
solve  ! Run the FLOTRAN solution procedure.
```

newstep.mac

```
! Changes the duration of a single time step for both models.
!
! Takes as an argument the factor with which the old time step must be multiplied in order to get
! the new time step.

*cfopen,step,cmd  ! Write the macro's argument to a file else it will be lost when the database
                  ! files change.
*vwrite,arg1
(F4.2)
*cfclos

finish
*use,getnames.mac
/filname,%outfile%  ! Open the magma database file.
resume

*dim,b,array,1  ! retrieve the macro's argument.
*vread,b(1),step,cmd
(F4.2)
factor=b(1)
b=

/solu
/com,,Transient Analysis,1
*get,oldstep,fldata,time,step  ! Get the old time step.
stepnew=factor*oldstep  ! Update it.
fldata,time,step,stepnew  ! Install it.
save
```

```
finish
*use,getnames.mac
/filname,%infile%   ! Open the country rock database file.
resume

*dim,b,array,1   ! retrieve the macro's argument.
*vread,b(1),step,cmd
(F4.2)
factor=b(1)
b=

/solu
/com,,Transient Analysis,1
*get,oldstep,fldata,time,step   ! Get the old time step.
stepnew=factor*oldstep   ! Update it.
fldata,time,step,stepnew   ! Install it.
save
```

savebcs.mac

```
! Writes the current contact surface temperature and heat flux boundary conditions to file
! "bcstore.cmd".

*cfopen,bcstore,cmd
*vwrite,temps(1)
(F10.5)
*vwrite,fluxes(1)
(F10.5)
*cfclos
```

getbcs.mac

```
! Retrieves boundary condition lists "fluxes" and "temps" from file "bcstore.cmd".

temps=
fluxes=
*dim,temps,array,elnodes
*dim,fluxes,array,elnodes

*dim,a,array,2*elnodes   ! Temporary array for reading in fluxes and temperatures.
```

```
*msg,ui
Retrieving flux and temperature arrays...
*vread,a(1),bcstore,cmd
(F10.5)
*do,m,1,elnodes
    temps(m) = a(m)
    fluxes(m) = a(elnodes+m)
*enddo
a=
m=
```

getnames.mac

```
! Retrieves the names of the magma chamber and country rock database files (in that order) from
! the file "fnames.cmd". It is assumed that the file names have the extension "db" hence only the
! first parts of the names are used.

outfile=
infile=

*dim,a,char,2
*vread,a(1),fnames,cmd
(A)

outfile=a(1)
infile=a(2)
a=
```